

Clinical applications of infrared and Raman spectroscopy in the fields of cancer and infectious diseases

Maria Paraskeva^{a,b}, Baker J. Matthew^c, Butler J. Holly^c, Byrne J. Hugh^d, Chakkumpulakkal P. V. Thulya^e, Christie Loren^{c,f}, Crean StJohn^g, Gardner Peter^h, Gassner Callum^e, Kazarian G. Sergeiⁱ, Kochan Kamila^e, Kyrgiou Maria^{a,j}, Lima M. G. Kássio^k, Martin-Hirsch L. Pierre^l, Paraskevaidis Evangelos^m, Pebotuwa Savithri^{e,n}, Adegoke A. John^e, Sala Alexandra^{c,f}, Santos Marfran^k, Sulé-Suso Josep^o, Tyagi Gunjanⁱ, Walsh Michael^p, and Wood Bayden^e



^aDepartment of Metabolism, Digestion and Reproduction, Faculty of Medicine, Imperial College London, Hammersmith Campus, London, United Kingdom; ^bSchool of Pharmacy and Biomedical Sciences, University of Central Lancashire (UCLan), Preston, United Kingdom; ^cDxcover Ltd, Royal College Building, Glasgow, United Kingdom; ^dFOCAS Research Institute, Technological University Dublin, Dublin, Ireland; ^eCentre for Biospectroscopy, School of Chemistry, Monash University, Clayton, Victoria, Australia; ^fDepartment of Pure and Applied Chemistry, University of Strathclyde, Technology and Innovation Centre, Glasgow, United Kingdom; ^gVice-Chancellor's Group, University of Central Lancashire, Preston, United Kingdom; ^hManchester Institute of Biotechnology, The University of Manchester, Manchester, United Kingdom; ⁱDepartment of Chemical Engineering, Imperial College London, London, United Kingdom; ^jWest London Gynaecological Cancer Centre, Imperial College Healthcare NHS Trust, London, UK; ^kBiological Chemistry and Chemometrics, Institute of Chemistry, Federal University of Rio Grande do Norte, Natal, Brazil; ^lDepartment of Obstetrics and Gynaecology, Lancashire Teaching Hospitals, NHS Foundation Trust, Preston, United Kingdom; ^mDepartment of Obstetrics and Gynaecology, University of Ioannina, Ioannina, Greece; ⁿDepartment of Microbiology, Monash University, Clayton, Victoria, Australia; ^oSchool of Pharmacy and Bioengineering, Keele University and Cancer Centre, University Hospitals of North Midlands, Stoke on Trent, United Kingdom; ^pDepartment of Materials Science and Biomedical Engineering, University of Wisconsin - Eau Claire, Eau Claire, WI, USA

ABSTRACT

Analytical technologies that can improve disease diagnosis are highly sought after. Current screening/diagnostic tests for several diseases are limited by their moderate diagnostic performance, invasiveness, costly and laborious methodologies or the need for multiple tests before a definitive diagnosis. Spectroscopic techniques, including infrared (IR) and Raman, have attracted great interest in the medical field, with applications expanding from early disease detection to monitoring and real-time diagnosis. This review highlights applications of IR and Raman spectroscopy, with a focus on cancer and infectious diseases since 2015, and underscores the diverse sample types that can be analyzed, such as biofluids, cells and tissues. Studies involving more than 25 participants per group (disease and control group; if no control group >25 in disease group) were considered eligible, to retain the clinical focus of the paper. Following literature searches, we identified 94 spectroscopic studies on different cancers and 30 studies on infectious diseases. The review

KEYWORDS

Infrared spectroscopy; Raman spectroscopy; cancer; infectious disease; disease diagnostics; health economics; clinical translation

CONTACT Maria Paraskeva  m.paraskeva@imperial.ac.uk  Department of Metabolism, Digestion and Reproduction, Faculty of Medicine, Imperial College London, Hammersmith Campus, W12 0NN, London, United Kingdom

© 2021 The Author(s). Published with license by Taylor & Francis Group, LLC

This is an Open Access article distributed under the terms of the Creative Commons Attribution-NonCommercial-NoDerivatives License (<http://creativecommons.org/licenses/by-nc-nd/4.0/>), which permits non-commercial re-use, distribution, and reproduction in any medium, provided the original work is properly cited, and is not altered, transformed, or built upon in any way.

suggests that such technologies have the potential to develop into an objective, inexpensive, point-of-care test or facilitate disease diagnosis and monitoring. Up-to-date considerations for the implementation of spectroscopic techniques into a clinical setting, health economics and successful applications of vibrational spectroscopic tests in the clinical arena are also discussed.

Introduction

Amidst the search for novel, cost-effective and rapid medical diagnostic tests, vibrational spectroscopy techniques have attracted increased interest in recent years. Current clinical tests, such as cytological evaluation, immunohistochemistry and imaging techniques have proven extremely efficacious in disease diagnostics. However, they necessitate costly, time-consuming methodologies while they may also lack automation, require user-dependent interpretation or involve a series of tests, some still providing mediocre diagnostic accuracy. In order to address these needs, Infrared (IR) and Raman spectroscopy have been suggested as an alternative means of detecting and diagnosing a broad range of diseases. By providing simultaneous information on multiple biological molecules, such technologies generate a holistic biochemical “fingerprint”, thus indicating the presence or absence of disease, and even the stage of disease progression.

Vibrational spectroscopy techniques employ the interaction of light with matter upon exposure to electromagnetic radiation of specific energy to study molecular vibrations. The vibrational characteristics of the chemical bonds of a molecule are characteristic of that molecule and the spectroscopic signature of transitions between discrete vibrational levels induced by incident light can therefore reveal information on specific molecules present in the sample. IR absorption and Raman, the two main vibrational spectroscopic techniques, have distinct physical origins, being light absorption and inelastic light scattering, respectively (Figure 1A). IR and Raman spectroscopy provide complementary information, due to different selection rules; vibrations are IR active when there is a change in the permanent dipole moment over the course of the vibration, whereas a change in the molecular polarizability is needed for a vibration to be Raman-active. The different experimental variants of IR and Raman, each with distinct benefits and limitations, are provided in Table 1^[1-6]. Vibrational spectroscopy has been successfully employed as an analytical tool for a number of applications in fields such as pharmacology^[7], archaeology^[8], forensic^[9], food^[10] and environmental science^[11], homeland security^[12] and biomedicine^[13].

Clinical spectroscopy is attracting increasing interest as an alternative test for the early detection, diagnosis or monitoring of human diseases, including kidney^[14], heart^[15] and neurodegenerative diseases^[16,17], asthma^[18], chronic obstructive pulmonary disease^[19] and diabetes^[20]. The last two decades have also seen a tremendous increase in IR and Raman spectroscopic studies in the fields of cancer (~15-20 fold increase) and infectious diseases (~7-30 fold increase) (Figure 2). Tissues, cells and biological fluids, including blood, urine, saliva or cerebrospinal fluid, are all suitable for spectroscopic analysis, generating characteristic spectra that are indicative of the content

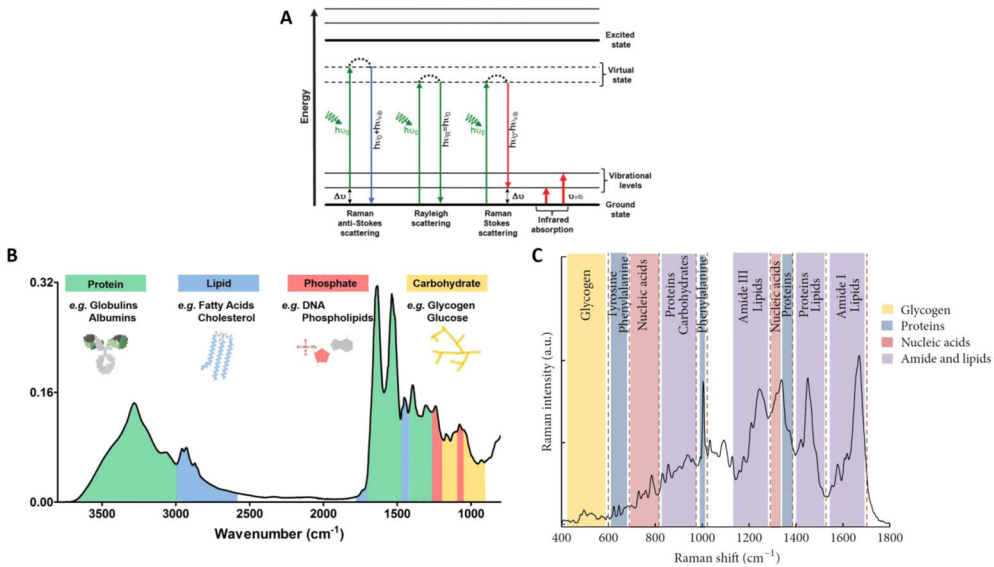


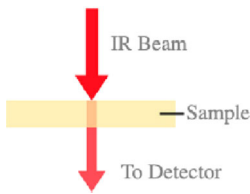
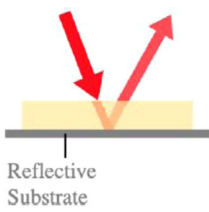
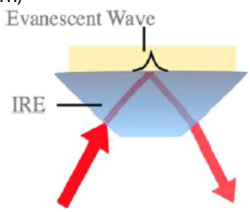
Figure 1. Principle of vibrational spectroscopic techniques and characteristic biological spectra serving as “fingerprints”. When an incident photon interacts with a molecule, it may be absorbed, during infrared (IR) absorption, or scattered. Vibrational energies are quantized and lie in the mid-IR region of the electromagnetic spectrum. Absorption of light is well defined, resonant frequencies give rise to a spectrum which is characteristic of the vibrations of a material. When light scattering occurs, the energy of incident and scattered photons can either remain the same (elastic or Rayleigh scattering) or differ (inelastic or Raman scattering). Depending on whether energy is lost or gained by the incident photon, Stokes or anti-Stokes scattering are observed, respectively. The spectrum of observed energy differences (Raman shifts) provides a similar fingerprint of the chemical composition of a sample.

(A) Energy diagram illustrating the electronic transitions of a molecule during Raman anti-Stokes and Stokes scattering, Rayleigh scattering and infrared absorption. Where $h\nu_0$ = incident energy; $h\nu_{\text{vib}}$ = vibrational energy; $h\nu_{\text{R}}$ = Rayleigh energy; $\Delta\nu$ = Raman shift; ν_{vib} = vibrational frequency. Characteristic spectra generated by analysis of biological samples using (B) IR and (C) Raman spectroscopy. Different spectral regions providing structural information for different biomolecules including proteins, lipids, nucleic acids and carbohydrates are highlighted. The IR spectrum was generated by analysis of human blood serum using Attenuated Total Reflection Fourier-transform IR (ATR-FTIR) whereas the Raman spectrum was obtained from cells of the cervical cancer cell line CaSki. Reproduced with permission from Baker *et al.*^[24], Gray *et al.*^[159] and Ramos *et al.*^[170]

of biomolecules such as proteins, lipids, nucleic acids and carbohydrates (Figure 1B and C).

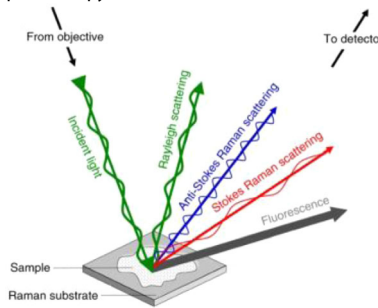
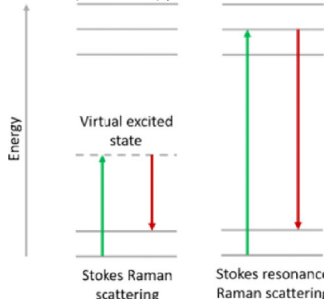
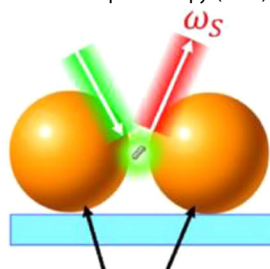
This paper will provide a comprehensive review of studies since 2015 that have utilized clinical spectroscopy as a means of studying cancer and infectious diseases toward the development of a cost-effective, rapid diagnostic and/or monitoring test. Studies involving more than 25 participants were deemed eligible for this review, to retain its clinical focus and explore the potential of spectroscopy in a clinical context. Smaller-scale studies have been excluded to avoid those focusing mainly on technology/methodology development. For further information and studies with an emphasis on innovation and emerging trends in biomedical spectroscopy, the readers are directed to the following reviews^[1,13,21–28]. Herein, we include both *ex vivo* and *in vivo* studies as

Table 1. Experimental variants of infrared and Raman spectroscopic techniques along with their benefits and limitations. Graphics reproduced and adapted with permission from^[1–6].

	Experimental mode	Benefits	Limitations
Infrared Spectroscopy	<p>Transmission</p> 	<p>Can be employed in Macro or Microscopic mode Spatial resolution of $\sim 5\mu\text{m}$ Ratioing technique, in which signal is normalized to source intensity High signal-to-noise ratio Most commonly performed in Fourier Transform mode Interrogation area up to $150\times 150\mu\text{m}$ with multidetector Focal Plane arrays</p>	<p>Need for IR transparent substrate Restrictions in sample thickness ($<12\mu\text{m}$) Laborious sample preparation of tissue samples Spectral artifacts due to (i) reflection from top surface, (ii) resonant scattering Susceptible to water interference</p>
	<p>Transflection</p> 	<p>As for IR Transmission Sample absorbance doubled to improve signal-to-noise ratio for thin samples Low-cost reflective substrates High signal-to-noise ratio</p>	<p>As for IR Transmission Normally only employed in Microscopic configuration Restrictions in sample thickness ($<5\mu\text{m}$) Spectral artifacts due to (i) reflection from top surface, (ii) resonant scattering, (iii) electric field standing wave effects</p>
	<p>Attenuated Total Reflection (ATR)</p> 	<p>As for IR Transmission Higher spatial resolution for imaging ($1\text{-}2\mu\text{m}$) Spectral artifacts due to (i) reflection from top surface, (ii) resonant scattering are minimized Minimal sample preparation Low-cost substrate (Biofluids can be directly deposited on crystal without the need for substrate) Ideal for biofluids</p>	<p>Possibility for sample destruction due to contact Tissue samples more prone to destruction Limited penetration depth, which varies across the mid-IR ($\sim 5\text{-}10\mu\text{m}$).</p>

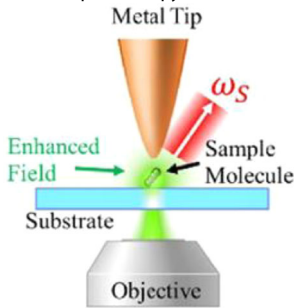
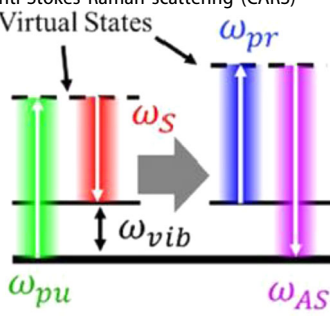
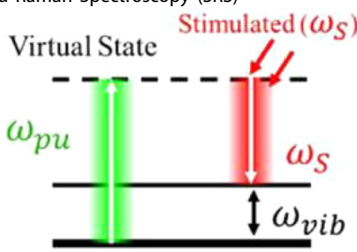
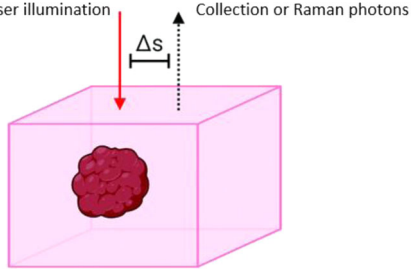
(continued)

Table 1. Continued.

Raman Spectroscopy	Experimental mode	Benefits	Limitations
	<p data-bbox="221 202 403 231">Raman Spectroscopy</p> 	<p data-bbox="772 202 974 714"> Most commonly performed in backscattering, microscopic mode Spatial resolution of $<1\ \mu\text{m}$ Confocal operation available, to allow 3D imaging Narrower, better defined spectral features than in IR Incident radiation not absorbed by the process, so penetration is limited by focal depth Minimal sample preparation required Relatively small signals from water </p>	<p data-bbox="1001 202 1176 1052"> Relatively weak signal No normalization to input intensity Susceptible to interference from stray light scattering and/or fluorescence Susceptible to instrument calibration drift High intensity at the sample can cause photothermal and/or photochemical degradation Most commonly performed in dispersive mode, in which the spectrum of a point is dispersed onto a multidetector array. Lateral coverage is by point-to-point mapping, rather than imaging of an area, resulting in long acquisition times. </p>
	<p data-bbox="221 1091 551 1120">Resonance Raman Spectroscopy (RRS)</p> 	<p data-bbox="772 1091 974 1381"> As for Raman Spectroscopy 106 signal enhancement High signal-to-noise ratio for resonant moieties (typically carotenes, heme, and other conjugated structures) </p>	<p data-bbox="1001 1091 1176 1236"> As for Raman Spectroscopy Spectrum dominated by resonant moieties </p>
	<p data-bbox="221 1439 618 1468">Surface Enhanced Raman Spectroscopy (SERS)</p>  <p data-bbox="376 1738 591 1777">Metal Nano-particles</p>	<p data-bbox="772 1439 974 1825"> Commonly employed using colloidal suspensions, or substrates. 10³–10¹⁰ Raman signal enhancement Quenches fluorescence Low detection limit Narrower, better defined spectral features than in IR Molecular labelling Suitable for biofluids </p>	<p data-bbox="1001 1439 1176 1758"> Poor reproducibility of spectral profiles and intensities Molecular selectivity to nanoparticle adherence Limited range ($\sim 10\text{nm}$) Increased sample preparation steps </p>

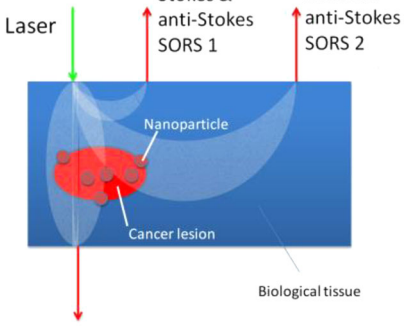
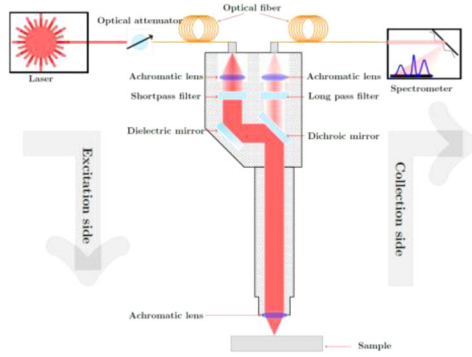
(continued)

Table 1. Continued.

Experimental mode	Benefits	Limitations
<p>Tip Enhanced Raman Spectroscopy (TERS)</p>  <p>Metal Tip</p> <p>Enhanced Field</p> <p>Sample Molecule</p> <p>Substrate</p> <p>Objective</p> <p>ω_S</p>	<p>Tip-dependent spatial resolution ($\sim 10\text{-}100\text{nm}$)</p> <p>Low detection limit</p> <p>Quenches fluorescence</p> <p>Narrower, better defined spectral features than in IR</p>	<p>Increased experimental complexity</p> <p>Sample heating effect at tip apex</p> <p>Poor reproducibility</p> <p>Surface sensitive ($\sim 10\text{nm}$)</p>
<p>Coherent anti-Stokes Raman scattering (CARS)</p>  <p>Virtual States</p> <p>ω_{pu}</p> <p>ω_S</p> <p>ω_{AS}</p> <p>ω_{vib}</p> <p>ω_{pr}</p>	<p>As for Raman Spectroscopy</p> <p>$10^3\text{-}10^6$ signal enhancement</p> <p>Spatial resolution improved by nonlinearity of response ($\sim 200\text{-}500\text{nm}$)</p> <p>No fluorescence interference</p>	<p>As for Raman Spectroscopy</p> <p>Nonresonant background can dominate weak resonance signals</p> <p>Spectral distortion</p> <p>Increased risk of photothermal sample damage</p> <p>Currently limited to single wavenumber measurement, which can be discretely tuned</p>
<p>Stimulated Raman Spectroscopy (SRS)</p>  <p>Virtual State</p> <p>Stimulated (ω_S)</p> <p>ω_{pu}</p> <p>ω_S</p> <p>ω_{vib}</p>	<p>As for CARS</p> <p>Not affected by fluorescence and nonresonant background</p> <p>High sensitivity (1 in 10^6 photons)</p>	<p>As for Raman Spectroscopy</p> <p>Increased risk of photothermal sample damage</p> <p>Currently limited to single wavenumber measurement, which can be discretely tuned</p>
<p>Spatially Offset Raman Spectroscopy (SORS)</p>  <p>Laser illumination</p> <p>Collection or Raman photons</p> <p>Δs</p>	<p>As for Raman</p> <p>Increased depth measurements (several mm)</p>	<p>As for Raman</p> <p>Relatively weak signal</p> <p>Reduced reproducibility</p>

(continued)

Table 1. Continued.

Experimental mode	Benefits	Limitations
<p data-bbox="225 208 577 260">Surface Enhanced Spatially Offset Raman Spectroscopy (SESORS)</p> 	<p data-bbox="772 208 960 328">As for SORS Detects SERS signals up to 50 mm beneath the sample surface</p>	<p data-bbox="1008 208 1142 280">Requires nanoparticle introduction</p>
<p data-bbox="225 656 712 685">Shifted-Excitation Raman Difference Spectroscopy (SERDS)</p> 	<p data-bbox="813 656 927 724">As for Raman Fluorescence rejection</p>	<p data-bbox="1008 656 1149 801">As for Raman Difference spectra are reconstructed using peak fitting</p>

well as different experimental modes allowing for point spectroscopic assessment or imaging. A health economic evaluation is also provided, to highlight the cost benefit of vibrational spectroscopic techniques in healthcare systems compared to currently used tests. Recent startup companies that have successfully moved forward to translational clinical research are also discussed. Finally, we present a general workflow of clinical spectroscopy and emphasize the requirements for integrating such technologies into a clinical context.

Search strategy: eligibility and exclusion criteria

The literature search was conducted in PubMed for articles that were published between January 2015 and May 2021. Independent reviewers extracted the data and identified eligible studies. Studies were deemed eligible for inclusion if they included more than 25 participants per group (disease and control; if no control group >25 in disease group) to study any cancer type or infectious disease (bacterial, fungal, parasitic, viral). All experimental variants of mid-IR and Raman spectroscopy were considered eligible

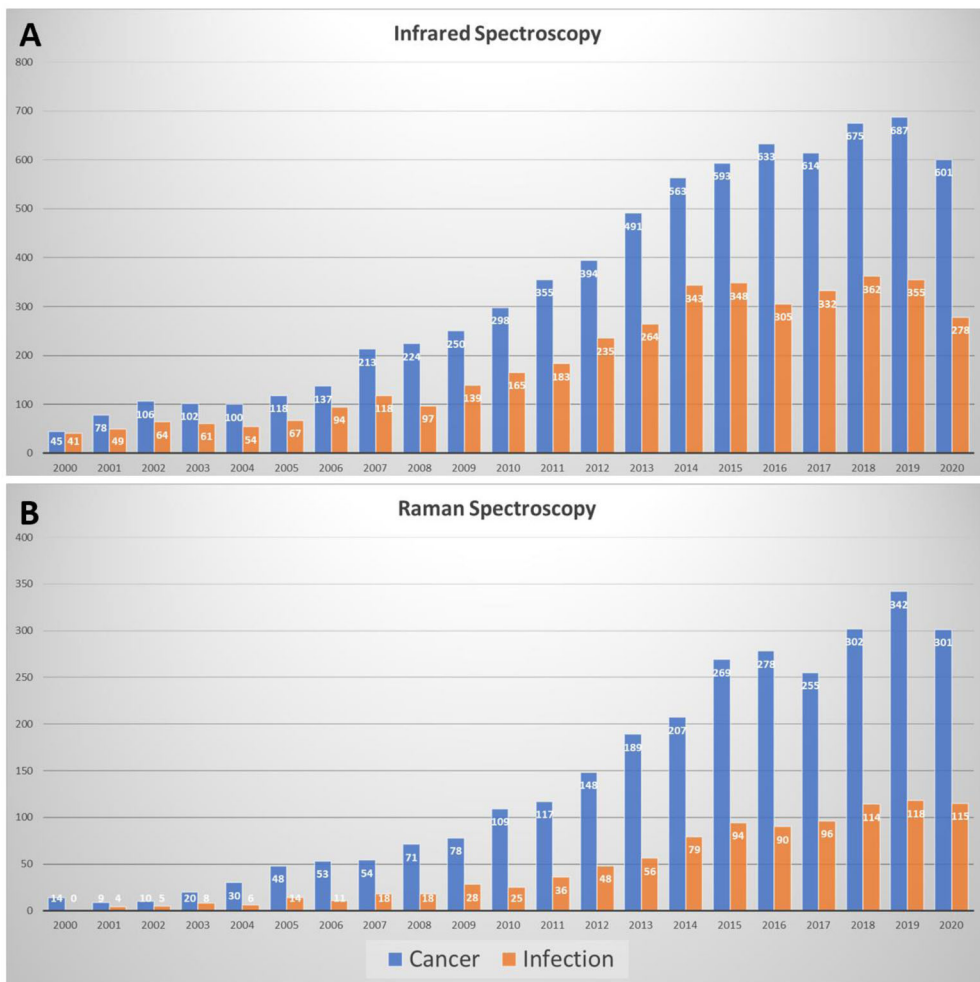


Figure 2. PubMed search to determine the number of publications that have utilized (A) Infrared and (B) Raman spectroscopy to study cancers and infections during the period 2000–2020. A significant increase of relevant clinical spectroscopy studies is observed in recent years.

for inclusion. Studies that analyzed different human sample types (biofluids, cells and tissues) were included.

Articles that used cell lines or non-human samples (animal models) were excluded. Review articles, commentaries and opinion papers were also excluded, as were near-IR studies and those with a focus on drug delivery/development. Non-English articles and those with <25 participants per group (disease and control) were also excluded. The cut off of 25 participants per group was based on the study by Beleites *et al.* on optimum sample sizes for classification models^[29].

IR and Raman spectroscopy in cancer research

Overall, 94 studies were found to satisfy the inclusion criteria: four in bladder cancer, ten studies in brain tumor, five studies in breast cancer, five in colon cancer, seven in

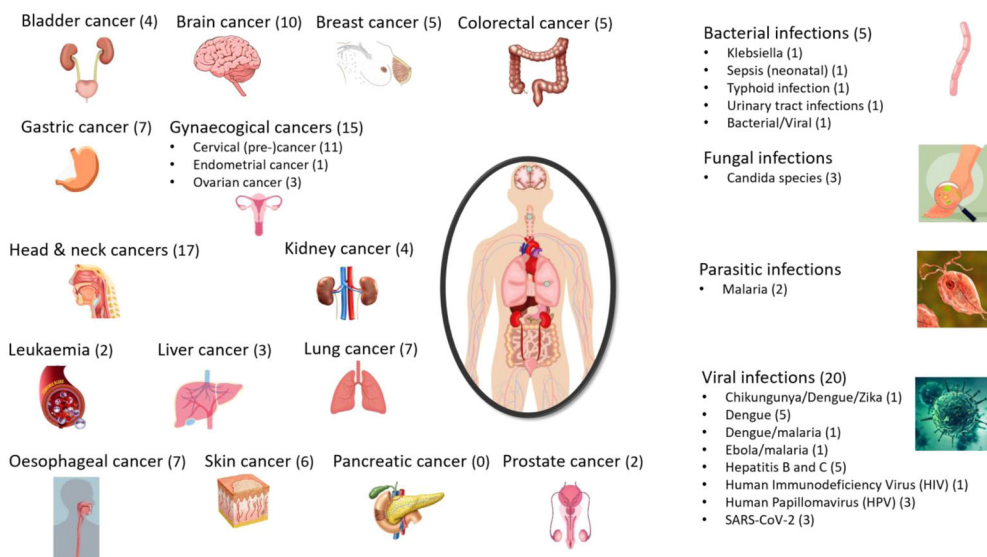


Figure 3. Clinical spectroscopy in cancer and infectious diseases. Infrared (IR) and Raman spectroscopic techniques have been used for the early detection, diagnosis or monitoring of the depicted cancers and infectious diseases (numbers of identified studies are provided in parenthesis). Different experimental variants, sampling modes and sample types have been used for *in vivo* or *ex vivo* clinical studies. Details for each disease and main findings of each study published between 2015–2021 are provided in [Tables 2 and 3](#).

gastric cancer, 15 studies in gynaecological cancers (11 cervical precancer/cancer; one endometrial cancer; three ovarian cancer), 17 in head and neck cancers, four in kidney, two in leukemia, three in liver cancer, seven in lung cancer, seven in esophageal cancer, six in skin cancer, two in prostate cancer ([Figure 3](#)). No studies of pancreatic cancer were found with >25 participants.

Bladder cancer

The literature searches for applications of spectroscopy for the diagnosis of bladder cancer identified four papers that met our inclusion criteria, with two using serum, one using tissue and one using cytology.

Li *et al.*^[30] applied surface enhanced Raman spectroscopy (SERS) to the serum of 36 normal healthy volunteers and 55 patients with bladder cancer. SERS spectra were acquired with a 785 nm laser at 0.5mW and used silver nanoparticles with an acquisition time of 10 seconds. SERS spectra were subjected to genetic algorithms combined with linear discriminant analysis (GA-LDA), which identified six key spectral peaks associated with bladder cancer (associated with proteins, nucleic acids and lipids). Using these six spectral bands it was determined that a sensitivity of 91% and specificity of 100% could be obtained to classify serum derived from normal patients compared to bladder cancer patients. Chen *et al.*^[31] also investigated the use of SERS on serum from bladder cancer patients however focused on the discrimination of muscle invasive bladder cancer from non-muscle invasive bladder cancer, which is a critical determination

Table 2. Overview of infrared and Raman studies in the field of oncology between January 2015 and May 2021. Studies were deemed eligible for inclusion if they included more than 25 participants per group (disease and control; if no control group >25 in disease group).

Disease	Author, Year, Country	Spectroscopic technique	Population [Sample type]	Main findings
Biofluids				
Bladder cancer	Chen, 2019, China ^[31]	SERS	30 healthy control, 60 cancer (28 non-muscle invasive and 32 muscle invasive) [Blood serum]	Multiple models for diagnosis presented, overall diagnostic accuracy was 93%
Bladder cancer	Li, 2015, China ^[30]	SERS	36 healthy control, 55 cancer [Blood serum]	Using genetic algorithms combined with linear discriminant analysis had a diagnostic sens of 91% and spec of 100%
Brain cancer (IDH1 detection)	Cameron, 2020, UK ^[39]	ATR-FTIR coupled with centrifugal filtration (for serum samples); Synchrotron (for tissue samples)	(i) 72 gliomas (36 IDH1 mutated vs 36 IDH1 wild-type) [Blood serum] (ii) 79 gliomas (21 IDH1 mutated and 78 for IDH1 wild-type. Some were lost during sample prep so exact numbers for each are not known) [FFPE tissue]	Serum-based analysis gave ~70% sens and spec; 82% sens and 83% spec in distinguishing IDH1 mutated vs IDH1 wildtype using synchrotron on tissues
Brain tumour	Cameron, 2020, UK ^[37]	ATR-FTIR	87 healthy control, 554 cancer (Lymphoma and primary: glioma, meningioma and metastatic) [Blood serum]	92% sens, 97% spec for lymphoma vs controls; 96% sens, 95% spec for gliomas vs controls; 95% sens, 98% spec for meningiomas vs controls; 96% sens, 95% spec for metastatic brain cancers vs controls; brain cancer subtypes were differentiated with ~71-94% sens and 82-96% spec; primary vs metastatic cancers achieved 91% sens and 66% spec
Brain cancer	Butler, 2019, UK ^[38]	ATR-FTIR	237 non-cancer, 487 cancer; external validation with 104 prospectively recruited patients [Blood serum]	92% sens and 93% spec for cancer vs non-cancer; 83% sens and 87% spec in prospective validation study
Brain cancer	Cameron, 2019, UK ^[36]	ATR-FTIR	237 non-cancer, 478 cancer, 41 additional lymphoma patients [Blood serum]	91% sens and spec for cancer vs non-cancer; best result for glioblastoma vs lymphoma was 90% sens and 86% spec (done using 112 patients overall)

(continued)

Table 2. Continued.

Disease	Author, Year, Country	Spectroscopic technique	Population [Sample type]	Main findings
Brain tumour	Mehta, 2018, India ^[40]	Raman	35 controls, 35 cancers (meningiomas) [Blood serum]	When tested in independent dataset: 70% accuracy for meningiomas vs controls; 72% accuracy for Grade I meningiomas vs controls; 80% accuracy for Grade II meningiomas vs controls
Brain cancer	Smith, 2016, UK ^[35]	ATR-FTIR	122 non-cancer, 311 cancer [Blood serum]	93% sens and 92% spec; feature selection coupled with 2D correlation analysis was employed to improve the diagnostic values from the Hands, 2016 study (below)
Brain tumour	Hands, 2016, 2016 ^[34]	ATR-FTIR	122 non-cancer, 311 cancer (primary: glioma, meningioma and metastatic) [Blood serum]	92% sens and 83% spec
Breast cancer	Sitnikova, 2020, Russia ^[44]	ATR-FTIR	80 healthy controls, 66 cancer [Blood serum]	92% sens and 87% spec was obtained
Breast cancer	Lin, 2020, China ^[45]	SERS	30 health controls, 30 cancer at two different time points (before and after surgical treatment), [Blood serum]	95% and 100% diagnostic accuracies were achieved for pre-surgery vs post-surgery and pre-surgery vs normal groups, respectively
Breast cancer	Elmi, 2017, Iran ^[47]	FTIR (transmission mode)	43 healthy controls, 43 cancer [Blood serum]	Diagnostic sens of 84%, spec of 74%, and accuracy of 83% based on 3090-3700 cm^{-1} spectral region
Cervical cancer	Shrivastava, 2021, India ^[61]	Confocal Raman microscopy	30 controls, 63 cancer (serial samples from 3 time points: before, during or 6months after treatment – chemoradiotherapy with external radiotherapy) [Blood serum]	93% sens and 86% spec for control vs cancer before treatment; sens and spec ranged between 50-74% and 25-66% respectively when cancer samples from different time points of treatment were compared (ie. before vs during treatment; during vs after; before vs after)

(continued)

Table 2. Continued.

Disease	Author, Year, Country	Spectroscopic technique	Population [Sample type]	Main findings
Cervical precancer and cancer	Lu, 2020, China ^[62]	SERS-based immunoassay	30 healthy controls, 30 CIN1, 30 CIN2, 30 CIN3, 30 cervical cancer [Blood serum]	Simultaneous detection of two cancer-associated serum biomarkers (squamous cell carcinoma antigen and osteopontin). Good selectivity and reproducibility with low detection limits and consistent results to ELISA methods
Colon cancer	Toraman, 2019, Turkey ^[51]	FTIR	40 healthy controls, 30 cancer [Blood plasma]	Sens of 93% and spec of 95% for SVM and 96% for multilayer perceptron model
Colon cancer	Li, 2016, China ^[49]	Raman	75 healthy controls, 65 pre-operative colon cancer, 60 post-operative colon cancer patients [Blood Serum]	Diagnostic accuracy of 91% and spec of 93%
Colon, breast, lung, oral and ovarian cancers	Moisoiu, 2019, Romania ^[50]	SERS	39 normal, 109 colorectal, 42 breast, 33 lung, 17 oral, 13 ovarian cancer [Blood serum]	98% sens and 91% spec for normal vs cancer (all types); overall diagnostic accuracy of 88% for oral, 86% for colorectal, 80% for ovarian, 76% for breast and 59% for lung cancer
Endometrial cancer and atypical hyperplasia	Paraskevasidi, 2020, UK ^[72]	ATR-FTIR	242 healthy controls, 68 atypical hyperplasia, 342 cancer (Type I: 258; Type II: 64; Mixed: 20) [Blood plasma]	87% sens and 78% spec for controls vs cancer (all types); 91% sens and 81% spec for Type I cancer vs controls; 100% sens and 88% spec for atypical hyperplasia vs controls
Gastric Cancer	Chen, 2018, China ^[56]	SERS	116 healthy control, 104 cancer (20 early gastric cancer, 84 advanced gastric cancer) [Saliva]	80% sens and 88% spec
Gastric Cancer	Liu, 2017, China ^[58]	FTIR	30 healthy control, 40 cancer [Red blood cells]	95% sens and 70% spec
Gastric and Colon cancer	Guleken, 2021, Turkey ^[57]	FTIR	43 healthy control, 45 gastric cancer, 45 colon cancer [Blood serum]	PCA discrimination demonstrated

(continued)

Table 2. Continued.

Disease	Author, Year, Country	Spectroscopic technique	Population [Sample type]	Main findings
Gastric cancer	Bahreini, 2019, Iran ^[54]	Raman	40 healthy control, 20 cancer [Blood serum]	88% ability to discriminate between control and cancer
Gastric cancer and gastritis	Li, 2016, China ^[55]	SERS	42 control, 45 atrophic gastritis patients, 43 pre-operation gastric cancer patients, 40 post-operation gastric cancer patients [Blood serum]	Accuracies of 97%, 89% and 87% were obtained for PCA-SVM, PCA-LDA and PCA-CART
Head and Neck cancer	Liang, 2020, China ^[81]	SERS	32 benign, 70 thyroid cancers [Blood plasma]	90% discrimination accuracy between benign and malignant thyroid tumour
Head and Neck cancer	Lin, China, 2019 ^[80]	SERS	30 normal, 30 nasopharyngeal carcinoma [Blood plasma]	Sens of 89% and 86%, spec 71% and 79%, for 633 and 785 nm respectively
Head and Neck cancer	Adeeba, 2018, Pakistan ^[82]	ATR-FTIR	20 healthy controls, 60 "niswar" (a dipping tobacco product) users, 67 oral cancer [Blood plasma]	90% classification rate
Head and Neck cancer	Xue, 2018, China ^[79]	SERS	135 Oral Squamous Cell Carcinoma (OSCC) samples of different stages and histologic grades [Blood serum]	All accuracies of detection and classification reached above 85%
Head and Neck cancer	Tan, 2017, China ^[78]	SERS	145 old maxillofacial fracture and healthy volunteers as normal control, 90 mucoepidermoid carcinoma as positive control, 135 OSCC [Blood serum]	OSCC discriminated from the normal with 81% sens and 84% spec
Head and Neck cancer	Brindha, 2017, India ^[83]	Raman	80 normal, 57 oral premalignant, 60 oral malignant patients [Urine]	96% accuracy for normal vs premalignant; 96% accuracy for normal vs malignant; 93% accuracy across normal, premalignant and malignant groups
Head and Neck cancer	Sahu, 2015, India ^[76]	Raman	126 healthy controls, 47 premalignant, 35 disease controls (non-oral cancer malignancy control) and 120 oral cancer [Blood serum]	64% sens and 80% spec for normal vs abnormal

(continued)

Table 2. Continued.

Disease	Author, Year, Country	Spectroscopic technique	Population [Sample type]	Main findings
Head and Neck cancer	Yan, 2015, China ^[77]	SERS	31 normal controls, 60 parotid gland tumours patients (20 pleomorphic adenoma, 21 Wartin's tumour and 19 mucoepidermoid carcinoma) [Blood serum]	84-88% classification accuracy, 82-97% sens and 74-87% spec
Leukaemia	Bai, 2020, China ^[97]	Raman	30 healthy volunteers, 33 diffuse large B-cell lymphoma patients, 39 chronic lymphocytic leukemia patients [Blood plasma]	For the chronic lymphocytic leukemia model, sens was 93% and spec was 100%, whereas for the diffuse large B-cell lymphoma model, sens was 80% and spec was 92%
Leukaemia	Féré, 2020, France ^[98]	Raman	61 healthy individuals and one group of 79 untreated CLL patients [Whole blood smears]	88% mean sens and 74% mean spec
Lung Cancer	Qian, 2018, China ^[102]	SERS	66 healthy controls, 61 cancer [Saliva]	95-97% sens and 100% spec were achieved using leave-one-out and random forest algorithms for controls vs cancer
Lung, Liver and Breast cancers	Xiao, 2016, China ^[103]	SERS	60 normal controls, 47 hepatocellular carcinoma, 55 lung cancer, 68 breast cancer [Blood serum]	OPLS-DA classification method differentiated all cancers from controls as well as between the different cancer types
Liver cancer and cirrhosis	Li, 2015, China ^[99]	SERS	44 healthy controls, 45 liver cancer, 42 post-treatment liver cancer and 45 liver cirrhosis [Blood serum]	Between 89% and 92% accuracy depending on model used
Liver and nasopharyngeal cancers	Yu, 2018, China ^[100]	SERS	95 healthy volunteers, 104 liver cancer patients, 100 nasopharyngeal cancer patient [Blood serum]	91% diagnostic accuracy on unknown testing set.

(continued)

Table 2. Continued.

Disease	Author, Year, Country	Spectroscopic technique	Population [Sample type]	Main findings
Oesophageal adenocarcinoma	Maitra, 2019, UK ^[109] (ATR-FTIR) Maitra, 2020, UK ^[110] (Raman)	ATR-FTIR Raman	(i) 35 control, 18 inflammatory, 27 Barrett's, 6 low-grade dysplasia (LGD), 12 high-grade dysplasia (HGD), 22 oesophageal adenocarcinoma (OAC) [Blood plasma] (ii) 36 control, 19 inflammatory, 28 Barrett's, 6 LGD, 12 HGD, 23 OAC [Blood Serum] (iii) 38 control, 19 inflammatory, 27 Barrett's, 6 LGD, 12 HGD, 22 OAC [Saliva] (iv) 38 control, 19 inflammatory, 27 Barrett's, 6 LGD, 11 HGD, 25 OAC [Urine]	ATR-FTIR: 100% sens and spec for controls vs disease in plasma/urine samples; 95-100% sens and 50-100% spec for controls vs disease in serum (for OAC: 100% sens and spec); 87-100% sens, 63-100% spec for controls vs disease in saliva (for OAC: 100% sens, 95% spec). Raman: For saliva/urine samples, 100% of correct predictions of all oesophageal stages. For plasma/serum samples, accuracy values >90% were achieved for all oesophageal stages
Oesophageal cancer	Feng, 2017 ^[111]	SERS	52 controls, 55 cancer [Urine]	The oesophageal cancer and control groups were separated with 100% sens and spec
Ovarian cancer	Perumal, 2019, Singapore ^[73]	SERS	57 benign, 54 cancer (29 Stage I, 3 Stage II, 15 Stage III, 7 Stage IV) [Ovarian cyst fluid]	SERS-based assay to quantify haptoglobin (Hp); normalized mean values of Hp were significantly higher in cancer cases (1.85 vs 0.6); 94% sens and 91% spec for benign vs cancer; sens was high for all stages (97% Stage I; 100% Stage II; 93% Stage III, 86% for Stage IV)
Ovarian cancer	Paraskevaidi, 2018, UK ^[74]	Raman and SERS	28 benign, 27 cancer (17 Stage I, 10 Stage II-IV cancer) [Blood plasma]	Raman: 94% sens and 96% spec for benign vs cancer; 93% sens and 97% spec for Stage I cancer vs benign SERS: 87% sens and 89% spec; 80% sens and 94% spec for Stage I cancer vs benign
Prostate cancer	Medipally, 2020, Ireland ^[122]	FTIR (ATR and transmission modes) and Raman spectroscopy	33 healthy, 43 cancer [Blood plasma]	Sens and spec ranging between 90-99% (PLSA-DA) for healthy vs cancer

(continued)

Table 2. Continued.

Disease	Author, Year, Country	Spectroscopic technique	Population [Sample type]	Main findings
Prostate cancer	Medipally, 2019, Ireland ^[123]	FTIR (transmission)	53 cancer patients (at five different time points: prior treatment, after hormone treatment, end of radiotherapy, two months post radiotherapy and eight months post radiotherapy) [Blood plasma]	Discrimination between patients at each treatment stage and follow-up time point, as well as between patients with acute and late toxicity and toxicity grade. High sens and spec (80-99%) were achieved
Cytology				
Bladder cancer	Gok, 2016, Turkey ^[32]	Transmission and ATR FTIR	34 control, 137 cancer [Cell pellets from bladder washes]	Successful discrimination of normal and cancer
Cervical precancer and cancer	Karunakaran, 2020, India ^[63]	SERS (label-free)	47 normal, 41 HSIL, 36 cervical squamous carcinomas [exfoliated cervical cells in LBC: single cells, cell pellet and extracted DNA]	Average diagnostic accuracy of 94% (in single cells), 74% (in cell pellets) and 92% (in extracted DNA) for the three groups
Cervical precancer	Traynor, 2019, Ireland ^[64]	Confocal Raman microscopy	64 normal, 69 CIN3 [LBC: single cells]	Samples stored at -80°C were not suitable (lack of cellular material and presence of cellular debris); fresh LBC samples and those stored at -25°C were suitable; 86% sens and 90% spec for normal vs CIN3 (fresh samples); 91% sens and 92% spec for normal vs CIN3 (-25°C samples)
Cervical precancer	Jusman, 2016, Malaysia ^[65]	FTIR	650 normal, 160 LSIL, 40 HSIL [LBC: single cells]	92% overall diagnostic accuracy in differentiating normal, LSIL and HSIL; proposed an automated screening FTIR system for cervical precancer detection
Cervical precancer	Ramos, 2016, Ireland ^[66]	Confocal Raman microscopy	88 normal (negative cytology), 35 LSIL (CIN1), 43 HSIL (21 CIN2/22 CIN3) [LBC: single cells]	Histological assessment (CIN) provided higher diagnostic accuracy when compared to cytological assessment (SIL); 91-100% sens and 97-100% spec for detecting normal, CIN1/2/3; 86-100% sens and 95-100% spec for detecting negative, LSIL, HSIL

(continued)

Table 2. Continued.

Disease	Author, Year, Country	Spectroscopic technique	Population [Sample type]	Main findings
Head and Neck cancer	Sahu, 2017, India ^[84]	Raman	20 healthy volunteers with tobacco habits, 27 oral premalignant conditions (n = 27) [Oral exfoliated cells]	Oral premalignant conditions identified with ~70% sens in the three-group model and 83% in a two-group model
Head and Neck cancer	Sarkar, 2018, India ^[85]	Fluorescence, atomic absorption and FTIR	20 non-smokers, 60 smokers, 20 clinically diagnosed oral leucoplakia and 19 OSCC patients [Oral exfoliated cells]	No diagnostic classification performed. Highlighted effect of smoking on cellular bioenergetic and hememetabolic pathways, which may be important for early cancer development.
Skin Cancer	Wald, 2015, Belgium ^[116]	FTIR imaging	51 cancer patients (26 primary and 25 metastatic tumours) [Melanoma cells]	No differences between primary and metastatic melanomas, but PLS-DA differentiated between Stage I-II and Stage III-IV primary tumours with 89% sens and 71% spec.
Tissue				
Bladder cancer and cystitis	Witzke, 2019, Germany ^[33]	FTIR imaging	19 low-grade cancer, 43 high-grade/invasive cancers and 41 severe cystitis [Fresh frozen tissue]	95% sens and spec when comparing cancerous and non-cancerous tissue
Brain tumour	Lilo, 2020, UK ^[41]	ATR-FTIR	99 tumour patients (grade I (n = 70), II meningiomas (n = 24) and recurrent grade I meningiomas (n = 5)) [FFPE tissue]	80% sens and 73% spec for grade I vs II meningiomas; 94% sens and 94% spec for grade I vs grade I recurrence; 97% sens and 100% spec for grade II vs grade I recurrence
Brain tumour	Morais, 2019, UK ^[42]	Raman imaging	90 tumour patients (66 Grade I and 24 Grade II meningiomas) [FFPE tissue]	86% sens and 100% spec (96% accuracy) for Grade I vs Grade II meningiomas
Brain cancer	Livermore 2019, UK ^[43]	Raman	62 gliomas (36 astrocytoma, IDH-wild-type; 21 astrocytoma, IDH-mutated; 5 oligodendroglioma) [Fresh tissue] 79 gliomas (19 astrocytoma, IDH-wild-type; 41 astrocytoma, IDH-mutated; 19 oligodendroglioma) [Snap-frozen tissue] 120 gliomas (41 astrocytoma, IDH-wild-type; 51 astrocytoma, IDH-mutated; 28 oligodendroglioma) [FFPE tissue]	79%–94% sens and 90%–100% spec for distinguishing between the 3 glioma genetic subtypes. IDH mutation gave 91% sens and 95% spec Seventy-nine cryosections, 120 FFPE samples, and glioma cell lines also successfully classified

(continued)

Table 2. Continued.

Disease	Author, Year, Country	Spectroscopic technique	Population [Sample type]	Main findings
Breast cancer	Talari, 2019, UK ^[46]	Raman spectroscopy	132 breast biopsies from four cancer subtypes: luminal A, luminal B, HER2 and triple negative [Tissue microarray biopsies]	Spec of 70%, 100%, 90% and 97% for distinguishing luminal A, luminal B, HER2 and triple negative subtypes
Breast cancer	Surmacki, 2015, Poland ^[48]	Raman imaging	82 samples from two sites of cancer patients (safety margin and tumour section) [Tissue cryosection]	86% sens and 72% spec for distinguishing margin vs tumour
Cervical precancer and cancer	Wang, 2021, China ^[67]	Confocal Raman microscopy	60 cervical inflammation (cervicitis), 30 CIN1, 30 CIN2, 30 CIN3, 30 cervical squamous cell carcinomas, 30 cervical adenocarcinomas [FFPE tissue]	86% overall diagnostic accuracy: precancerous lesions (CIN1-3) were correctly identified with diagnostic accuracy ranging from 80-89%; squamous cell carcinoma and adenocarcinoma were found with 100% and 86% accuracy respectively.
Cervical cancer	Zhang, 2021, China ^[68]	Raman	44 cervical adenocarcinomas, 49 cervical squamous cell carcinomas [FFPE tissue]	Different classifications models were evaluated reaching diagnostic accuracies between 85-96% in distinguishing cervical adenocarcinomas vs squamous cell carcinomas
Cervical cancer	Zheng, 2019, China ^[69]	Raman	45 cervical adenocarcinomas, 50 cervical squamous cell carcinomas [FFPE tissue]	93% diagnostic accuracy in distinguishing cervical adenocarcinomas vs squamous cell carcinomas
Cervical precancer and cancer	Daniel, 2018, India ^[70]	Confocal Raman microscopy	64 normal, 36 precancer and 145 cancer (19 well differentiated, 40 moderately differentiated and 86 poorly differentiated squamous cell carcinoma) [Snap frozen tissue]	95% overall accuracy in correctly classifying the 3 groups: normal (97% correct), precancerous (70% correct) and cancerous samples (99% correct) using PC-LDA; 94% overall accuracy for detecting well/moderately/poorly differentiated squamous cell carcinoma using PC-LDA

(continued)

Table 2. Continued.

Disease	Author, Year, Country	Spectroscopic technique	Population [Sample type]	Main findings
Cervical cancer	Daniel, 2016, India ^[71]	Polarized Raman and Raman	36 normal, 25 cancer [not specified tissue]	Polarized Raman: 96% sens and 97% spec (97% accuracy) for normal vs cancer; Raman: 92% sens and 72% spec (80% accuracy) for normal vs cancer
Colon cancer	Kuepper, 2016, Germany ^[52]	FTIR (transflection mode)	16 well differentiated, 90 moderately differentiated and 19 poorly differentiated colon cancer patients [FFPE, tissue microarray]	94% sens and 100% spec of colon cancer grading.
Colon cancer	Petersen, 2017, Germany ^[53]	Fibre-optic Raman	101 normal tissues, 22 adenocarcinoma, 141 tubular adenomas, 79 hyperplastic polyps [Ex vivo fresh tissue]	High-risk lesions vs low-risk lesions have 79% sens and 74% spec. Cancer vs normal tissue has a sens of 79%, and spec of 83%
Gastric cancer	Ghassemi, 2021, Iran ^[59]	ATR-FTIR	30 adenocarcinoma patients with adjacent normal tissue [FFPE tissue]	Discrimination of normal adjacent and cancerous tissue (82% diagnostic accuracy)
Gastric cancer	Lin, 2016, Singapore ^[60]	<i>In vivo</i> Raman	Total of 157 gastric patients with measurements taken from cancerous and healthy tissues. [<i>In vivo</i>]	Sens ranged from 75% to 89% and spec from 82% to 92% depending on model used
Head and Neck cancer	Bhattacharjee, 2021, India ^[92]	<i>In vivo</i> Raman	Tumour and contralateral regions of 94 OSCC patients [<i>In vivo</i>]	Prediction of disease recurrence with a prediction error of <0.25
Head and Neck cancer	Jeng, 2020, Taiwan ^[87]	Raman/ autofluorescence	35 control, 35 oral cancer, 35 cancer lesions [Oral biopsies]	Raman: Cancer vs normal: 83% accuracy, 80% sens, and 86% Combination: 97% accuracy, 100% sens 94% spec
Head and Neck cancer	Chundayil Madathil, 2019, India ^[89]	SERS Catheter	37 patient samples [Oral biopsies]	Malignant OSCC, verrucous carcinoma, premalignant leucoplakia, and disease-free conditions are detected and classified with an accuracy of 97% Correct classification of tumours into three grades with an accuracy of 98% in OSCC

(continued)

Table 2. Continued.

Disease	Author, Year, Country	Spectroscopic technique	Population [Sample type]	Main findings
Head and Neck/ Mixed cancers	Vohra, 2018, USA ^[88]	SERS	25 samples from human cervical lymph nodes, tonsils, oropharyngeal mucosa, sinus mucosa, and thyroid gland [RNA extracted from snap frozen tissue]	100% sens, 89% spec in distinguishing H&NSCC from other tissue types such as thyroid cancer and benign lymphoid tissue
Head and Neck cancer	Hoesli, 2017, USA ^[90]	SRS	Tissue from 50 patients, from which 42 tumor samples and 42 normal adjacent controls were chosen. [Fresh oral biopsies]	91% sens and 95% spec for neoplastic vs non-neoplastic images
Head and Neck cancer	Malik, 2017, India ^[91]	<i>In vivo</i> Raman	Tumour and contralateral normal mucosa in 99 patients with oral cancer [<i>In vivo</i>]	The sens of Raman spectroscopy in predicting recurrences was 80% and the spec was 29.7%
Head and Neck cancer	Sun, 2016, China ^[86]	Raman	35 non-cancerous, 39 nasopharyngeal cancer [Fresh biopsy tissue smears]	87% sens and 86% spec for differentiating nasopharyngeal cancer from non-cancerous smears
Kidney cancer	He, 2021, China ^[93]	Raman	77 Renal cell carcinoma patients [Tissue biopsy - 38 fresh and 39 from a frozen tissue bank]	Distinguish human renal tumour from normal tissues and fat with an accuracy of 93% Classification of renal tumour subtypes and grades with an accuracy of 87% and 90%, respectively
Kidney cancer	Sablinskas, 2020, Lithuania ^[96]	Fiber ATR IR	34 cancer patients [Fresh tissue]	27 of 34 kidney tumour samples were correctly classified as tumour tissues
Kidney cancer	Liu, 2017, China ^[94]	Raman	63 patients receiving radical or partial nephrectomy. Distal renal parenchymas were collected as a normal, control group [Fresh needle biopsy]	83% accuracy for normal vs tumour. 92% sens and 71% spec for malignant vs benign tumours. 87% accuracy for low-grade vs high-grade tumours. Clear cell renal carcinoma was differentiated from oncocytoma (100%) and angiomyolipoma (89%). Histological subtypes of cell carcinoma distinguished (94% accuracy)

(continued)

Table 2. Continued.

Disease	Author, Year, Country	Spectroscopic technique	Population [Sample type]	Main findings
Kidney cancer	Mert, 2015, Turkey ^[95]	SERS	40 Renal cell carcinoma and transitional cell carcinoma patients (28 T1 stage, 12 T2–T3 stages) [Homogenized tissue]	Discrimination of tissue regions of normal and different tumour stages up to 100%
Lung Cancer	Bangaol, 2020, Philippines ^[104]	ATR-FTIR	66 benign, 54 cancer [FFPE tissue]	98% sens, 92% spec, 95% accuracy, 91% positive predictive value and 98% negative predictive value for benign vs cancer
Lung Cancer	Weng, 2017, USA ^[105]	CARS imaging	83 normal, 156 adenocarcinoma, 111 squamous cell carcinoma, 38 small-cell carcinoma [Snap frozen tissue]	89% accuracy in classifying the four classes
Lung Cancer	McGregor, 2017, Canada ^[106]	<i>In vivo</i> endoscopic Raman spectroscopy	80 cancer patients (72 high grade dysplasia/malignant lesions tissue sites and 208 benign lesions/normal tissue sites) [<i>In vivo</i>]	High grade dysplasia and malignant lesions were detected with 90% sens and 65% spec
Lung Cancer	Akalin, 2015, USA ^[107]	FTIR imaging	80 normal, 61 benign, 308 cancer [FFPE tissue, microarray]	Clear distinction between the different adenocarcinoma subtypes. SVM classifier separated benign from malignant lesions with 99% accuracy
Lung Cancer	Großerueschkamp, 2015, Germany ^[108]	FTIR Imaging	92 patient samples of lung cancer [Snap frozen tissue]	Identification of NSCLC, ADC, SqCC, SCLC, hamartochondroma, carcinoids, thymoma, large cell neuroendocrine carcinoma and diffuse malignant mesothelioma with accuracy of 97% and subclasses of adenocarcinomas with 95% accuracy
Liver cancer	Zhang, 2018, China ^[101]	SERS	46 normal patients and 56 liver cancer patients [Tissue section – not specified]	100% sens and spec

(continued)

Table 2. Continued.

Disease	Author, Year, Country	Spectroscopic technique	Population [Sample type]	Main findings
Oesophageal cancer	Wu, 2020, China ^[112]	Synchrotron FTIR (transmission mode)	32 control, 39 cancer [Hair]	90% sens, 88% spec, 90% positive predictive value and 89% accuracy
Oesophageal cancer	Maitra, 2020, UK ^[113]	Raman	35 normal vs 18 inflammatory vs 27 Barrett's oesophagus vs 6 LGD vs 12 HGD vs 22 OAC [Tissue section - not specified]	90-100% sens, and 71-100% spec (91-100% accuracy) for correctly identifying each class
Oesophageal cancer	Ishigaki, 2016, Japan ^[114]	Raman	50 normal tissues, 73 cancer (42 invasive cancer stage I; 25 epithelial cancer stage 0; 6 suspicious lesions) [Fresh tissue]	81% sens, 94% spec for normal vs cancer stage I
Oesophageal cancer	Wang, 2015, Singapore ^[115]	<i>In vivo</i> Raman	48 oesophageal patients [<i>In vivo</i>]	93% sens and 94% spec for oesophageal squamous cell carcinoma identification
Ovarian cancer	Theophilou, 2016, UK ^[75]	ATR-FTIR	35 benign, 30 borderline, 109 cancer (46 high grade serous, 9 low grade serous, 15 endometrioid carcinoma, 4 mixed, 12 mucinous, 12 clear cell, 13 carcinosarcoma) [FFPE]	Optimal discrimination was observed between benign, borderline and cancer after GA-LDA analysis; no sens or spec reported. Classification of different ovarian carcinoma subtypes was performed with overall diagnostic accuracy ranging between 87-100% after two-group comparisons with GA-LDA
Skin cancer	Schleusener, 2015, Germany ^[117]	<i>In vivo</i> Raman	104 control (normal skin), 35 basal cell carcinoma (BCC), 22 squamous cell carcinoma (SCC) [<i>In vivo</i>]	Non-melanoma skin cancers were discriminated from normal skin (n = 104) with 63% sens and 83% spec (73% accuracy) for BCC only, whilst 74% sens and 82% spec (78% accuracy) were achieved for BCC/SCC (n = 57) vs controls

(continued)

Table 2. Continued.

Disease	Author, Year, Country	Spectroscopic technique	Population [Sample type]	Main findings
Skin cancer	Zhao, 2016, Canada ^[119] Zhao, 2015, Canada ^[118]	<i>In vivo</i> Raman	46 benign lesions, 74 precancerous lesions and cancers [<i>In vivo</i>]	Zhao, 2016: Wavenumber selection-based analysis to improve diagnostic spec. Increase of spec from 17-65% to 20-75% with sens fixed to 99-90%. Zhao, 2015: Differentiation performed using a retrospective analysis of a previous cohort of 518 lesions as training set, obtaining an AUC-ROC of ~0.90
Skin cancer	Santos, 2018, Netherlands ^[120]	High-wavenumber Raman	Common nevi and melanoma in situ for a total of 128 lesions [Fresh tissue]	PCA-LDA diagnostic model was built on 78 common nevi and melanoma in situ lesions and validated on an independent dataset of 50 common nevi and melanoma in situ lesions. With a fixed sens of 100%, spec amounted to 44%.
Skin cancer	Feng, 2018, USA ^[121]	<i>In vivo</i> Raman	44 healthy controls, 44 non-melanoma skin cancer (basal cell carcinoma (n = 14); squamous cell carcinoma (n = 20); actinic keratosis (n = 10)) [<i>In vivo</i>]	95% sens, 10% spec

Abbreviations: ADC: Adenocarcinoma; ATR: Attenuated total reflection; CART: Classification and regression tree; CIN: Cervical Intraepithelial neoplasia; DMM: Diffuse malignant mesothelioma; FFPE: Formalin fixed paraffin embedded; FTIR: Fourier transform infrared spectroscopy; HGD: High-grade dysplasia; HSIL: High-grade squamous intraepithelial lesion; IDH1: Isocitrate dehydrogenase 1; LBC: Liquid-based cytology; LGD: Low-grade dysplasia; LOOVC: Leave-one-out cross validation; LSIL: Low-grade squamous intraepithelial lesion; NSCLC: Non-small cell lung carcinomas; OAC: oesophageal adenocarcinoma; OPLS-DA: orthogonal partial least squares discriminant analysis; OSCC: Oral squamous cell carcinoma; PCA-LDA: Principal component-linear discrimination analysis; PLS-DA: Partial least squares discriminant analysis; SCLC: Small cell lung cancer; Sens: Specificity; SERS: Surface enhanced Raman spectroscopy; Spec: Specificity; SqCC: Squamous cell carcinoma; SVM: Support vector machine

in the staging, prognosis and treatment options of bladder cancer patients. SERS spectra were acquired from 30 healthy volunteers, 28 non-muscle invasive bladder cancers and 32 muscle invasive bladder cancers. Raman spectra were acquired with a 785 nm laser using silver nanoparticles with a 10 second integration time. Overall diagnostic accuracy using partial least squares-discriminant analysis (PLS-LDA) was found to be 93%, with a 98% accuracy in discriminating between normal and cancer and 93% between non-muscle invasive and muscle invasive bladder cancer.

Fourier transform Infrared spectroscopy (FTIR) has also been investigated for its utility in bladder cancer by Gok *et al.* using cytology^[32] and Witzke *et al.* on formalin-fixed paraffin embedded (FFPE) tissue sections^[33]. Gok *et al.*^[32] examined cytology samples

acquired from bladder washes using transmission FTIR from 37 bladder cancer patients and 34 normal controls. This was then confirmed using a separate cohort using attenuated total reflection-FTIR (ATR-FTIR) on 44 bladder cancer patients and 21 normal controls. The cancer group had a mix of carcinomas, papillomas and papillary urothelial neoplasm of low malignant potential. Spectra from both FTIR approaches were subjected to principal component analysis (PCA) and hierarchical clustering analysis (HCA) that led to specificities ranging from 53% to 81% and sensitivities ranging from 82% to 100% depending on the techniques, spectral range analyzed and whether the normal patients were compared to all bladder cancers or just the carcinoma sub-group. Witzke *et al.*^[33] also investigated the application of FTIR in the bladder and combining this approach with identifying regions of interest for laser capture microdissection and later liquid chromatography-mass spectrometry (LC-MS). One part of the study (sample set 2) focused on the application of FTIR imaging to fresh frozen bladder tissues to discriminate between low-grade bladder cancer (19), high grade bladder cancer (43) and severe cystitis (41). Spectra were classified using Random Forest which have 95% sensitivity and specificity when comparing between cancerous and non-cancerous tissue.

Brain tumor

The literature search included the keywords: meningioma, glioblastoma (GBM), astrocytoma and lymphoma. Of the 10 eligible studies, six used a biofluid-based ATR-FTIR/Raman approach, one study included biofluids and brain tissues using a synchrotron-based spectrometer while three studies used tissue samples and ATR-FTIR/Raman.

Hands *et al.*^[34] involved the investigation of blood serum using ATR-FTIR spectroscopy. 122 non-cancer samples were compared against 311 primary tumor samples (gliomas, meningiomas and metastatic). Following a stratified approach, the mean sensitivity and specificity for cancer versus non-cancer was 90% and 78%, which increased to 92% and 83% when using feature selection method via a fed-support vector machine (SVM) approach. In a follow up study by Smith *et al.*^[35], the patient cohort was the same as in the Hands *et al.* study. However, further feature selection coupled with generalized 2D correlation analysis to augment the machine learning algorithm was employed to improve the sensitivity and specificity results. Using a random forest model for the second derivate normalized spectra, outputs gave a sensitivity of 93% and a specificity of 92%. Cameron *et al.*^[36] published a study in 2019 which attempted to stratify brain tumor patients by using serum-based ATR-FTIR, aiming particularly to distinguish between glioblastoma and lymphoma patients. 765 samples were analyzed (healthy controls ($n = 237$), brain tumors ($n = 487$) and additional lymphoma samples ($n = 41$)). When assessing healthy versus brain cancer using PLS-DA, the sensitivity and specificity were $\sim 91\%$. Using the same technique to differentiate GBM ($n = 71$) from lymphoma, results accounted for up to 90% sensitivity and 86% specificity. Another study by Cameron *et al.*^[37] delves further into determining brain tumor types using the same method, in order to aid in secondary care. In this study, 87 healthy controls were collected alongside 554 tumor samples which included several subtypes (lymphoma and primary: glioma, meningioma and metastatic). Overall, this test achieved sensitivities

and specificities in the high 90% range in distinguishing between brain tumor samples (all subtypes) and healthy controls. When primary and metastatic cancers were compared, 91% sensitivity and 66% specificity were achieved. Butler *et al.*^[38] employed ATR-FTIR spectroscopy to investigate biofluids from the same dataset of 237 non-cancer and 478 cancer samples from Cameron *et al.*^[36] but without the additional lymphoma samples. This study aimed to develop a rapid, high-throughput technique capable of triaging brain cancer patients and yielded 93% sensitivity and sensitivity using an SVM-based classification approach.

The final study involving ATR-FTIR^[39], aimed to determine whether a patient with a glioma primary brain tumor possessed the isocitrate dehydrogenase 1 (IDH1) mutation, which indicates a better prognosis, or had IDH1 wild-type lesion. Both serum and tissue samples were investigated, with ATR-FTIR used on the dried serum samples, whilst the tissue samples were investigated using the MIRIAM beamline at the Diamond Light Source synchrotron facility (UK). Serum samples were collected from 36 patients for each IDH1 type and, when investigated using centrifugal filtration coupled with ATR-FTIR, gave a sensitivity and specificity of around 70% respectively. A number of tissue samples ($n=21$ for IDH1-mutated and $n=78$ for IDH1-wild-type) were lost during sample preparation, and therefore 79 glioma patients were analyzed. Using this method to separate mutated from wild-type IDH1, the authors reported a sensitivity of 82% and a specificity of 83%.

A serum-based Raman study was also completed by Mehta *et al.*^[40] to investigate meningiomas ($n=35$) versus controls ($n=35$). 25 healthy and 25 meningioma samples underwent PCA and principal component-linear discrimination analysis (PC-LDA), the latter model being subjected to Leave-One-Out Cross-Validation (LOOCV); when tested using an independent test set, the PC-LDA model gave a classification efficiency of 70%. For healthy controls ($n=25$) against grade I meningiomas ($n=15$), the classification efficiency when tested against an independent test set was 70% and 75% respectively. For healthy ($n=25$) against grade II meningiomas ($n=16$), the specificity was only 69%, given a number of the meningiomas incorrectly classified; only 10 healthy samples were used for the independent test set which gave a classification efficiency of 80%.

Several studies employed the use of FTIR and Raman spectroscopy on tissue samples to attempt to differentiate between cancer subtypes. Once such study conducted by Lilo *et al.*^[41] used ATR-FTIR to analyze FFPE brain tissue samples coupled with subtype classification via a PLS-LDA model. Utilizing these methods gave a sensitivity and specificity of 80% and 73% for grade I vs grade II meningiomas, 94% sensitivity and 94% specificity for grade I vs grade I recurring and finally 97% sensitivity and 100% specificity for grade II vs grade I recurring meningiomas.

Alternatively, Morais *et al.*^[42] used Raman microspectroscopy imaging to investigate brain tissue samples to determine the grading of the brain tumor. 90 samples were analyzed in total, 66 grade I and 24 grade II meningiomas. The models with the best classification performance were principal component analysis -quadratic discriminant analysis (PCA-QDA) and successive projections algorithm-quadratic discriminant analysis (SPA-QDA). Both models yielded a sensitivity of 86% with a specificity of 100%, with an area under the curve (AUC) of 0.929.

Finally, with regards to tissue sampling, Livermore *et al.*^[43] investigated the use of Raman spectroscopy in classification of gliomas. This study involved the use of fresh tissue ($n = 62$), FFPE tissues ($n = 120$), cryosections ($n = 79$) and LN18 cell lines. For identifying astrocytomas, IDH-wild-type, the PC-LDA model gave a sensitivity of 94% and a specificity of 90%. Astrocytomas with IDH-mutated gave a sensitivity of 91% and specificity of 95% and for Oligodendroglioma, the sensitivity was 79% with 100% specificity. Using the cryosections for astrocytomas with IDH-wild-type, the sensitivity was 78% and specificity 85%, for astrocytomas with IDH-mutant it was 79% and 89% and for oligodendrogliomas, 74% sensitivity and 90% specificity. Finally, for the FFPE sections, astrocytomas with IDH-wild-type the sensitivity was 81% with 84% specificity, for astrocytomas with IDH-mutant the sensitivity and specificity was 72% and 87%, with the oligodendrogliomas having a sensitivity of 79% and a specificity of 93%.

Breast cancer

After the literature search for breast cancer, 54 publications were identified, out of which five were eligible for the current review based on our inclusion and exclusion criteria.

Blood serum of 66 breast cancer patients was investigated by FTIR spectroscopy and compared to blood serum collected from 80 healthy controls^[44]. A combinatorial approach of PCA and principal component regression was applied yielding correct identification of cancer cases with sensitivity of 92% and specificity of 87%. These diagnostic values match closely to those of mammography and ultrasound emphasizing the potential of the technique for clinical diagnosis. Similar results were demonstrated by Lin *et al.*^[45], who obtained pre- and post-surgery breast cancer samples along with healthy controls after a serum-based analysis. The approach for surgical evaluation and screening, based on label-free SERS using silver nanoparticles coupled with PCA-LDA, achieved 95% and 100% diagnostic accuracies for pre-surgery versus post-surgery and pre-surgery versus normal groups, respectively. Talari *et al.* used Raman spectroscopy with PCA and LDA to identify cancer subgroups^[46]. To distinguish between luminal A, luminal B, HER2 and triple negative subtypes, 132 tissue microarray breast biopsies were examined. Biochemical alterations linked with lipids, collagen and nucleic acid were identified achieving a specificity of 70%, 100%, and 90% and 97%, for luminal A, luminal B, HER2, and triple negative subtypes respectively. In another study with similar objective, Elmi *et al.*^[47] utilized PCA-LDA to distinguish blood serum samples from 43 breast cancer patients and 43 healthy controls. Differences in FTIR spectra were observed for wavenumbers associated with sugar, collagen, esters and NH stretching region. The results showed that breast cancer could be distinguished from controls with 84% sensitivity, 74% specificity (83% accuracy) in the 3090-3700 cm^{-1} spectral region. The NH stretching vibration in this region was primarily found to be the classifying factor, indicating that the prominent differences in the spectra were due to protein modifications.

Tissue sections in various forms are also frequently analyzed in spectroscopy diagnostic studies. Raman spectral imaging analysis of 82 samples from two sites of cancer patients (safety margin and tumor section) was employed to identify, characterize and

discriminate structures in normal and cancerous tissues in a study by Sumacki *et al.*^[48]. The main differences between normal and cancerous tissues were found in regions characteristic of vibrations of carotenoids, fatty acids, proteins and interfacial water. PCA and PLS-DA diagnostic models were built to evaluate the diagnostic value of Raman. The sensitivity and specificity obtained from PLS-DA and cross validation were 86% and 72% respectively, reinforcing Raman imaging as a promising diagnostic tool.

Colon cancer

A literature search identified five papers that met the inclusion criteria for using vibrational spectroscopy to identify colon cancer.

Three papers were focused on measuring biofluids for colon cancer detection. Li *et al.*^[49] used Raman spectroscopy (514.5 nm, 100mW) of serum samples from 75 healthy volunteers, 65 pre-op colon cancers and 60 post-op colon cancers. Spectra were analyzed using PCA and k-nearest neighbors (KNN) and discrimination was identified to be principally due to the nucleic acids, amino acids and chromophores. KNN of the obtained principal components (PCs) demonstrated a diagnostic accuracy of 91%. A study by Moisoiu *et al.*^[50] applied SERS to discriminate between normal (n = 39), and cancers of the colon (n = 109), breast (n = 42), lung (n = 33), oral (n = 17) and ovaries (n = 13) using blood serum. The study used silver nanoparticle and a 532 nm laser at 10mW with a 40 second acquisition time. Derived spectra were analyzed using PCA-LDA and classification of normal from cancer was achieved with a sensitivity of 98% and specificity of 91%. Cancer types were correctly classified with an accuracy of 88% for oral cancer, 86% for colorectal cancer, 80% for ovarian cancer, 76% for breast cancer and 59% for lung cancer. A study by Toraman *et al.*^[51] investigated using FTIR on plasma samples from 30 colon cancer patients and 40 healthy patients. FTIR spectra had 16 spectral features derived which were then subjected to multilayer perceptron neural network and support vector machine (SVM). Numerous classification comparisons were shown with maximum accuracies for SVM of 94 (1300-1000 cm⁻¹ spectral range) and 96 for multilayer perceptron model (1300-1000 cm⁻¹) spectral range.

Two studies were identified which applied spectroscopy to tissue to diagnose colon cancer. Kuepper *et al.*^[52] used transflection mode FTIR imaging to scan tissue microarrays that consisted of 16 well differentiated, 90 moderately differentiated and 19 poorly differentiated colon cancer patients. Spectra were classified using two consecutive random forest classifiers, the first to identify cancerous regions and the second to identify the grade of differentiation. This approach allowed for tumor tissue identification to be made with a 94% sensitivity and 100% specificity. Overall, the classifiers accurately predicted 85% of the cancer grading. Petersen *et al.*^[53] used fiber optic Raman spectroscopy (785 nm, 300mW, 2 second integration) of colon biopsy samples to extract spectra from adenocarcinoma (n = 22), tubular adenomas (n = 141), hyperplastic polyps (n = 79) and normal tissue (n = 101). Classification results demonstrated high-risk lesions could be differentiated from low-risk lesions with a sensitivity of 79% and specificity of 74%, whereas cancer and normal tissue could be discriminated with a sensitivity of 79% and specificity of 83%. This work may allow for future *in-vivo* measurements to be taken.

Gastric cancer

A literature search identified seven papers that investigated the application of spectroscopic techniques to gastric cancer that met the selection criteria, with five using biofluids and two using tissues.

Three studies used Raman to examine biofluids for the detection of gastric cancer. Bahreni *et al.*^[54] examined whether Raman spectra acquired (532 nm laser, 70mW, 1 second acquisition time) from serum could correlate with traditional enzymatic tests often used for gastric cancer, with correlation above 94% between the Raman spectra and the enzymatic tests. Furthermore, it was shown that 87.5% of samples were correctly classified as being from healthy patients (n=40) or gastric cancer subjects (n=20) using PLS regression. A study by Li *et al.*^[55] also examined serum from gastric cancer patients however used SERS (632.8 nm laser, 3.5mW, 10 s exposure time, silver nanoparticles) to discriminate between atrophic gastritis (n=45), pre-op (n=43) and post-op (n=40) gastric cancers and healthy individuals (n=42). Obtained SERS spectra were subjected to PCA and then with either SVM, LDA or classification and regression tree (CART), with accuracies demonstrated of 97%, 89% and 87% respectively. Another study that was performed using SERS to detect gastric cancer was conducted by Chen *et al.*^[56] using saliva samples. This study used SERS sensors based on graphene oxide nanoscrolls wrapped in gold nanoparticles (785 nm laser at 35mW with a 10 second acquisition time). It was demonstrated that discrimination between early and advanced gastric cancers (n=104) could be achieved with a specificity over 88% and sensitivity over 80%.

Two studies investigated the use of FTIR on biofluids for gastric cancer diagnosis. A study by Guleken *et al.*^[57] applied FTIR to serum derived from 43 control patients, 45 gastric cancer patients and 45 colon cancer patients. Significant spectral differences were observed in the Amide III and Amide I spectral regions between the cancers and normal patients. PCA analysis demonstrated clustering of the cancers together and separated from the normal cluster. Liu *et al.*^[58] also used FTIR to diagnose gastric cancer however focused on measurements from red blood cells. The study compared the red blood cells spectra from 30 normal patients to 40 gastric cancer patients identified spectral changes associated with protein secondary structures, structure and content of sugars and relative amounts of proteins and sugars. The spectra were subjected to canonical discriminant analysis which gave a 95% sensitivity and 70% specificity.

Two studies were identified that have applied spectroscopy to tissue sections to diagnose gastric cancer, one using ATR-FTIR and one using fiber optic Raman spectroscopy. Ghassemi *et al.*^[59] demonstrated that ATR-FTIR applied to tissue samples could discriminate between normal adjacent and cancerous tissue from the FFPE tissue sections from 30 patients. Data modeling techniques such as PCA, SVM and KNN allowed for classifications with a final classification accuracy of 82% reported. Lin *et al.*^[60] demonstrated the simultaneous use of fingerprint and high-wavenumber Raman spectroscopy with a beveled fiber-optic probe for *in-vivo* measurements during gastroscopy of the pre-cancerous lesion, gastric intestinal metaplasia. In the study they obtained measurements from 157 gastric patients in which they recorded a total of 4,178 spectra from normal tissue and 432 spectra from gastric intestinal metaplasia. PCA and LDA

algorithms were used for classification which resulted in an AUC of 0.92 for disease classification.

Gynaecological cancers

After a literature search for gynaecological cancers since 2015, 214, 53 and 83 studies were identified for cervical, endometrial, and ovarian cancers, respectively, out of which 11, one and three were deemed relevant to the current review based on our inclusion criteria.

Cervical cancer

Women with low- and high-grade cervical precancer as well as invasive carcinoma were investigated. The majority of the studies performed spectroscopic analysis on tissues derived after a biopsy (5/11 studies) and cells that were stored in a preservative medium, namely a liquid-based cytology (LBC) sample (4/11 studies), whereas only 2/11 studies used blood serum samples.

Shrivastava *et al.*^[61] used confocal Raman microscopy in blood serum from controls and cancer patients for diagnostic purposes, achieving 93% sensitivity and 86% specificity. Serial samples were collected from all patients at three different time points (before, during and 6 months post-treatment) to also monitor the effect of treatment. Chemoradiation-related changes were identified in the serial samples with proteins and nucleic acids showing a decrease while phospholipids were elevated. The authors concluded that the observed variations could either be due to treatment or caused by persistence of disease at 6-months, which would therefore necessitate a longer follow-up. Raman profiles from patients after treatment were trending toward the healthy controls, although protein alterations persisted even post-treatment. Such an approach holds promise in disease detection and potentially in treatment monitoring; further studies in longitudinal samples during the course of treatment are required.

In a study using a SERS-based immunoassay of blood serum, two cancer-associated blood biomarkers (squamous cell carcinoma antigen and osteopontin) were simultaneously detected with low detection limits and good selectivity and reproducibility^[62]. Healthy subjects as well as histologically confirmed precancer (cervical intraepithelial neoplasia (CIN) 1, 2 and 3) and cancer samples were analyzed with the SERS-based platform and enzyme-linked immunosorbent assay (ELISA) experiments, showing consistent results.

Karunakaran *et al.*^[63] used three different sample preparation approaches (single cells, cell pellets and extracted DNA) to analyze the cytological material from LBC samples. Using a label-free SERS approach, the average diagnostic accuracy for differentiating between normal, high-grade precancer (high-grade-intraepithelial lesions (HSIL)) and cancer samples was higher for single cells and extracted DNA (92-94%), whereas a lower diagnostic accuracy of 74% was achieved in cell pellets.

Three different spectroscopic studies using single cells from LBC samples investigated cervical precancer of low and high grades^[64-66]. One study highlighted that cytological samples were suitable for analysis of fresh samples or after storage at -25°C , but not -80°C ^[64]. After comparison of controls with high-grade precancer across all three

studies, the sensitivity and specificity were found to be between 86-100% and 90-100% respectively; sensitivity and specificity for detecting low-grade lesions were 94% and 95-98% respectively. The authors proposed an automated screening system for cervical cancer^[65] and also highlighted that histological assessment provided higher diagnostic accuracy in comparison to cytological assessment^[66].

Using tissue samples and Raman spectroscopy, five different studies demonstrated high diagnostic accuracies in detecting cervical precancer and cancer^[67-71]. Wang *et al.*^[67] classified and identified six different tissue types (inflammation, CIN1, CIN2, CIN3, squamous cell carcinomas and adenocarcinomas) with 86% overall diagnostic accuracy. Precancerous lesions (CIN1-3) were identified with 80-89% accuracy while squamous cell carcinomas and adenocarcinomas were found with 100% and 86% accuracy. Two studies did not include a control group but rather assessed the ability of the approach to differentiate between different cancer subtypes (adenocarcinomas and squamous cell carcinomas)^[68,69]. Using different classification algorithms, they achieved diagnostic accuracies ranging between 85-96% in distinguishing the two subtypes of cancer. Using snap frozen tissue sections, Daniel *et al.*^[71] correctly detected normal, precancer and cancer subjects with 70-99% accuracy while also achieving 94% accuracy in detecting well/moderately/poorly differentiated squamous cell carcinomas. Polarized Raman and Raman were both found to accurately discriminate control and cancer subjects, with polarized Raman achieving higher diagnostic values (96% sensitivity, 97% specificity, 97% accuracy versus 92% sensitivity, 72% specificity, 80% accuracy)^[71].

Endometrial cancer

One blood-based ATR-FTIR study in endometrial cancer was eligible for inclusion^[72]. Using blood plasma samples from healthy controls as well as women with atypical hyperplasia and endometrial cancer of different subtypes, controls were differentiated from all cancers (mixed) with 87% sensitivity and 78% specificity. Endometrioid adenocarcinomas (Type I), the most common subtype of endometrial cancer, were detected with 91% sensitivity and 81% specificity. Precursor lesions of atypical hyperplasia were also identified with high diagnostic accuracy (100% sensitivity and 88% specificity), which may allow fertility sparing management and cancer prevention.

Ovarian cancer

Of the eligible studies for inclusion ($n = 3$), two performed analysis of biological fluids (ovarian cyst fluid^[73] and blood plasma^[74] and one used ovarian tissue samples^[75].

A SERS-based method was used to detect and quantify haptoglobin (Hp) in ovarian cyst fluid as a diagnostic biomarker for epithelial ovarian cancers^[73]. A significantly higher concentration of Hp was identified in malignant in comparison to benign cysts (normalized mean values of 1.85 vs 0.6). Verified against histology, SERS achieved 94% sensitivity and 91% specificity for benign versus malignant samples, while sensitivity was also high (86-100%) for all the different cancer stages (stage I-IV). For comparison, a cancer antigen 125 (CA-125) test was performed on the same patients achieving lower sensitivity and specificity of 85% and 90%, respectively.

Using both Raman and SERS, Paraskevaïdi *et al.* analyzed blood plasma samples from benign and ovarian cancer cases^[74]. Both techniques provided satisfactory diagnostic accuracy for the detection of ovarian cancer (stage I-IV) (Raman: 94% sensitivity and 96% specificity; SERS: 87% sensitivity and 89% specificity), as well as for early ovarian cancers (stage I) (Raman: 93% sensitivity and 97% specificity; SERS: 80% sensitivity and 94% specificity). SERS achieved slightly lower diagnostic values, which may be due to poor reproducibility of spectral profiles and intensities. Nevertheless, these findings suggest improved diagnostic accuracy compared to clinically-used molecular biomarkers for ovarian cancer.

Theophilou *et al.*^[75] employed ATR-FTIR spectroscopy to analyze dewaxed FFPE tissues from benign, borderline and cancer patients. Different algorithms were employed (PCA-LDA, successive projections algorithm-LDA (SPA-LDA) and GA-LDA), with GA-LDA providing optimal discrimination between the three classes. Classification of different ovarian carcinoma subtypes (high- and low-grade serous, endometrioid, mixed, mucinous, clear cell and carcinosarcomas) was also performed and achieved overall diagnostic accuracies ranging between 87-100% after two-group comparisons using GA-LDA.

Head and neck cancers

The literature search for Head and Neck cancers included cancer of the pharynx, oropharynx, hypopharynx, larynx, mouth and tongue, and encompassed dysplasia, neoplasia and carcinoma. A total of 278 results were retrieved, 17 of which were deemed to be relevant to the current review (8/17 on biofluids, 2/17 cytology, 5/17 excised tissue, 2/17 *in vivo*).

Multiple studies have explored the applications of Raman, SERS and IR spectroscopic analysis of human blood plasma and serum for diagnostic applications in human head and neck cancers. Sahu *et al.*^[76] explored the use of using a fiber-optic Raman microprobe (785 nm) of serum samples of 328 subjects belonging to healthy controls, premalignant, disease controls (non-oral cancer), and oral cancer groups. Samples were measured in liquid drop form and PCA-LDA was employed for discriminant analysis, achieving 77% classification efficiency between normal and oral premalignant groups, 89% for normal and disease control groups, and 87% for normal and oral cancer groups. In a four way model, the normal versus abnormal could be differentiated with 64% sensitivity and ~80% specificity. The study also explored the feasibility of differentiating two different types of cancers (oral and glioma), showing ~89% efficiency.

A number of studies have sought to enhance the sensitivity of Raman based techniques using SERS, which may be particularly suited to the analysis of relatively dilute biofluids. In the study of Yan *et al.*^[77], the serum of 60 patients with parotid gland tumors was analyzed and compared with that of 31 normal patients. The patients were further stratified into a pleomorphic adenoma group, Wartin's tumor group and mucoepidermoid carcinoma group. Measurements at 633 nm were made of drops of serum mixed with gold nanoparticles. Using SVM-based analysis, spectra were classified with ~86% accuracy, ~90% sensitivity and ~80% specificity. Tan *et al.*^[78] similarly explored SERS (633 nm) for the analysis of blood serum in liquid form, but for the diagnosis of oral squamous cell

carcinoma (OSCC). The study included 135 patients with OSCC, 90 patients with mucoepidermoid carcinoma, selected as the positive control group, while 145 patients with old maxillofacial fracture and healthy volunteers were used as the normal control group. PCA-LDA demonstrated that OSCC could be successfully discriminated from the normal control groups with a sensitivity of 81% and a specificity of 84%. Using similar methodology, Xue *et al.*^[79] analyzed the serum of 135 OSCC patients, grouped according to tumor size, positive lymph nodes, metastases, and histological grade. Accuracies of detection and classification of >85% were achieved for all categories. Lin *et al.*^[80] used a silver nanoparticle serum mixture to measure the SERS response to differentiate 30 nasopharyngeal carcinoma patients and 30 healthy volunteers. Diagnostic sensitivities of 89% and 86%, and corresponding specificities of 71% and 79%, were achieved, using either 785 or 633 nm, respectively. Liang *et al.*^[81] employed SERS for differentiation of benign ($n = 30$) and malignant ($n = 70$) thyroid tumors from blood plasma which had been subjected to ultrafiltration, resulting in 90% discrimination accuracy.

Using ATR-FTIR spectroscopy, Adeeba *et al.*^[82] analyzed dried plasma samples of 67 oral cancer patients, 60 "niswar" (a dipping tobacco product) users (considered to be normal, but high risk), and 20 healthy controls. Discriminant analysis resulted in a 90% classification rate.

In an alternative approach, Brindha *et al.*^[83] explored the application of Raman (785 nm) spectroscopy in the high wavenumber region for the analysis of human urine samples, and the detection of oral cancer. Samples from 80 normal subjects, 57 oral premalignant and 60 oral malignant patients were examined, yielding 96% accuracy for classification of normal versus premalignant; 96% accuracy for normal versus malignant; and 93% accuracy across normal, premalignant and malignant groups.

Spectroscopic analysis of oral exfoliated cells has also been employed for oral cancer diagnostics. Sahu *et al.*^[84] harvested samples from 20 healthy volunteers, 20 healthy volunteers with tobacco habits, and 27 with oral premalignant (OPL) conditions. Using Raman spectroscopic analysis (785 nm) of cell pellets, OPL patients could be identified with ~70% sensitivity in the three-group model, or ~83% in two-group model, indicating that tobacco consumption may be a confounding factor. Sarkar *et al.*^[85] employed a combination of fluorescence, atomic absorption and FTIR to explore the relative expression level of relevant biomolecules in exfoliated cell samples of clinically diagnosed and histopathologically confirmed oral leucoplakia ($n = 20$) and OSCC ($n = 19$) patients, compared to those from 20 nonsmokers, 60 smokers. Although no diagnostic classification was undertaken, the study indicated the effect of smoking on cellular bioenergetic and hememetabolic pathways, which may be important for early cancer development.

Clinically relevant studies of tissue samples have been carried out using Raman, SERS and Infrared spectroscopies. Sun *et al.*^[86] examined smears from cancerous ($n = 39$) and non-cancerous nasopharyngeal tissues ($n = 35$) using confocal Raman spectroscopy (785 nm), establishing a diagnostic sensitivity of 87% and specificity of 86% for differentiation of the two tissue types. Jeng *et al.*^[87] used a combination of visually enhanced lesion imaging and Raman microspectroscopy to examine cryopreserved tissue samples from 35 oral cancer patients who had undergone surgery. Thirty-five cancer lesions and thirty-five control samples with normal oral mucosa were analyzed. PCA-LDA of Raman spectra

resulted in diagnostic accuracy of 83%, sensitivity 80%, and specificity 86%. Regions of interest of the autofluorescence images were differentiated with 90% accuracy, 100% sensitivity, and 80% specificity. The combination of the two techniques differentiated cancer and normal groups with 97% accuracy, 100% sensitivity, and 94 % specificity. Vohra *et al.*^[88] used a functionalized “nanorattle” SERS (785 nm) based technique to target cyto-keratin nucleic acid biomarkers specific to head and neck squamous cell carcinoma (HNSCC). Patients were chosen from adults with HNSCC, thyroid papillary carcinoma, lymphoma, or benign lymphoid or tonsillar disease, and 25 samples were obtained from human cervical lymph nodes, tonsils, oropharyngeal mucosa, sinus mucosa, and thyroid gland tissue. Tissues were flash frozen, before RNA extraction and functionalized SERS measurement, resulting in a diagnostic sensitivity of 100% and specificity of 89% in distinguishing HNSCC from other tissue types. Chundayil Madathil *et al.*^[89] designed a novel SERS catheter device and demonstrated its potential using samples from 37 patients with abnormal oral lesions. Regions of oral tissues identified as disease-free, malignant oral squamous cell carcinoma (OSCC), verrucous carcinoma and premalignant leucoplakia were detected and classified with an accuracy of 97%. Correct classification of OSCC tumors into three grades was achieved with an accuracy of 98%. Stimulated Raman Scattering was explored by Hoesli *et al.*^[90] to differentiate normal and cancerous tissue from head and neck cancer patients. 42 tumor samples and 42 normal adjacent controls were derived from 50 patients, and diagnostic sensitivities and specificities of 91 and 95% were achieved, respectively, for neoplastic vs non-neoplastic images.

In vivo Raman studies were carried out by both Malik *et al.*^[91] and Bhattacharjee *et al.*^[92] In the first study, Raman spectroscopy was performed on tumor and contralateral normal mucosa in 99 oral cancer patients. Patients were then followed up to track the reappearance of cancerous lesions. Recurrences of lesions were predicted with a sensitivity of 80% and specificity 30%. The latter study aimed to explore the potential of Raman spectroscopy for prediction of disease-free survival of oral cancer patients. Raman spectra were obtained from the tumor and contralateral regions of 94 OSCC patients. Based on identified spectral markers, a model for disease free survival rates (>1000 days) were established, with a prediction error of <0.25.

Kidney cancer

The literature search for Kidney cancer included kidney and renal cancer, including dysplasia, neoplasia, carcinoma, Grawitz tumor, hypernephroma and nephrocarcinoma. A total of 138 results were retrieved, four of which were deemed to be relevant to the current review.

Renal cell carcinoma in tissue samples has been studied using both Raman^[93,94] and SERS^[95]. He *et al.*^[93] established a (785 nm) Raman spectroscopy-based SVM model to classify (n=77 samples) human renal tumor from normal and fat regions of tissue with an accuracy of 93%. Liu *et al.*^[94] collected needle biopsy kidney tissue samples from 63 patients who had received radical or partial nephrectomy. Raman spectroscopy (532 nm), coupled with discriminant analysis, could distinguish tumor and normal tissues with an accuracy of 83%, and malignant versus benign tumors with sensitivity and specificity of 92% and 71%. Low-grade and high-grade tumors were classified with an accuracy of 87%. In addition, clear cell renal carcinoma was differentiated from oncocytoma and

angiomyolipoma with accuracies of 100% and 89%, respectively. Histological subtypes of cell carcinoma were distinguished with an accuracy of 94%. Mert *et al.*^[95] employed SERS (830 nm) to examine normal and abnormal homogenized tissue samples collected from 40 patients at different cancer stages. In a range of different diagnostic comparisons, the study demonstrated sensitivity, specificity, and total accuracy as high as 100%

Sablinskas *et al.*^[96] employed the less explored technique of Fiber ATR-IR to examine fresh kidney tissue, resected from patients undergoing surgery. Spectra of tissue were measured inside the operation theater, immediately after resection, using an ATR silver halide fiber probe. A classification accuracy of 79% of kidney tumor was achieved.

Leukemia

The literature search for Leukemia produced a total of 98 results, of which only two blood-based studies were deemed relevant to the current review.

In the study of Bai *et al.*^[97], Raman spectroscopy was employed to study the features of blood plasma of 33 patients with diffuse large B-cell lymphoma (DLBCL) and 39 with chronic lymphocytic leukemia (CLL), compared to 30 healthy volunteers. Measurements were made in droplet form using a 785 nm laser source. Classification models were constructed using orthogonal partial least squares discriminant analysis, resulting in 93% sensitivity and 100% specificity of 100% for the CLL model, whereas for the DLBCL model resulted in 80% sensitivity and 92% specificity.

Féré *et al.*^[98] explored a number of different classification strategies, applied to the (532 nm) Raman spectra of blood smears spread on glass slides, for the diagnosis of chronic lymphocytic leukemia. The study included one group of 61 healthy patients and one group of 79 untreated CLL patients, and explored different scenarios, dependent on the clinical objective, i.e., balanced sensitivity and specificity, maximum sensitivity, or maximum specificity. Classification accuracies of up to ~88% were achieved.

Liver cancer

After a literature search for spectroscopic techniques to diagnose liver disease, three papers were deemed eligible based on the search criteria.

Two papers, Li *et al.*^[99] and Yu *et al.*^[100] investigated the application of SERS using silver nanoparticles to serum samples from patients with liver diseases. Li *et al.*^[99] used SERS to discriminate between 44 healthy patients, 45 liver cancer patients, 42 post-treatment liver cancer patients and 45 liver cirrhosis patients. Spectra were acquired using a 632 nm laser at 3.5 mw with a 10 second acquisition time. The SERS spectra were subjected to SVM, PLS and artificial neural networks, which resulted in accuracies of 92%, 89% and 90% respectively. Yu *et al.*^[100] also used SERS on blood serum however applied this approach to a different cohort with 104 healthy volunteers, 104 liver cancer patients and 100 nasopharyngeal patients. SERS spectra were acquired using laser at 785 nm at 0.1mW with a 10 second acquisition time and subjected to either PLS or PCA for dimensionality reduction which were then used in SVM with a Gaussian radio basis function. Diagnostic accuracies of 95% were achieved for the training set and 91% for the validation set.

Zhang *et al.*^[101] also investigated the application of SERS with silver nanoparticles to liver disease however took measurements from liver tissues slices from 56 patients, with

46 normal adjacent tissue and 56 from cancer tissue. SERS spectra were acquired using a 532 nm laser with a four second acquisition time. The SERS spectra were subjected to PCA-LDA which resulted in sensitivities and specificities of 100% between cancerous and normal adjacent tissue. They found that 838, 1448, and 1585 cm^{-1} peaks were significantly altered in the cancerous tissue regions.

Lung cancer

Out of the 55 results obtained from the literature search in lung cancer, seven were deemed eligible for this review (2/7 using biofluids; 5/7 using tissue samples).

In a study by Qian *et al.*^[102], saliva samples of 61 lung cancer patients and 66 healthy controls were examined using a portable SERS system with a nano-modified chip. A SVM diagnostic model was built using random forest algorithms with LOOCV, achieving 95-97% sensitivity and 100% specificity.

Xiao *et al.*^[103] attempted to detect and compare serum metabolic profiles in three cancer types, lung, breast and liver *via* SERS along with healthy controls. Vibrational frequencies associated with metabolites like tryptophan, phenylalanine, proline, valine, adenine and thymine were used as discriminative factors. Diagnostic accuracy was assessed using an orthogonal PLS-DA (OPLS-DA) multivariate algorithm. All cancers were clearly distinguished from healthy controls as well as between the different cancer types, highlighting the potential of SERS as a label-free, noninvasive approach for metabolites profiling and diagnosis of cancer.

Five different studies investigated lung cancer using tissues (*ex vivo* or *in vivo*). Bangaol *et al.*^[104] used FTIR to analyze benign ($n = 66$) and malignant (deparaffinized) FFPE tissues ($n = 54$). PCA and hierarchical cluster analysis distinctly clustered benign from malignant tissues with 98% sensitivity and 93% specificity (95% accuracy), which is in agreement with histopathological assessment. Weng *et al.*^[105] demonstrated the feasibility of applying a deep learning algorithm to automatically differentiate normal and three types of lung cancerous tissues (adenocarcinoma, squamous cell carcinoma and small-cell carcinoma) using coherent anti-Stokes Raman scattering (CARS) imaging. Images were acquired after thawing of tissues that had been snap-frozen and analyzed in real-time. The computational model achieved 89% accuracy in classifying the four classes which could provide instant information and accelerate clinical decision-making. McGregor *et al.*^[106] presented the use of a real-time endoscopy Raman system to improve the diagnostic specificity of localizing lung cancer in central airways. Results were based on data obtained from 280 tissue sites (72 malignant lesions, 208 normal) in 80 patients, subjected to multivariate analyses and waveband selection methods. The model demonstrated that malignant lesions can be detected with 90% sensitivity but lower specificity of 65%. Akalin *et al.*^[107] demonstrated the potential of spectral histopathology by acquiring data from normal and lung cancer cases (commercial tissue microarrays) and benign lesions (standard excised tissues). The hyperspectral data set acquired from tissue imaging was analyzed by multivariate analysis, revealing changes in the biochemical composition between tissue types, and between various stages and states of disease. LOOCV-based SVM classifier could separate benign from malignant lesions with 99% accuracy while clear distinction was seen between the different

adenocarcinoma subtypes. Großerueschkamp *et al.*^[108] performed automated marker-free identification of lung tumor classes and subtypes of adenocarcinoma by FTIR imaging and a novel trained random forest classifier. The tissue imaging analysis led to identification of non-small cell lung carcinomas, adenocarcinomas, squamous cell carcinoma, small cell lung cancer, hamartochondroma, carcinoids, thymoma, large cell neuroendocrine carcinoma and diffuse malignant mesothelioma with accuracy of 97% and subclasses of adenocarcinoma tumors with an accuracy of 95%.

Esophageal cancer

A total of 32 results were recovered after a literature search for esophageal cancer, seven of which were considered relevant for the current review (3/7 using biofluids; 4/7 using tissue samples).

Using a number of different biofluids (plasma, serum, saliva and urine), Maitra *et al.*^[109] evaluated the ability of ATR-FTIR to discriminate stages of esophageal transformation into adenocarcinoma. Different chemometric models were applied (PCA-quadratic discriminant analysis (PCA-QDA), SPA-QDA, GA-QDA) to discriminate controls from individuals with disease, with PCA/GA-QDA achieving optimal results (100% sensitivity and specificity) when using blood plasma or urine samples. The same group also analyzed samples from the same cohort of patients using Raman spectroscopy^[110], achieving similar results with GA-LDA providing 100% accuracy for all classes when using saliva or urine samples and >90% accuracy when using blood samples. Feng *et al.*^[111] used SERS to obtain the complete biochemical profile of modified nucleosides in urine samples from 52 controls and 55 esophageal cancer patients. The ability of SERS to discriminate cancer from healthy participants was tested using PLS-LDA, which allowed complete separation of the two classes with 100% accuracy.

In a study by Wu *et al.*^[112], synchrotron infrared microspectroscopy was employed to differentiate between healthy controls (n=32) and esophageal cancer patients (n=39) using hair samples. Spectral data was analyzed using PCA as an exploratory technique and discriminant analysis as a classification technique. Clear differentiation was observed between the two groups, with a sensitivity of 90% and specificity 88%. A different study by Maitra *et al.*^[113] used Raman microspectroscopy to discriminate stages of esophageal transformation to adenocarcinoma in human tissues. Normal, inflammatory, Barrett's esophagus, low-grade and high-grade dysplasia as well as esophageal adenocarcinoma samples were analyzed and three chemometric techniques were tested for classification (PCA-QDA, SPA-QDA and GA-QDA). Sensitivity and specificity ranged between 90-100% and 71-100% respectively (91-100% accuracy) for identifying each class. Overall GA-LDA provided optimal results. Ishigaki *et al.*^[114] used Raman spectroscopy to detect early-stage esophageal cancer (stage I) using 50 normal and 42 fresh tissues. Through partial least squares regression analysis (PLS-R) and self-organization maps (SOMs), it was possible to discriminate between normal and cancerous samples, although a relatively large overlap was observed. Using LDA on six Raman bands that were statistically different provided an 81% sensitivity and 94% specificity after comparison of normal versus stage I cancerous tissues.

Wang *et al.*^[115] evaluated the potential of *in vivo* Raman spectroscopy as a real-time diagnostic tool for esophageal squamous cell carcinoma (ESCC). Spectra were acquired from 48 esophageal cancer patients using a Raman fiber optic endoscopic tool that was developed for rapid analysis. Using PLS-DA, the sensitivity and specificity for detecting ESCC were 93% and 94% respectively.

Skin cancer

The literature search for Skin cancers included malignant, pre- and neoplastic lesions, involving melanoma and non-melanoma skin cancers (NMSC), such as basal cell skin cancer (BCC), squamous cell carcinoma (SCC) and actinic keratosis (AK) of the skin. Out of 404 studies identified since 2015, six were deemed relevant for this review based on our inclusion criteria. The majority of the studies (5/6) was performed on tissue samples using Raman spectroscopy; only one study included the use of infrared imaging on histological samples.

In 2015, Wald and Goormaghtigh^[116] employed FTIR imaging and PLS-DA to analyze histological sections and identify the main cell types found in melanoma tumors, achieving an accuracy of over 90%. The same study compared melanoma cells in patients with primary (n = 26) and metastatic tumors (n = 25), although no class differences were identified. Discrimination of different stages (stage I/II versus stage III/IV) of primary tumors was assessed, achieving 89% sensitivity and 71% specificity.

Two *in vivo* studies were carried out using Raman spectroscopy to discriminate between cancerous and normal skin. Schleusener *et al.*^[117] collected Raman spectra from subjects with lesions of BCC (n = 35) and SCC (n = 22). BCC samples were successfully discriminated from normal skin (n = 104) with 63% sensitivity and 83% specificity (73% accuracy). All NMSC combined (BCC/SCC, n = 57) versus normal skin (n = 104) resulted in sensitivity and specificity of the PLS-DA model up to 74% and 82% respectively (78% accuracy). Zhao *et al.*^[118] examined skin cancer and precancerous lesions from 74 patients, which were compared to benign lesions from 46 participants. Performing a retrospective analysis using a previous cohort of lesions (n = 518) as training set, the AUC was found to be ~0.90. Using the same cohort, but including a wavenumber selection-based analysis, the same group improved the diagnostic specificity from a range of 17-65% to 20-75% when sensitivity was fixed to 90-99%^[119].

Santos *et al.*^[120] developed a method to improve diagnosis of melanoma based on Raman spectroscopy. High-wavenumber Raman spectra were collected from lesions suspicious for melanoma (common nevi and melanoma in situ: n = 128), with measurements performed on multiple locations within the lesions. A PCA-LDA diagnostic model was developed on a dataset of common nevi and melanoma in situ (n = 78) and then validated on an independent dataset (n = 50). The diagnostic model correctly classified all melanomas in the independent dataset with a highest possible specificity of 44% at a fixed sensitivity of 100%. Feng *et al.*^[121] explored the discriminating power between different types of NMSC (BCC, n = 14; SCC, n = 20; AK, n = 10) and healthy skin regions (n = 44) from the same patients using receiver operating characteristic

(ROC) curve analysis; the results showed high sensitivity up to 95% with a rather low specificity of 10%.

Pancreatic cancer

The literature search for pancreatic cancers included malignant, pre- and neoplastic lesions, involving exocrine and endocrine cancers, such as adenocarcinomas (PDAC) and neuroendocrine tumors (NET) of the pancreas. A total of 98 results were found for the chosen time interval, of which 4 studies were deemed to be clinically relevant; however, none of them were based on a required number of patients to be included in this review.

Prostate cancer

The literature search for prostate cancer resulted in 22 studies, of which only 2 blood-based were deemed relevant to the current review.

In a study by Medipally *et al.*^[122], Raman and IR spectra were recorded from blood plasma samples obtained from 33 healthy controls and 43 prostate cancer patients. Significant spectral differences were observed between the spectra of two categories exhibiting different Gleason scores. The acquired spectra were analyzed by PCA, PLS-DA and classical least squares fitting to discriminate samples with and without disease and provide insights into the underlying molecular species. The PLS-DA classifier was able to classify the presence of disease with sensitivities and specificities ranging between 90-99%. The CLS fitting identified several analytes that are involved in the development and progression of prostate cancer. Another study from the same group monitored radiotherapeutic response in blood plasma of prostate cancer patients reflected in the spectral profiles after FTIR analysis^[123]. Samples were acquired from 53 prostate cancer patients at five different time points (prior treatment, after hormone treatment, at the end of radiotherapy, two months post radiotherapy and eight months post radiotherapy) and analyzed using PCA. Discrimination was observed between spectra recorded at baseline versus follow up time points, as well as between spectra from patients showing minimal and severe acute and late toxicity. The diagnostic model achieved sensitivity and specificity rates ranging from 80% to 99%^[50].

IR and Raman spectroscopy in infectious diseases

Overall, 30 studies were identified in the literature to satisfy the inclusion criteria. Five studies in bacterial/viral (1/5 sepsis, 1/5 *Typhoid* infection, 1/5 Urinary tract infection, 1/5 *Klebsiella* and 1/5 bacterial/viral (not specified)), three in fungal (*Candida* infections, *Candida* or *T. rubrum*), two in parasitic (malaria) and 20 in viral infections (Chikungunya; Dengue; Ebola; Hepatitis B and C (HBV and HCV); Human Immunodeficiency Virus (HIV); Human Papillomavirus (HPV); Severe acute respiratory syndrome coronavirus 2 (SARS-CoV-2)) (Figure 3).

Table 3. Overview of infrared and Raman studies in infectious diseases between January 2015 and May 2021. Studies were deemed eligible for inclusion if they included more than 25 participants per group (disease and control; if no control group >25 in disease group).

Disease	Author, Year, Country	Spectroscopic technique	Population [Sample type]	Main findings	
Biofluids					
Bacterial infection	Sepsis (neonatal)	Yunanto, 2019, Indonesia ^[125]	FTIR	60 newborns: 30 healthy and 30 with risk of sepsis [Saliva]	Exploratory study, identified spectral regions that were significantly different between the groups
	Typhoid infection (<i>Salmonella typhi</i>)	Naseer, 2020, Pakistan ^[124]	Raman	60 healthy volunteers, 60 patients (typhoid-confirmed) [Blood serum]	Characteristic spectral signatures associated with infection. PCA discrimination between healthy volunteers and patients showed clear discrimination along PC1
	Urinary-Tract-Infection (UTI)	Tien, 2018, Taiwan ^[126]	SERS	108 UTI patient samples [Urine]	SERS chip used to capture/detect bacteria (no culturing); culturing used a reference method; culturing identified 97 of the samples as infected; SERS approach identified 93 of them directly and remaining 4 – after concentration
Fungal infection	Candida infection	Wohlmeister, 2017, Brazil ^[129]	FTIR	48 <i>Candida</i> infections (C. albicans (n = 36), C. glabrata (n = 10), C. krusei (n = 2) [Vaginal discharge]	93% of infected samples were correctly classified using Soft Independent Modelling by Class Analogy (SIMCA)
	Candida infection	Silva, 2016, Portugal ^[130]	ATR-FTIR	82 clinical isolates from 12 different <i>Candida spp.</i> from distinct biological products [Vaginal exudate, urine, blood and sputum]	~100% accuracy in identifying clinical isolates according to developed PLS-DA model
Parasitic infection	Malaria	Mwanga, 2019, Tanzania ^[133]	ATR-FTIR	173 healthy controls, 123 malaria infected patients [Dried blood spots]	93% sens and 92% spec (92% accuracy) for detecting <i>Plasmodium falciparum</i> infection; 85% sens and spec (85% accuracy) for detecting mixed malaria infection (<i>P. falciparum</i> and ovale)

(continued)

Table 3. Continued.

Disease	Author, Year, Country	Spectroscopic technique	Population [Sample type]	Main findings
Dengue, malaria	Patel, 2019, India ^[140]	Raman	54 healthy controls, 39 dengue, 37 malaria [Blood serum]	Sens/spec of 96% for dengue vs healthy controls and 95% for malaria vs healthy controls PC-LDA
Dengue, Zika, Chikungunya	Santos, 2018, Brazil ^[139]	ATR–FTIR	45 healthy controls, 45 dengue, 30 zika, 10 chikungunya infections [Blood]	Healthy, dengue and chikungunya classes were identified with 100% sens and spec (using PCA-LDA/SPA-LDA/GA-LDA models); Zika infections were identified with sensitivity and specificity ranging between 92-100% and 86-100% respectively
Dengue virus	Khan, 2017, Pakistan ^[138]	Raman	55 healthy controls, 45 dengue infections [Blood serum]	91% sens and spec (91% accuracy) using random forest algorithm
Dengue virus	Amin, 2017, Pakistan ^[137]	Raman	28 healthy controls, 32 dengue infections [Blood serum]	93% sens and 100% spec (97% accuracy) by PCA-LDA
Dengue virus	Khan, 2016, Pakistan ^[135]	Raman	53 dengue negative samples, 31 dengue infections [Blood serum]	73% sens and 93% spec (85% accuracy) by SVM model
Dengue virus	Khurram, 2016, Pakistan ^[136]	Raman	104 dengue infected samples [Blood serum]	Comparative study between Raman spectroscopy and ELISA. Raman vs. IgM: 61% sens and 72% spec (66% accuracy) by SVM model; Raman vs. IgG: 43 % sens and 52% spec (47% accuracy) by SVM model
Dengue virus	Khan, 2016, Pakistan ^[134]	Raman	25 healthy controls, 40 dengue infected samples [Blood serum]	Reported discriminatory spectral features between controls and infected individuals
Ebola, Malaria	Sebba, 2018, USA ^[146]	SERS nanotagging technology	100 Ebola positive vs 486 negative; 163 Malaria positive vs 233 negative [Whole blood and serum]	Simultaneous detection of Ebola, Lassa and malaria within the same sample. Ebola detection: 90% sens, 98% spec; malaria detection: 100% sens and spec

(continued)

Table 3. Continued.

Disease	Author, Year, Country	Spectroscopic technique	Population [Sample type]	Main findings
HBV	Lu, 2020, China ^[145]	Raman	499 healthy controls, 435 HBV [Blood serum]	Diagnostic accuracy of 96% by multiscale convolution independent circulation neural network
HBV	Tong, 2019, China ^[144]	Raman	500 non-HBV samples (including suspected bacterial infections with serum procalcitonin test results >0.5 µg/L, HCV patients, liver cirrhosis, liver cancer patients and healthy controls), 500 HBV [Blood serum]	100% sens and 88% spec (93% accuracy) were established using adaptive iterative weighted penalty least squares method (airPLS) - PCA- particle swarm optimization (PSO) -SVM method
HBV and Hepatitis C (HCV)	Roy, 2019, Australia ^[143]	ATR-FTIR	114 controls, 117 HBV, 130 HCV (Sample measurement: sample on ATR crystal) [Blood serum] 191 controls, 142 HBV, 164 HCV (Sample measurement: sample on glass coverslip) [Blood serum] 40 controls, 40 HBV, 40 HCV (Sample measurement: ultrafiltration) [Blood serum]	On ATR crystal: HBV vs control: 84% sens, 93% spec; HCV vs control: 80% sens, 97% spec HBV vs HCV: 77% sens, 83% spec On coverslip: HBV vs control: 69% sens, 74% spec; HCV vs control: 51% sens, 91% spec Ultrafiltration: Using the high-molecular weight fraction: HBV vs control: 88% sens, 95% spec; HCV vs control: 82% sens, 90% spec
HBV	Khan, 2018, Pakistan ^[142]	Raman	84 control, 119 HBV infected [Blood serum]	97% sens and 100% spec (98% accuracy) in distinguishing HBV from controls using support vector machine (SVM)
HCV	Sohail, 2018, Pakistan ^[141]	Raman	105 healthy controls, 122 HCV [Blood serum]	97% sens, 94% spec (95% accuracy) for controls vs HCV
Human immunodeficiency virus (HIV)	Silva, 2020, Brazil ^[147]	ATR-FTIR	80 healthy controls, 40 HIV-positive patients [Blood plasma]	83% sens and 92% spec by GA-LDA model

(continued)

Table 3. Continued.

	Disease	Author, Year, Country	Spectroscopic technique	Population [Sample type]	Main findings
	Human papilloma virus (HPV)	Chen, 2020, China ^[148]	Raman	196 HPV negative, 58 HPV positive [Cervical secretion]	94% sens and 100 % spec (99% accuracy)
	SARS-CoV-2	Barauna, 2021, Brazil ^[151]	ATR-FTIR	111 SARS-CoV-2 negative patients, 70 SARS-CoV-2 positive (based on RT-PCR) [Saliva]	95% blind sens and 89% spec by GA-LDA model
	SARS-CoV-2	Carlomagno, 2021, Italy ^[152]	SERS	33 age/sex-matched healthy controls, 38 SARS-CoV-2 negative, 30 SARS-CoV-2 positive [Saliva]	Control vs SARS-CoV-2 positive: 98% sens and spec (98% accuracy) Control vs SARS-CoV-2 negative: 96% sens and 99% spec (97% accuracy) SARS-CoV-2 positive vs negative sample: 87% sens and 95% spec (91% accuracy) Comparison between the three groups: 84% sens and 92% spec (88% accuracy) by Leave-One-Patient-Out Cross-Validation
	SARS-CoV-2	Wood, 2021, Australia ^[153]	FTIR with purpose-built transfection accessory	29 SARS-CoV-2 positive and 28 SARS-CoV-2 negative (confirmed by RT-qPCR) [Saliva]	93 % sens (27/29) and 82 % spec (23/28) by MCDVCV modelling approach.
	Cytology				
Bacterial/Viral infection	Bacterial and viral infections (not specified)	Agbariaa, 2020, Israel ^[127]	FTIR	113 controls, 89 inaccessible bacterial infections, 54 accessible bacterial infections, 60 inaccessible viral infections, 27 accessible viral infections. [White blood cells]	Controls vs infections (bacterial & viral): 95% accuracy. Diagnosis of the etiology of accessible infections (bacterial or Viral): >94% sens and > 90% spec. Error rate <6%. Results within 1h from collection
Bacterial infection	Klebsiella - <i>K. pneumoniae</i> ; <i>K. variicola</i> ; <i>K. quasipneumoniae</i>)	Dinkelacker, 2018, Germany ^[128]	FTIR	57 patients (68 isolates were used, of which 53 <i>K. pneumoniae</i> ; 11 <i>K. variicola</i> ; 4 <i>K. quasipneumoniae</i>) [Anal and pharyngeal swabs]	A high discriminatory power compared to the WGS reference, which was reflected by an adjusted R index of 0.837

(continued)

Table 3. Continued.

	Disease	Author, Year, Country	Spectroscopic technique	Population [Sample type]	Main findings
Parasitic infection	Malaria	Heraud, 2019, Thailand ^[132]	FTIR	318 patients with clinical symptoms of malaria: 151 positive, 167 negative according to qPCR and PCR [Red blood cells]	PLS-DA achieved 90% sens and 91% spec. SVM analysis showed better classification with 92% sens and 97% spec for discriminating malaria infection. Data were pre-analysed, and modelled to generate a diagnosis which can be accessed by patients over the cloud-based system
Viral infection	HPV	Mo, 2020, China ^[150]	FTIR	50 healthy controls, 50 high-risk HPV positive [Cervical exfoliated cells]	98% sens and 98% spec (98% accuracy) using PCA-LDA model
	HPV	Zheng, 2020, China ^[149]	Raman	33 normal, 30 high-risk HPV positive [Cervical exfoliated cells]	100% sens and 97% spec (98% accuracy) by leave-one-patient-out cross-validation method.
Tissue					
Fungal infection	<i>T. rubrum</i> or <i>Candida</i> species - <i>C. parapsilosis</i> (sensu lato), <i>C. glabrata</i> , <i>C. albicans</i>)	Kourkoumelis, 2017, Greece ^[131]	Raman	26 controls, 52 clippings infected either by <i>T. rubrum</i> / <i>Candida</i> [Nails]	The classification for the test set yielded 100% accuracy, with low RMSEP: 0.24 for the classification of <i>T. rubrum</i> vs <i>Candida</i> species vs controls

Abbreviations: ATR: Attenuated total reflection; FTIR: Fourier transform infrared spectroscopy; GA-LDA: Genetic algorithm-linear discriminant analysis; HBV: Hepatitis B; HCV: Hepatitis C; HPV: Human papillomavirus; IgG: Immunoglobulin G; IgM: Immunoglobulin M; MCDCV: Monte Carlo Double Cross Validation; PCA-LDA: Principal component-linear discrimination analysis; PLS-DA: Partial least squares-discriminant analysis; Sens: Sensitivity; SERS: Surface enhanced Raman spectroscopy; SPA-LDA: Successive projections algorithm-linear discriminant analysis; Spec: Specificity; SVM: Support vector machine; UTI: Urinary tract infection; WGS: Whole Genome Sequencing

Bacterial infections

Patients diagnosed with any bacterial infection were investigated. Five studies were finally included in the review based on the inclusion criteria (biofluid-based: 1/5 using blood serum; 1/5 urine; 1/5 saliva; 1/5 anal and pharyngeal swabs; cytology-based: 1/5 white blood cells).

Naseer *et al.*^[124] used serum-based Raman spectroscopy to discriminate between participants infected with *Salmonella typhi* (n = 60) and healthy controls (n = 60). PCA was used as an exploratory approach, whereby two principal components (PCs) were chosen (90% of variance). The authors identified characteristic spectral signatures that differed between the two classes. However, no other classification approach was employed. In an exploratory study, Yunanto *et al.*^[125] used FTIR of saliva samples to

facilitate the diagnosis of neonatal sepsis. Spectral information was obtained from newborns at risk of sepsis ($n = 30$) and healthy ($n = 30$) and significantly different spectral regions were reported, showing changes in nucleic acid/protein regions, which might be resulting from an inflammatory process. Tien *et al.*^[126] used SERS cylindrical chips to identify pathogens in patients with urinary tract infection (UTI) ($n = 108$). Urine was sent for bacterial culture as a reference method and also analyzed using SERS chips to identify bacteria. Of the 108 patients, 97 samples with a single bacterial species were identified by conventional urine culture. In the others, mixed flora was observed, which was not possible to detect by SERS. SERS identified 93 samples directly, while the remaining four samples required concentration to identify bacteria. The use of SERS in conjunction with the recognition software could allow a quicker and less expensive identification of pathogens.

Using white blood cells and FTIR spectroscopy, Agbaria *et al.*^[127] assessed accessible and inaccessible bacterial and viral infections. In this study, spectra from 343 individuals were collected, including 113 controls, 89 inaccessible bacterial infections, 54 accessible bacterial infections, 60 inaccessible viral infections, and 27 accessible viral infections. The authors used SVM which resulted to the classification between controls vs infected (95% accuracy). It was also possible to identify the etiology of accessible infections with >94% sensitivity and >90% specificity in one hour after blood collection with a < 6% error rate. The authors concluded that the classification results demonstrate the methodology's ability to diagnose the etiology of inaccessible infections with high reliability. Dinkelacker *et al.*^[128] used FTIR spectroscopy as a tool for the rapid typing *Klebsiella* clinical isolates and compared their results with whole genome sequencing (WGS) (gold standard). Samples from 57 patients were used (anal and pharyngeal swabs – 68 isolates, of which 53 *K. pneumoniae*; 11 *K. varicella*; 4 *K. quasipneumoniae*). 75% similarity was chosen as a cutoff value for grouping, and applying this value to the dendrogram, 28 groups were observed that comprized 8 isolates. The cluster congruence was quantified with the adjusted Rand index (ARI). $ARI = 1$ means total congruence between two methods. Comparing the FTIR-based to the WGS-based method (gold standard), there was a high similarity, which was reflected in an ARI of 0.837. A congruent result in relation to the WGS phylogeny was obtained for 63 isolates (~93%). The results demonstrated that FTIR spectroscopy has the ability to evaluate the relationship of *Klebsiella* strains exhibiting high congruence with the WGS gold standard method.

Fungal infections

Three studies were identified which examined fungal infections (2/3 using biofluids; 1/3 using tissues).

Wohlmeister *et al.*^[129] used FTIR (reflectance mode) associated with Soft Independent Modeling by Class Analogy (SIMCA) to identify of *Candida* species isolated from vaginal secretions. The study included samples of vaginal secretions from 48 women infected with a *Candida* species (*C. albicans* ($n = 36$), *C. glabrata* ($n = 10$), *C. krusei* ($n = 2$)). PCA was applied as an exploratory analysis technique, while SIMCA maximized interclass distance and class prediction (internal and external validation). Through the application of SIMCA, ~93% ($n = 45$) of the samples were correctly

classified. Silva *et al.*^[130] used ATR-FTIR to discriminate clinically relevant *Candida* species. The analyzed isolates were obtained from different biological samples (vaginal exudate, urine, blood and sputum). In this study, an exploratory analysis of the spectra of these clinical isolates with PCA was performed, and classification analysis was performed with PLS-DA. For the classification, different analyses were performed to discriminate between *C. albicans*, *C. glabrata*, *C. krusei*, *C. parapsilosis* and *C. tropicalis* species (most important clinical infections) with PLS-DA achieving ~100% correct detection of the clinical isolates.

Kourkoumelis *et al.*^[131] evaluated the ability of Raman spectroscopy to detect fungal infections by analyzing healthy (n = 26) and infected nails (n = 52). Using PCA, efficient differentiation of healthy, *T. rubrum* and *Candida* species infected nails was achieved. SIMCA and PLS-DA were further applied to generate diagnostic algorithms for the classification of Raman spectra. Both techniques succeeded in classifying clinical nail samples in three groups according to their mycological categories. The authors demonstrated that Raman spectroscopy is a promising method for the differentiation of healthy vs. diseased nails, including efficient differentiation between onychomycosis caused by *T. rubrum* and *Candida* species.

Parasitic infections

Studies on parasitic infections including Malaria, Babesiosis and Leishmania were identified since 2015. Out of the 64 results obtained, only two fit into the inclusion criteria. Two studies investigating parasitic infections (malaria) were identified after literature search (1/2 using dried blood spots; 1/2 using red blood cells).

Two independent studies on the detection of malaria parasites have extended spectroscopic approaches to large clinical pilot trials. Heraud *et al.*^[132] tested 318 patients exhibiting malaria symptoms from four regional clinics in Thailand. Blood samples from all patients were pre-analyzed using three different conventional testing methods namely optical microscopy using a Giemsa staining, rapid diagnostic tests (RDT), and qPCR (gold standard). According to qPCR, 151 tested positive while 167 patients tested negative for malaria infection. Spectral data were acquired using a portable ATR-FTIR spectrometer, which can be operated from a laptop computer or a mobile telephone with in-built software that guides the user through the sample measurement. To minimize the effect of confounding variables such as spectral noise, water vapor, background fluctuations, and possible contamination by sample fixation, an independent quality control software suite was designed to ensure each spectrum acquired passed the stipulated criteria for data modeling. PLS-DA and SVM algorithms were employed to create classification models, with PLS-DA achieving 90% sensitivity and 91% specificity while SVM analysis showed better classification with 92% sensitivity and 97% specificity for discriminating *P. falciparum* malaria infection. Finally, spectral data were encrypted and automatically uploaded to a cloud-based diagnostic system where spectra are pre-processed using the classifier located in the “Cloud”. This system will enable non-experts to rapidly process and receive a malaria diagnosis within 5 minutes.

Mwanga *et al.*^[133] carried out a similar pilot trial in Tanzania. A malaria parasite survey was conducted using RDTs and PCR assays across 1486 households. Blood samples

obtained were further re-analyzed by optical microscopy to ascertain the presence of malaria parasites. Finger prick volumes of blood were acquired from all participants and subsequently dried on to filter paper to form a dried blood spot. Altogether, positive ($n = 123$) and negative ($n = 173$) PCR pre-confirmed samples were scanned directly using a portable ATR-FTIR spectrometer. Seven independent machine learning algorithms were used to analyze the spectral data including k-nearest neighbors, logistic regression, SVM, naïve Bayes, XGBoost, random forest and Multilayer perceptron. Logistic regression models gave the best results, having an overall classification accuracy of 92% for *P. falciparum* and 85% for predicting mixed infections of *P. falciparum* and *Plasmodium ovale*.

Viral infections

The literature search for viral infections included Human Papillomavirus (HPV), Ebola, Hepatitis B and C (HBV and HCV), Zika, Dengue, Chikungunya, Yellow fever, Human Immunodeficiency Virus (HIV), and Severe acute respiratory syndrome coronavirus 2 (SARS-CoV-2). Of the total 53 studies retrieved, 20 were deemed to be relevant based on the inclusion criteria (7/20 Dengue; 5/20 HBV and HCV; 3/20 HPV; 3/20 SARS-CoV-2; 1/20 HIV; 1/20 Ebola infections)

Dengue & other infections

Globally, diseases caused by viruses are regarded as a major public health issue. Global dengue incidences have risen dramatically in recent decades. There are four distinct but closely related dengue virus (DENV) serotypes, namely DENV-1, DENV-2, DENV-3, and DENV-4. Hitherto, several diagnostic methods have been developed, that includes serological (ELISA) and virological assays (reverse transcriptase-polymerase chain reaction (RT-PCR)). Despite the advancement in the point of care combination tests, considerable challenges endured in the clinical management of dengue-infected patients, including the non-existences of definitive biomarkers^[10].

Most of the studies to date are based on serum analysis. In 2016, Khan *et al.*^[134], examined the biochemical changes associated with dengue infections from 40 infected individuals and 25 healthy controls and distinctive Raman peaks were apparent in infected samples. Most notably, a Raman line at 750 cm^{-1} was assigned to adenosine diphosphate (ADP), which is expected to be excreted into extra-cellular media during cell rupture. However, no chemometric investigation was conducted to prove the diagnostic prediction of the proposed approach. A different study from the same group exploited the combination of Raman spectroscopy and SVM algorithm to elucidate the biochemical disparities between 31 dengue positive and 53 negative samples^[135]. Similar Raman bands were observed ($750, 850, 1450, \text{ and } 1660\text{ cm}^{-1}$ which were assigned to ADP, Tryptophan- immunoglobulin G (IgG), IgG, and Amide I (proteins)) in the dengue-infected samples. When analyzing the spectra of three independent SVM models using kernel functions including Gaussian radial basis function, polynomial function, and a linear function, the best performance was achieved with the polynomial kernel with sensitivity of 73% and a specificity of 93% (85% accuracy).

In another study, two different conventional approaches, such as IgG and immunoglobulin M (IgM) – captured ELISA, were evaluated in comparison with Raman spectroscopy^[136]. The sensitivity, specificity, and accuracy for Raman spectroscopy in

comparison to IgM and IgG captured with the ELISA assay were 61%, 72%, and 66%, and 43%, 52%, and 47%, respectively. Authors explained the rationale behind the 'low sensitivity' concern with Raman analysis as being due to the greater number of false-negative results. There were 21 samples (20%) misdiagnosed as dengue negative with Raman spectroscopy, whilst IgM values of ELISA predicted them as dengue positive. However, the spectroscopic approach provides preferable specificity along with sensitivity and a very low false positive rate in comparison to IgM than IgG assays.

In 2017, Amin *et. al.*^[137] identified unique spectral signatures associated with 32 dengue infected serum samples including Raman bands that were not reported earlier. These Raman bands provided an exceptional sensitivity of 93%, specificity of 100%, and diagnostic accuracy of 97% using PCA-LDA. Khan *et.al.*^[138] also demonstrated that Raman spectroscopy with a random forest algorithm could correctly classify 100 dengue suspected samples (sensitivity, specificity of 91%). Analysis of the spectra demonstrated discernible variations in the peak intensities and additional Raman bands were observed, which were indicative of elevated lactate level in the infected samples.

A successful attempt has been made to evaluate the potential of ATR-FTIR spectroscopy in conjunction with multivariate classification techniques between healthy versus dengue versus chikungunya versus zika blood samples^[139]. Since these viruses belong to the same family (i.e., Flaviviridae) and have similar surface proteins, cross-reactivity is a pertinent concern in clinical diagnostic routines. A combination of ATR-FTIR spectroscopy and different multivariate algorithms (PCA-LDA, SPA-LDA, and GA-LDA) showed an excellent sensitivity and specificity of 100% in healthy, dengue, and chikungunya classes. However, classification of zika samples exhibited a 100% sensitivity and 92% specificity with PCA-LDA and SPA-LDA models whilst GA-LDA showed sensitivity of 92% and specificity of 86%.

Similarly, due to the overlapping clinical symptoms between malaria and dengue infections, a precise diagnosis remains challenging. Recently, Patel *et al.*^[140] reported a Raman spectroscopy-based stratified analysis on 130 subjects (37 malaria, 39 dengue, and 54 healthy controls). The authors showed a classification efficiency of 83% for both dengue and malaria whilst 100% efficacy was achieved with control data sets for the 3-model system (malaria vs dengue vs controls) using PC-LDA and validated using a LOOCV approach. Besides, a ROC displayed a sensitivity/specificity of 0.95 for malaria versus controls and 0.96 for dengue versus controls. As compared with existing diagnostic approaches, the acquired classification efficiency to stratify malaria versus dengue is enhanced. Nevertheless, machine-learning involving larger-cohorts analysis would be highly recommended before clinical translations.

HBV & HCV infections

HBV and HCV cause both acute and chronic infections. In 2018, Sohail *et al.*^[141] analyzed 227 samples, (105 healthy individuals, 122 HCV infected). Raman spectroscopy combined with a proximity-based machine learning technique was utilized to obtain a sensitivity of 97%, specificity of 94%, and a diagnostic accuracy of 95%. Significant spectral changes were observed due to variation peak intensities of lectin, chitin, lipids, ammonia and viral proteins as a consequence of the HCV infection. A better specificity of 100% and an accuracy of 98% was achieved with a Raman spectroscopy-SVM model

in differentiating 84 normal sera samples from 119 HBV infected samples^[142]. A SVM model was built on two separate kernels i.e., polynomial function and Gaussian RBF for extracting Raman spectral features of control sera and infected sera samples. The best classification performance was achieved using a polynomial kernel of order-2. In another study, Roy *et al.*^[143] employed three sample preparation methodologies including sera deposited onto glass cover slips, airdried and placed onto the ATR crystal, whole serum dried directly onto the ATR crystal, and ultrafiltration to deplete high- and low-molecular weight serum components and the high-molecular weight fraction placed directly onto the ATR-FTIR diamond window and dried. PLS-DA was applied to all three cases and sensitivity of 84%, 80%, and 77% and specificity of 93%, 97%, and 83% were established in HBV versus control, HCV versus control, and HBV versus HCV classification sets with the first approach (direct deposition onto ATR crystal). The depletion of high molecular weight components from low molecular weight fraction slightly enhanced sensitivity and specificity. The sensitivity of 88% and 82%, and specificity of 95% and 90% were achieved in HBV versus control, HCV versus control samples.

Tong *et al.*^[144], applied a combination of Raman spectroscopy and adaptive iterative weighted penalty least squares method, PCA, particle swarm optimization algorithm, and SVM (airPLS-PCA-PSO-SVM) approaches on 500 HBV and 500 non-HBV clinical samples (including suspected bacterial infections with serum procalcitonin (PCT) test results $>0.5 \mu\text{g/L}$, HCV patients, liver cirrhosis, liver cancer patients) and healthy controls. A sensitivity of 100%, specificity of 88%, and accuracy of 93% were attained. More recently, Lu *et al.*^[145] demonstrated the discrimination potential of Raman spectroscopy with a multiscale convolution independent circulation neural network between 499 healthy people and 435 HBV patients and accuracy of the approach was determined to be 96%.

Ebola & other infections

In regard to Ebola disease diagnosis, point of need diagnostic methods are critical. The initial clinical symptoms of the disease mimicking other endemic diseases, such as malaria, are certainly hindering the effective diagnosis. Sebba *et al.*^[146] developed a multiplexed POC immunoassay platform that uses surface-enhanced Raman scattering (SERS) tags to simultaneously detect antigens from Ebola, Lassa and malaria within a single blood sample. The SERS assay design comprises of a Raman reporter placed on the surface of a gold nanoparticle which enhances the strength of the scattering ($\sim 4\text{-}8$ orders of magnitude). The team has showed a sensitivity and specificity of 90% and 98% for Ebola detection ($n = 100$), whilst 100% for Malaria detection ($n = 163$). Besides these excellent statistics, the proposed assay does have limitations. The performance of SERS technology in human samples in an outbreak is undetermined. Moreover, the challenges due to the sample matrix including the disparities between fresh versus frozen blood or serum versus whole blood samples are remaining, which affect the potential of this assay technology.

HIV infections

Very recently, Silva *et al.*^[147] successfully detected HIV infection in pregnant women using ATR-FTIR spectroscopy. The authors used blood plasma samples from 80 healthy

controls and 40 HIV-positive patients obtaining a sensitivity of 83% and specificity of 92% after using GA-LDA.

HPV infections

In 2020, three spectroscopic studies focused on HPV infection, out of which two studies exploited Raman spectroscopy whilst the other study utilized FTIR. Chen *et al.*^[148] applied Raman spectroscopy in cervical secretions with a combination of a few multivariate data analysis techniques (airPLS-PLS-GA-SVM model), which achieved 94% sensitivity and 100% specificity (99% accuracy). Similarly, Zheng *et al.*^[149] analyzed Raman spectral data from 33 normal and 30 high-risk HPV positive cervical exfoliated cell samples using a LOOCV method, which provided 100% sensitivity, 97% specificity and 98% accuracy. Mo *et al.*^[150] investigated the performance of FTIR combined with PCA-LDA to facilitate the rapid and noninvasive screening of 50 high-risk HPV infections using cervical exfoliated cell samples. The method was able to produce sensitivity and specificity of 98%.

SARS-CoV-2 infections

SARS-CoV-2 has been emerged as a threat to humanity due to its severity in swift spreading of infection. As yet there are only three studies on the utilization of vibrational spectroscopic approaches for SARS-CoV-2 diagnosis. Barauna *et al.*^[151] proposed the exploitation of ATR-FTIR spectroscopy with a GA-LDA algorithm to detect and discriminate infected from healthy control samples. In total, saliva samples from 111 SARS-CoV-2 negative patients and 70 SARS-CoV-2 positive patients were used (confirmed by RT-PCR) and provided a 95% blind sensitivity and 89% specificity. Interestingly infrared spectra of the purified virus showed no evidence of amide modes. Carlomagno *et al.*^[152] used a Raman-based deep learning classification model to discriminate the signal collected from COVID-19 saliva samples with accuracy, precision, sensitivity and specificity of more than 95%. However, the control versus SARS-CoV-2 positive versus negative sample model provided 84% sensitivity and 92% specificity (88% accuracy) by LOOCV. More recently, Wood *et al.*^[153] investigated the utilization of infrared spectroscopy for the rapid point-of-care detection of COVID-19 markers in saliva from 29 SARS-CoV-2 positive patients and 28 negative using a portable infrared spectrometer with a purpose-built transfection accessory. This study demonstrated a sensitivity of 93 % (27/29) and a specificity of 82 % (23/28) using a Monte Carlo Double Cross Validation algorithm with 50 randomized test and model sets. Furthermore, they isolated and purified the virion particles from cell culture and identified the specific infrared and Raman marker bands associated with SARS-CoV-2 virus from RNA, proteins and lipids. The isolation of the virion particles was confirmed by transmission electron microscopy that clearly showed the virion particles with the characteristic corona and glycoprotein spikes.

Health economic considerations

The extensive research reported is a testament to the potential of vibrational spectroscopy as a platform in medical analysis. Whilst the capability of these approaches and

applications has been explored comprehensively, the barriers to translation still exist, as is shown by the number of technologies and products that have actually entered the medical market. A potential reason for this lack of translation is perhaps a predisposition in research to focus upon the technology performance in a given clinical niche, or a more superficial exploration of the medical application itself. Interaction with key opinion leaders and close consideration of the wider influences in health care are essential for translation.

For any new medical technology, it is essential that it is safe and effective, but also that it *contains* healthcare expenditures – essentially creating a balance between efficacy and cost^[154]. As well as providing the evidence required for approval for use, health economic assessments are a recommended way of further exploring the use of a technology within a clinical area and establishing clinical utility.

In the area of IR and Raman spectroscopy, the subject of ‘cost’ is predominantly associated with the cost of instrumentation, substrates, and occasionally reagents^[155–158]. It could be assumed that the gross value of these components together would infer the relative cost of a technology. However, health economics is not simply a comparison of these costs between different instruments, or approaches. The entire clinical pathway, and the technology’s position within it, needs to be assessed so that comparisons within that pathway can be made. A topical example would be a [hypothetical] technology that was positioned as a screening test for COVID-19, which would need to compete with the existing test (PCR) in terms of cost per analysis, as well as critical factors such as sample throughput. Whereas a low-cost device may be able to compete, some instrumentation may be unsuitable. In this example there is an obvious comparator technology; however, in some instances this may not be the case, and a close economic evaluation will be required to truly understand the cost-benefit implications.

A series of health economic studies have been published with regards to a blood serum test for brain tumor detection^[159,160]. Initially, the current clinical pathway for brain cancer diagnosis is described, and the position of the test within that pathway is explored^[159]. This study took into consideration proof-of-principal results, and factored this test performance into a cost-effectiveness calculation, showing that the spectroscopic test could provide cost savings in a primary and secondary care setting. A follow-up study explored the health economic model further, by using prospective data, as well as an additional cost-consequence analysis for tumor type discrimination^[160]. These studies are invaluable for enabling translation, and the examples described here are good resources for future studies and applications.

Successful startups toward clinical translation

Over the last 5 – 10 years there has been a welcome increase in entrepreneurial activity within the clinical spectroscopic field. However, we start this section with a discussion of an early trailblazer, River D (formerly known as River Diagnostics) (<https://www.riverd.com/>). River D was formed in 2002 and is a spin-out of the Erasmus Medical Center in Rotterdam, Netherlands. River D’s main product within a clinical application is the gen2-SCA, a highly sensitive confocal Raman system for *in vivo* skin analysis that can determine molecular concentration profiles from the skin surface within minutes and with high spatial resolution. This can help to study penetration and transdermal

delivery of topically applied materials. PitchBook shows that River D is a well-established company with its latest deal as a Series B (<https://pitchbook.com/profiles/company/58999-87>).

Other companies backed by strong patent portfolios are appearing in the space (note some of the authors are directors of these companies). Dxclover Ltd is a spin-out of the Department of Pure and Applied Chemistry at the University of Strathclyde (<https://www.dxclover.com/>). Dxclover Ltd formed in 2016 and spun out in 2019 with a seed funding. To date they have raised £5.1M to progress their novel spectroscopic liquid biopsy for the detection of cancer. Glyconics is a spin-out from research performed at the University of Swansea and are developers of medical diagnostics device design for early detection of exacerbation (<https://glyconics.com/>). Glyconics use FTIR to diagnose and monitor acute and chronic diseases from the molecular analysis of sputum to detect chronic obstructive pulmonary disease in patients with respiratory problems. Invenio (<https://www.invenio-imaging.com>) are pioneering Stimulated Raman Histology (SRH) that allows 3-D imaging of thick tissue specimens for the detection of disease. This technology enables analysis that does not require physical sectioning, performing a spectroscopic measurement at each point and displaying the results as a pseudo-colour image for each molecular species. Crunchbase shows that Invenio Imaging is based upon research from the Department of Chemistry and Chemical Biology at Harvard University and have raised \$7.5 M in funding and now have headquarters in silicon valley (<https://www.crunchbase.com/organization/invenio-imaging>).

There is also a burgeoning market in new instrumentation represented by new companies and mergers / acquisitions of other companies within the spectroscopic field. These companies do not have the company mission of translating clinical spectroscopy in a similar fashion to the companies named above but worth noting is the acquisition of Cobalt Light Systems by Agilent. The instrumentation developed by Cobalt can rapidly and accurately identify materials hidden inside objects or through barriers (such as the skin). IRSweep are developing the next generation of fast broadband and high-resolution dual-comb spectrometers (<https://irsweep.com/>) and Photothermal Spectroscopy Group who have pioneered the development of instruments for optical Photothermal Infrared (O-PTIR) (<https://www.photothermal.com>).

The descriptions above are by no means exhaustive and are representative of a developing area within spectroscopy and exemplify innovation that originated in research for both clinical spectroscopy and spectroscopic instrumentation that is progressing toward / completed commercial application.

Considerations for the translation of clinical spectroscopy

Translation of vibrational spectroscopy into the clinical environment has been relatively slow^[23]. The field of clinical spectroscopy would greatly benefit from multidisciplinary research centers that would not only assess the clinical potential of such technologies but also explore routes to the market and secure funding for large-cohort randomized clinical trials, which would facilitate and expedite clinical translation.

Standardization of pre-analytical, analytical and post-analytical steps is crucial for any analytical method intended for clinical implementation^[2,161–164]. Multinational

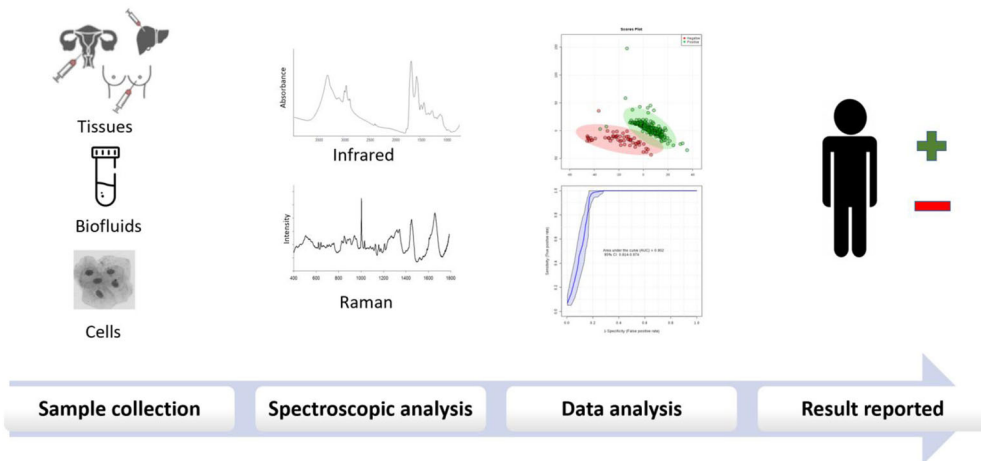


Figure 4. General workflow of clinical spectroscopy.

networks, such as the International Society for Clinical Spectroscopy (CLIRSPEC) (<https://clirspec.org/>) and Raman4Clinics (<https://www.raman4clinics.eu/>) founded in 2015, aim to pool expertise and develop collaborations between scientists, chemometricians, industrial and clinical partners in a concerted effort to promote the translation of spectroscopic techniques into the clinic. The objectives of these networks range from optimizing sample preparation protocols and determining instrumentation requirements suitable for clinical use, to developing data analysis/sharing protocols and assessing spectroscopy's clinical value and patient benefit.

Depending on the study design, the performance of spectroscopy needs to be evaluated as a screening/triage, diagnostic, prognostic or monitoring tool in large multi-center studies. In case the proposed spectroscopic test provides comparable or even superior accuracy to currently available tests, then it could be considered for implementation into the routine clinical practice. However, apart from assessing the diagnostic performance, other factors, such as health economics, automation, time for analysis and ease-of-use, should be taken into consideration and compared head-to-head with clinically validated approaches. Disruption of the normal clinical workflow should also be kept minimal to gain the support of the medical community. A general workflow of clinical spectroscopy is depicted in Figure 4, whereas suggested steps for clinical translation, from a preclinical phase to clinical trials along with technical considerations are provided in Figure 5^[3,171].

The ability of spectroscopy to analyze different sample types opens the technology up to different clinical applications. For instance, a highly-sensitive spectroscopic test of easily-accessible biofluids or cells (blood, urine, exfoliated cervical cells) would be valuable as a first-line screening tool, which may then require a secondary, more invasive (cerebrospinal fluid, tissue) but also specific test for a definite diagnosis. Such a two-step workflow has the potential to minimize unnecessary referrals to a secondary setting (as first-step highly sensitive) but also avoid over-diagnosis and over-treatment (as secondary-step highly specific).

Technological advancements in the field of spectroscopy have allowed the advent of portable, hand-held and miniaturized devices to permit point-of-care testing^[13]. The emergence

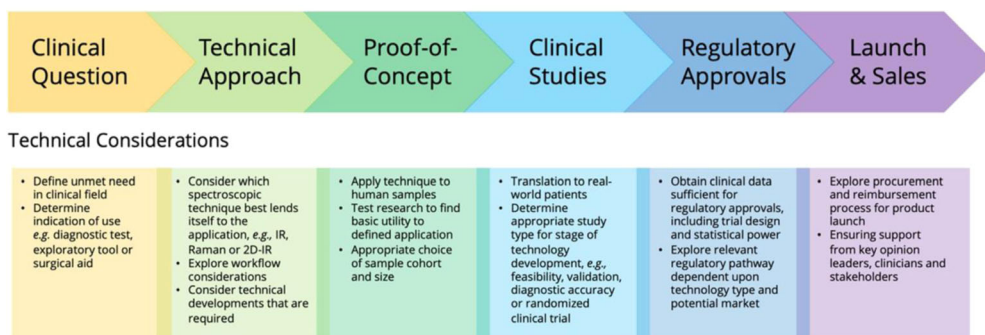


Figure 5. Steps toward clinical translation of vibrational spectroscopy. Reproduced with permission from Butler et al.^[3]

of quantum cascade lasers (QCLs), as high intensity light sources permitting IR measurements at discrete frequencies, is another important step forward into future clinical translation as they can decrease acquisition time and increase signal-to-noise ratio and resolution, thus enhancing the diagnostic capability^[165–168]. Development of fiber probes has also permitted *in vivo* applications for disease diagnostics or evaluation of surgical margin intra-operatively^[169]. However, despite the fact that fiber-based spectroscopy has proven its potential to facilitate diagnosis and guide treatment, large-scale trials confirming the promising results from proof-of-concept studies are still lacking. The requirements of instrumentation, such as resolution, portability, ease-of-use, speed of data acquisition/analysis, should be determined based on their clinical application and the setting for which these instruments are destined for (remote field trial, primary/secondary care, intra-operative).

Conclusion

It is clear that biomedical vibrational spectroscopy has shown promise in different clinical applications, from disease screening and diagnosis to treatment and monitoring of disease progression. Over the past last twenty years (2000 – 2020), there was a dramatic increase in the literature outputs for research in both IR and Raman spectroscopy for diagnosis of both cancer and infectious disease, although the rate of increase slowed significantly since ~ 2016. Notably, of the studies identified by the inclusion criteria, only ~10% of these were considered clinically relevant, based on the exclusion criteria, in the case of cancer diagnostics. This was highest for the case of esophageal cancer (~22%), in which tissue studies, including *in vivo*, dominate. Amongst the cancer studies deemed eligible, biofluid based diagnostics were most prevalent (~47%), followed by tissue (~45%). Clinically relevant cytological based studies were relatively few, although they featured strongly for bladder (25%) and gynaecological (27%) cancer diagnostics. In the area of infectious disease, clinically relevant virology studies dominated (~67%), and these were almost exclusively (90%) performed on biofluids.

The analysis of the literature first and foremost leads to the conclusion that increasing emphasis must be placed by the scientific community on the clinical relevance of studies intended to prove the concept of the applicability of vibrational spectroscopic techniques for clinical diagnostic applications. The exclusion criterion of <25

participants per group (disease and control) neglects many valuable fundamental and proof of concept studies^[1,13,21–27]. However, credible prospects of clinical translation can only be based on credible statistical analyses.

The predominance of biofluid based studies is also noteworthy. They are spatially homogeneous in their liquid form, or, as measured using the increasingly popular technique of ATR, the spatial inhomogeneity of dried droplets is automatically integrated in a single measurement. Time consuming and computationally demanding spatial imaging/mapping therefore is not required, as it is for tissue. Lower cost, portable/miniaturized IR and Raman instrumentation has become increasingly available, potentially for point-of-care diagnostics, and it is therefore not surprising that the past 5 years have seen significant activity toward the commercialization of biofluid based diagnostic techniques, supported in some cases by health economics studies to demonstrate the feasibility of clinical translation. In histo/cytological applications, progress toward the realization of clinical translation has advanced less rapidly. Although the proof-of-concept has been demonstrated, in many cases, with clinically relevant cohorts, feasibility in terms of clinical workflow and health economics may rely on emerging and further instrumental and data processing developments, to reduce acquisition and analysis times.

Increasing bibliometric attention has been mostly given to disease diagnostics which highlights the need for further large-scale studies into the latter clinical applications. Nevertheless, continuous advancements in the field will undoubtedly shed light on these applications in the years to come.

Herein, we have reported human studies of mid-IR and Raman spectroscopy investigating cancer and infectious diseases since 2015. Although the potential of such technologies in these diseases has been demonstrated, larger emphasis should be placed on the requirements for clinical translation. Standardization of study design and protocols, collaborations between the scientific, medical and industrial community, as well as randomized clinical trials are all of imminent importance for the translation of promising analytical tools into the clinic. This review has also considered the health economics of vibrational spectroscopy in the clinical arena and presented successful startup companies with a clinical focus.

References

1. Wang, D.; He, P.; Wang, Z.; Li, G.; Majed, N.; Gu, A. Z. Advances in Single Cell Raman Spectroscopy Technologies for Biological and Environmental Applications. *Curr. Opin. Biotechnol.* 2020, *64*, 218–229. doi:10.1016/j.copbio.2020.06.011 (2020).
2. Butler, H. J.; Ashton, L.; Bird, B.; Cinque, G.; Curtis, K.; Dorney, J.; Esmonde-White, K.; Fullwood, N. J.; Gardner, B.; Martin-Hirsch, P. L.; et al. Using Raman Spectroscopy to Characterize Biological Materials. *Nat. Protoc.* 2016, *11*, 664–687. doi:10.1038/nprot.2016.036
3. Butler, H. J.; Cameron, J. M.; Jenkins, C. A.; Hithell, G.; Hume, S.; Hunt, N. T.; Baker, M. J. Shining a Light on Clinical Spectroscopy: Translation of Diagnostic IR, 2D-IR and Raman Spectroscopy towards the Clinic. *Clin. Spectrosc.* 2019, *1*, 100003. doi:10.1016/j.clispe.2020.100003
4. Nicolson, F.; Kircher, M. F.; Stone, N.; Matousek, P. Spatially Offset Raman Spectroscopy for Biomedical Applications. *Chem. Soc. Rev.* 2021, *50*, 556–568. doi:10.1039/D0CS00855A
5. Gebrekidan, M. T.; Erber, R.; Hartmann, A.; Fasching, P. A.; Emons, J.; Beckmann, M. W.; Braeuer, A. Breast Tumor Analysis Using Shifted-Excitation Raman Difference

- Spectroscopy (SERDS). *Technol. Cancer Res. Treat.* 2018, 17, 1533033818782532. doi:10.1177/1533033818782532
6. Gardner, B.; Stone, N.; Matousek, P. Non-Invasive Chemically Specific Measurement of Subsurface Temperature in Biological Tissues Using Surface-Enhanced Spatially Offset Raman Spectroscopy. *Faraday Discuss.* 2016, 187, 329–339. doi:10.1039/c5fd00154d
 7. Wartewig, S.; Neubert, R. H. Pharmaceutical Applications of Mid-IR and Raman Spectroscopy. *Adv. Drug Deliv. Rev.* 2005, 57, 1144–1170. doi:10.1016/j.addr.2005.01.022
 8. Martínez Cortizas, A.; López-Costas, O. Linking Structural and Compositional Changes in Archaeological Human Bone Collagen: An FTIR-ATR Approach. *Sci. Rep.* 2020, 10, 17888. doi:10.1038/s41598-020-74993-y
 9. de Oliveira Penido, C. A. F.; Pacheco, M. T. T.; Lednev, I. K.; Silveira, L. Raman Spectroscopy in Forensic Analysis: identification of Cocaine and Other Illegal Drugs of Abuse. *J. Raman Spectrosc.* 2016, 47, 28–38. doi:10.1002/jrs.4864
 10. Li-Chan, E.; Chalmers J. M.; Griffiths P. R.. *Applications of vibrational spectroscopy in food science.* John Wiley & Sons; 2010. https://www.google.co.uk/books/edition/Applications_of_Vibrational_Spectroscopy/MTLoO-IJYIC?hl=en&gbpv=0
 11. Ong, T. T.; Blanch, E. W.; Jones, O. A. Surface Enhanced Raman Spectroscopy in Environmental Analysis, Monitoring and Assessment. *Sci. Total Environ.* 2020, 720, 137601. doi:10.1016/j.scitotenv.2020.137601
 12. Ben-Jaber, S.; Peveler, W. J.; Quesada-Cabrera, R.; Cortés, E.; Sotelo-Vazquez, C.; Abdul-Karim, N.; Maier, S. A.; Parkin, I. P. Photo-Induced Enhanced Raman Spectroscopy for Universal Ultra-Trace Detection of Explosives, Pollutants and Biomolecules. *Nat. Commun.* 2016, 7, 12189. doi:10.1038/ncomms12189
 13. Pahlow, S.; Weber, K.; Popp, J.; Wood, B. R.; Kochan, K.; Rütther, A.; Perez-Guaita, D.; Heraud, P.; Stone, N.; Dudgeon, A.; et al. Application of Vibrational Spectroscopy and Imaging to Point-of-Care Medicine: A Review. *Appl. Spectrosc.* 2018, 72, 52–84. doi:10.1177/0003702818791939
 14. Bispo, J. A. M.; de Sousa Vieira, E. E.; Silveira, L.; Fernandes, A. B. Correlating the Amount of Urea, Creatinine, and Glucose in urine from Patients with Diabetes Mellitus and Hypertension with the Risk of Developing Renal Lesions by Means of Raman Spectroscopy and Principal Component Analysis. *J. Biomed. Opt.* 2013, 18, 087004–087004. doi:10.1117/1.JBO.18.8.087004
 15. Haas, S. L.; Müller, R.; Fernandes, A.; Dzyek-Boycheva, K.; Würfl, S.; Hohmann, J.; Hemberger, S.; Elmas, E.; Brückmann, M.; Bugert, P.; et al. Spectroscopic Diagnosis of Myocardial Infarction and Heart Failure by Fourier Transform Infrared Spectroscopy in Serum Samples. *Appl. Spectrosc.* 2010, 64, 262–267. doi:10.1366/000370210790918508
 16. Nabers, A.; Hafermann, H.; Wiltfang, J.; Gerwert, K. Aβ and Tau Structure-Based Biomarkers for a Blood- and CSF-Based Two-Step Recruitment Strategy to Identify Patients with Dementia Due to Alzheimer’s Disease. *Alzheimers Dement. (Amst)* 2019, 11, 257–263. doi:10.1016/j.dadm.2019.01.008
 17. Paraskevaïdi, M.; Morais, C. L. M.; Lima, K. M. G.; Snowden, J. S.; Saxon, J. A.; Richardson, A. M. T.; Jones, M.; Mann, D. M. A.; Allsop, D.; Martin-Hirsch, P. L.; et al. Differential Diagnosis of Alzheimer’s Disease Using Spectrochemical Analysis of Blood. *Proc. Natl. Acad. Sci. U. S. A.* 2017, 114, E7929–E7938. doi:10.1073/pnas.1701517114
 18. Sahu, A.; Dalal, K.; Naglot, S.; Aggarwal, P.; Krishna, C. M. Serum Based Diagnosis of Asthma Using Raman Spectroscopy: An Early Phase Pilot Study. *Plos One.* 2013, 8, e78921. doi:10.1371/journal.pone.0078921
 19. Whiteman, S. C.; Yang, Y.; Jones, J. M.; Spiteri, M. A. FTIR Spectroscopic Analysis of Sputum: preliminary Findings on a Potential Novel Diagnostic Marker for COPD. *Ther. Adv. Respir. Dis.* 2008, 2, 23–31. doi:10.1177/1753465807087972
 20. Scott, D. A.; Renaud, D. E.; Krishnasamy, S.; Meriç, P.; Buduneli, N.; Cetinkalp, S.; Liu, K.-Z. Diabetes-Related Molecular Signatures in Infrared Spectra of Human Saliva. *Diabetol. Metab. Syndr.* 2010, 2, 48. doi:10.1186/1758-5996-2-48

21. Ralbovsky, N. M.; Lednev, I. K. Towards Development of a Novel Universal Medical Diagnostic Method: Raman Spectroscopy and Machine Learning. *Chem. Soc. Rev.* 2020, 49, 7428–7453. doi:10.1039/D0CS01019G
22. Baker, M. J.; Byrne, H. J.; Chalmers, J.; Gardner, P.; Goodacre, R.; Henderson, A.; Kazarian, S. G.; Martin, F. L.; Moger, J.; Stone, N.; et al. Clinical Applications of Infrared and Raman Spectroscopy: state of Play and Future Challenges. *Analyst* 2018, 143, 1735–1757. doi:10.1039/C7AN01871A
23. Byrne, H. J.; Baranska, M.; Puppels, G. J.; Stone, N.; Wood, B.; Gough, K. M.; Lasch, P.; Heraud, P.; Sulé-Suso, J.; Sockalingum, G. D. Spectropathology for the Next Generation: Quo Vadis? *Analyst* 2015, 140, 2066–2073. doi:10.1039/C4AN02036G
24. Baker, M. J.; Hussain, S. R.; Lovergne, L.; Untereiner, V.; Hughes, C.; Lukaszewski, R. A.; Thiéfin, G.; Sockalingum, G. D. Developing and Understanding Biofluid Vibrational Spectroscopy: A Critical Review. *Chem. Soc. Rev.* 2016, 45, 1803–1818. doi:10.1039/C5CS00585J
25. Chan, K. L. A.; Kazarian, S. G. Attenuated Total Reflection Fourier-Transform Infrared (ATR-FTIR) Imaging of Tissues and Live Cells. *Chem. Soc. Rev.* 2016, 45, 1850–1864. doi:10.1039/c5cs00515a
26. Kazarian, S. G. Perspectives on Infrared Spectroscopic Imaging from Cancer Diagnostics to Process Analysis. *Spectrochim. Acta A. Mol. Biomol. Spectrosc.* 2021, 251, 119413. doi:10.1016/j.saa.2020.119413
27. Lazaro-Pacheco, D.; Shaaban, A. M.; Rehman, S.; Rehman, I. Raman Spectroscopy of Breast Cancer. *Appl. Spectrosc. Rev.* 2020, 55, 439–475. doi:10.1080/05704928.2019.1601105
28. Kochan, K.; Perez-Guaita, D.; Adegoke, J.; Veettil, T. C.; Martin, M.; Roy, S.; Pebotuwa, S.; Heraud, P.; Wood, B. EXPRESS: Infrared Spectroscopy of Blood. *Appl. Spectrosc.* 2021, 71, 611–646. doi:10.1177/0003702820985856
29. Beleites, C.; Neugebauer, U.; Bocklitz, T.; Krafft, C.; Popp, J. Sample Size Planning for Classification Models. *Anal. Chim. Acta.* 2013, 760, 25–33. doi:10.1016/j.aca.2012.11.007
30. Li, S.; Li, L.; Zeng, Q.; Zhang, Y.; Guo, Z.; Liu, Z.; Jin, M.; Su, C.; Lin, L.; Xu, J.; et al. Characterization and Noninvasive Diagnosis of Bladder Cancer with Serum Surface Enhanced Raman Spectroscopy and Genetic Algorithms. *Sci. Rep* 2015, 5, 1–7. doi:10.1038/srep09582
31. Chen, S.; Zhu, S.; Cui, X.; Xu, W.; Kong, C.; Zhang, Z.; Qian, W. Identifying Non-Muscle-Invasive and Muscle-Invasive Bladder Cancer Based on Blood Serum Surface-Enhanced Raman Spectroscopy. *Biomed. Opt. Express.* 2019, 10, 3533–3544. doi:10.1364/BOE.10.003533
32. Gok, S.; Aydin, O. Z.; Sural, Y. S.; Zorlu, F.; Bayol, U.; Severcan, F. Bladder Cancer Diagnosis from Bladder Wash by Fourier Transform Infrared Spectroscopy as a Novel Test for Tumor Recurrence. *J. Biophotonics.* 2016, 9, 967–975. doi:10.1002/jbio.201500322
33. Witzke, K. E.; Großesueschkamp, F.; Jütte, H.; Horn, M.; Roghmann, F.; von Landenberg, N.; Bracht, T.; Kallenbach-Thieltges, A.; Käßlerlein, H.; Brüning, T.; et al. Integrated Fourier Transform Infrared Imaging and Proteomics for Identification of a Candidate Histochemical Biomarker in Bladder Cancer. *Am. J. Pathol.* 2019, 189, 619–631. doi:10.1016/j.ajpath.2018.11.018
34. Hands, J. R.; Clemens, G.; Stables, R.; Ashton, K.; Brodbelt, A.; Davis, C.; Dawson, T. P.; Jenkinson, M. D.; Lea, R. W.; Walker, C.; et al. Brain Tumour Differentiation: rapid Stratified Serum Diagnostics via Attenuated Total Reflection Fourier-Transform Infrared Spectroscopy. *J. Neurooncol.* 2016, 127, 463–472. doi:10.1007/s11060-016-2060-x
35. Smith, B. R.; Ashton, K. M.; Brodbelt, A.; Dawson, T.; Jenkinson, M. D.; Hunt, N. T.; Palmer, D. S.; Baker, M. J. Combining Random Forest and 2D Correlation Analysis to Identify Serum Spectral Signatures for Neuro-Oncology. *Analyst* 2016, 141, 3668–3678. doi:10.1039/c5an02452h
36. Cameron, J. M.; Butler, H. J.; Smith, B. R.; Hegarty, M. G.; Jenkinson, M. D.; Syed, K.; Brennan, P. M.; Ashton, K.; Dawson, T.; Palmer, D. S.; et al. Developing Infrared

- Spectroscopic Detection for Stratifying Brain Tumour Patients: glioblastoma Multiforme vs. *Analyst* 2019, *144*, 6736–6750. doi:10.1039/C9AN01731C
37. Cameron, J. M.; Rinaldi, C.; Butler, H. J.; Hegarty, M. G.; Brennan, P. M.; Jenkinson, M. D.; Syed, K.; Ashton, K. M.; Dawson, T. P.; Palmer, D. S.; et al. Stratifying Brain Tumour Histological Sub-Types: The Application of ATR-FTIR Serum Spectroscopy in Secondary Care. *Cancers (Basel)* 2020, *12*, 1710. doi:10.3390/cancers12071710
 38. Butler, H. J.; Brennan, P. M.; Cameron, J. M.; Finlayson, D.; Hegarty, M. G.; Jenkinson, M. D.; Palmer, D. S.; Smith, B. R.; Baker, M. J. Development of High-Throughput ATR-FTIR Technology for Rapid Triage of Brain Cancer. *Nat. Commun.* 2019, *10*, 4501. doi:10.1038/s41467-019-12527-5
 39. Cameron, J. M.; Conn, J. J. A.; Rinaldi, C.; Sala, A.; Brennan, P. M.; Jenkinson, M. D.; Caldwell, H.; Cinque, G.; Syed, K.; Butler, H. J.; et al. Interrogation of IDH1 Status in Gliomas by Fourier Transform Infrared Spectroscopy. *Cancers* 2020, *12*, 3682. doi:10.3390/cancers12123682
 40. Mehta, K.; Atak, A.; Sahu, A.; Srivastava, S.; C, M. K. An Early Investigative Serum Raman Spectroscopy Study of meningioma. *Analyst* 2018, *143*, 1916–1923. doi:10.1039/C8AN00224J
 41. Lilo, T.; Morais, C. L. M.; Ashton, K. M.; Pardilho, A.; Davis, C.; Dawson, T. P.; Gurusinghe, N.; Martin, F. L. Spectrochemical Differentiation of Meningioma Tumours Based on Attenuated Total Reflection Fourier-Transform Infrared (ATR-FTIR) Spectroscopy. *Anal. Bioanal. Chem.* 2020, *412*, 1077–1086. doi:10.1007/s00216-019-02332-w
 42. Morais, C. L. M.; Lilo, T.; Ashton, K. M.; Davis, C.; Dawson, T. P.; Gurusinghe, N.; Martin, F. L. Determination of Meningioma Brain Tumour Grades Using Raman Microspectroscopy Imaging. *Analyst* 2019, *144*, 7024–7031. doi:10.1039/c9an01551e
 43. Livermore, L. J.; Isabelle, M.; Bell, I. M.; Scott, C.; Walsby-Tickle, J.; Gannon, J.; Plaha, P.; Vallance, C.; Ansorge, O. Rapid Intraoperative Molecular Genetic Classification of Gliomas Using Raman Spectroscopy. *Neurooncol. Adv.* 2019, *1*, vdz008. doi:10.1093/oaajnl/vdz008
 44. Sitnikova, V. E.; Kotkova, M. A.; Nosenko, T. N.; Kotkova, T. N.; Martynova, D. M.; Uspenskaya, M. V. Breast Cancer Detection by ATR-FTIR Spectroscopy of Blood Serum and Multivariate Data-Analysis. *Talanta* 2020, *214*, 120857. doi:10.1016/j.talanta.2020.120857
 45. Lin, D.; Wang, Y.; Wang, T.; Zhu, Y.; Lin, X.; Lin, Y.; Feng, S. Metabolite Profiling of Human Blood by Surface-Enhanced Raman Spectroscopy for Surgery Assessment and Tumor Screening in Breast Cancer. *Anal. Bioanal. Chem.* 2020, *412*, 1611–1618. doi:10.1007/s00216-020-02391-4
 46. Talari, A. C.; Rehman, S.; Rehman, I. U. Advancing Cancer Diagnostics with Artificial Intelligence and Spectroscopy: identifying Chemical Changes Associated with Breast Cancer. *Expert Rev. Mol. Diagn.* 2019, *19*, 929–940. doi:10.1080/14737159.2019.1659727
 47. Elmi, F.; Movaghar, A. F.; Elmi, M. M.; Alinezhad, H.; Nikbakhsh, N. Application of FT-IR Spectroscopy on Breast Cancer Serum Analysis. *Spectrochim. Acta A. Mol. Biomol. Spectrosc.* 2017, *187*, 87–91. doi:10.1016/j.saa.2017.06.021
 48. Surmacki, J.; Brozek-Pluska, B.; Kordek, R.; Abramczyk, H. The Lipid-Reactive Oxygen Species Phenotype of Breast Cancer. Raman Spectroscopy and Mapping, PCA and PLSDA for Invasive Ductal Carcinoma and Invasive Lobular Carcinoma. Molecular Tumorigenic Mechanisms beyond Warburg Effect. *Analyst* 2015, *140*, 2121–2133. doi:10.1039/c4an01876a
 49. Li, X.; Yang, T.; Li, S.; Wang, D.; Song, Y.; Zhang, S. Raman Spectroscopy Combined with Principal Component Analysis and k Nearest Neighbour Analysis for Non-Invasive Detection of Colon Cancer. *Laser Phys.* 2016, *26*, 035702. doi:10.1088/1054-660X/26/3/035702
 50. Moisoiu, V.; Stefancu, A.; Gulei, D.; Boitor, R.; Magdo, L.; Raduly, L.; Pasca, S.; Kubelac, P.; Mehterov, N.; Chiş, V.; et al. SERS-Based Differential Diagnosis between Multiple Solid Malignancies: breast, Colorectal, Lung, Ovarian and Oral Cancer. *Int. J. Nanomedicine.* 2019, *14*, 6165–6178. doi:10.2147/ijn.S198684

51. Toraman, S.; Girgin, M.; Üstündağ, B.; Türkoğlu, İ. Classification of the Likelihood of Colon Cancer with Machine Learning Techniques Using FTIR Signals Obtained from Plasma. *Turk. J. Elec. Eng. & Comp. Sci.* 2019, 27, 1765–1779. doi:10.3906/elk-1801-259
52. Kuepper, C.; Großrueschkamp, F.; Kallenbach-Thieltges, A.; Mosig, A.; Tannapfel, A.; Gerwert, K. Label-Free Classification of Colon Cancer Grading Using Infrared Spectral Histopathology. *Faraday Discuss.* 2016, 187, 105–118. doi:10.1039/c5fd00157a
53. Petersen, D.; Naveed, P.; Ragheb, A.; Niedieker, D.; El-Mashtoly, S. F.; Brechmann, T.; Kötting, C.; Schmiegel, W. H.; Freier, E.; Pox, C.; et al. Raman Fiber-Optical Method for Colon Cancer Detection: Cross-Validation and Outlier Identification Approach. *Spectrochim. Acta. A. Mol. Biomol. Spectrosc.* 2017, 181, 270–275. doi:10.1016/j.saa.2017.03.054
54. Bahreini, M.; Hosseinzadegan, A.; Rashidi, A.; Miri, S. R.; Mirzaei, H. R.; Hajian, P. A Raman-Based Serum Constituents' Analysis for Gastric Cancer Diagnosis: In Vitro Study. *Talanta* 2019, 204, 826–832. doi:10.1016/j.talanta.2019.06.068
55. Li, X.; Yang, T.; Li, S.; Wang, D.; Song, Y.; Yu, K. Different Classification Algorithms and Serum Surface Enhanced Raman Spectroscopy for Noninvasive Discrimination of Gastric Diseases. *J. Raman Spectrosc.* 2016, 47, 917–925. doi:10.1002/jrs.4924
56. Chen, Y.; Cheng, S.; Zhang, A.; Song, J.; Chang, J.; Wang, K.; Zhang, Y.; Li, S.; Liu, H.; Alfranca, G.; et al. Salivary Analysis Based on Surface Enhanced Raman Scattering Sensors Distinguishes Early and Advanced Gastric Cancer Patients from Healthy Persons. *J. Biomed. Nanotechnol.* 2018, 14, 1773–1784. doi:10.1166/jbn.2018.2621
57. Guleken, Z.; Bulut, H.; Gültekin, G. İ.; Arıkan, S.; Yaylım, İ.; Hakan, M. T.; Sönmez, D.; Tarhan, N.; Depciuch, J. Assessment of Structural Protein Expression by FTIR and Biochemical Assays as Biomarkers of Metabolites Response in Gastric and Colon Cancer. *Talanta* 2021, 231, 122353. doi:10.1016/j.talanta.2021.122353
58. Liu, H.; Su, Q.; Sheng, D.; Zheng, W.; Wang, X. Comparison of Red Blood Cells from Gastric Cancer Patients and Healthy Persons Using FTIR Spectroscopy. *J. Mol. Struct.* 2017, 1130, 33–37. doi:10.1016/j.molstruc.2016.10.019
59. Ghassemi, M.; Barzegari, S.; Hajian, P.; Zham, H.; Mirzaei, H. R.; Shirazi, F. H. Diagnosis of Normal and Malignant Human Gastric Tissue Samples by FTIR Spectra Combined with Mathematical Models. *J. Mol. Struct.* 2021, 1229, 129493.
60. Lin, K.; Wang, J.; Zheng, W.; Ho, K. Y.; Teh, M.; Yeoh, K. G.; Huang, Z. Rapid Fiber-Optic Raman Spectroscopy for Real-Time in Vivo Detection of Gastric Intestinal Metaplasia during Clinical Gastroscopy. *Cancer Prev Res (Phila).* 2016, 9, 476–483. doi:10.1158/1940-6207.CAPR-15-0213
61. Shrivastava, A.; Aggarwal, L. M.; Krishna, C. M.; Pradhan, S.; Mishra, S. P.; Choudhary, S.; Patel, C. B.; Singla, S.; Singh, R. K. Diagnostic and Prognostic Application of Raman Spectroscopy in Carcinoma Cervix: A Biomolecular Approach. *Spectrochim. Acta, Part A.* 2021, 250, 119356.
62. Lu, D.; Ran, M.; Liu, Y.; Xia, J.; Bi, L.; Cao, X. SERS Spectroscopy Using Au-Ag Nanoshuttles and Hydrophobic Paper-Based Au Nanoflower Substrate for Simultaneous Detection of Dual Cervical Cancer-Associated Serum Biomarkers. *Anal. Bioanal. Chem.* 2020, 412, 7099–7112. doi:10.1007/s00216-020-02843-x
63. Karunakaran, V.; Saritha, V. N.; Joseph, M. M.; Nair, J. B.; Saranya, G.; Raghu, K. G.; Sujathan, K.; Kumar, K. S.; Maiti, K. K. Diagnostic Spectro-Cytology Revealing Differential Recognition of Cervical Cancer Lesions by Label-Free Surface Enhanced Raman Fingerprints and Chemometrics. *Nanomedicine* 2020, 29, 102276. doi:10.1016/j.nano.2020.102276
64. Traynor, D.; Duraipandian, S.; Bhatia, R.; Cuschieri, K.; Martin, C. M.; O'Leary, J. J.; Lyng, F. M. The Potential of Biobanked Liquid Based Cytology Samples for Cervical Cancer Screening Using Raman Spectroscopy. *J. Biophotonics.* 2019, 12, e201800377. doi:10.1002/jbio.201800377

65. Jusman, Y.; Isa, N. A. M.; Ng, S.-C.; Hasikin, K.; Osman, N. A. A. Automated Cervical Precancerous Cells Screening System Based on Fourier Transform Infrared Spectroscopy Features. *J. Biomed. Opt.* 2016, *21*, 75005. doi:10.1117/1.JBO.21.7.075005
66. Ramos, I. R.; Meade, A. D.; Ibrahim, O.; Byrne, H. J.; McMennamin, M.; McKenna, M.; Malkin, A.; Lyng, F. M. Raman Spectroscopy for Cytopathology of Exfoliated Cervical Cells. *Faraday Discuss.* 2016, *187*, 187–198. doi:10.1039/c5fd00197h
67. Wang, J.; Zheng, C. X.; Ma, C. L.; et al. Raman Spectroscopic Study of Cervical Precancerous Lesions and Cervical Cancer. *Lasers Med. Sci.* 2021, *1–10*. doi:10.1007/s10103-020-03218-5
68. Zhang, H.; Cheng, C.; Gao, R.; Yan, Z.; Zhu, Z.; Yang, B.; Chen, C.; Lv, X.; Li, H.; Huang, Z. Rapid Identification of Cervical Adenocarcinoma and Cervical Squamous Cell Carcinoma Tissue Based on Raman Spectroscopy Combined with Multiple Machine Learning Algorithms. *Photodiagnosis Photodyn. Ther.* 2021, *33*, 102104. doi:10.1016/j.pdpdt.2020.102104
69. Zheng, C.; Qing, S.; Wang, J.; Lü, G.; Li, H.; Lü, X.; Ma, C.; Tang, J.; Yue, X. Diagnosis of Cervical Squamous Cell Carcinoma and Cervical Adenocarcinoma Based on Raman Spectroscopy and Support Vector Machine. *Photodiagnosis Photodyn. Ther.* 2019, *27*, 156–161. doi:10.1016/j.pdpdt.2019.05.029
70. Daniel, A.; Prakasarao, A.; Ganesan, S. Near-Infrared Raman Spectroscopy for Estimating Biochemical Changes Associated with Different Pathological Conditions of Cervix. *Spectrochim. Acta. A. Mol. Biomol. Spectrosc.* 2018, *190*, 409–416. doi:10.1016/j.saa.2017.09.014
71. Daniel, A.; Prakasarao, A.; Dornadula, K.; Ganesan, S. Polarized Raman Spectroscopy Unravels the Biomolecular Structural Changes in Cervical Cancer. *Spectrochim. Acta. A. Mol. Biomol. Spectrosc.* 2016, *152*, 58–63. doi:10.1016/j.saa.2015.06.053
72. Paraskevaïdi, M.; Morais, C. L. M.; Ashton, K. M.; Stringfellow, H. F.; McVey, R. J.; Ryan, N. A. J.; O'Flynn, H.; Sivalingam, V. N.; Kitson, S. J.; MacKintosh, M. L.; et al. Detecting Endometrial Cancer by Blood Spectroscopy: A Diagnostic Cross-Sectional Study. *Cancers* 2020, *12*, 1256. doi:10.3390/cancers12051256
73. Perumal, J.; Mahyuddin, A.; Balasundaram, G.; Goh, D.; Fu, C. Y.; Kazakeviciute, A.; Dinish, U. S.; Choolani, M.; Olivo, M. SERS-Based Detection of Haptoglobin in Ovarian Cyst Fluid as a Point-of-Care Diagnostic Assay for Epithelial Ovarian Cancer. *CMAR.* 2019, *11*, 1115–1124. doi:10.2147/CMAR.S185375
74. Paraskevaïdi, M.; Ashton, K. M.; Stringfellow, H. F.; Wood, N. J.; Keating, P. J.; Rowbottom, A. W.; Martin-Hirsch, P. L.; Martin, F. L. Raman Spectroscopic Techniques to Detect Ovarian Cancer Biomarkers in Blood Plasma. *Talanta* 2018, *189*, 281–288. doi:10.1016/j.talanta.2018.06.084
75. Theophilou, G.; Lima, K. M. G.; Martin-Hirsch, P. L.; Stringfellow, H. F.; Martin, F. L. ATR-FTIR Spectroscopy Coupled with Chemometric Analysis Discriminates Normal, Borderline and Malignant Ovarian Tissue: classifying Subtypes of Human Cancer. *Analyst* 2016, *141*, 585–594. doi:10.1039/C5AN00939A
76. Sahu, A. K.; Dhoot, S.; Singh, A.; Sawant, S. S.; Nandakumar, N.; Talathi-Desai, S.; Garud, M.; Pagare, S.; Srivastava, S.; Nair, S.; et al. Oral Cancer Screening: serum Raman Spectroscopic Approach. *J. Biomed. Opt.* 2015, *20*, 115006. doi:10.1117/1.JBO.20.11.115006
77. Yan, B.; Li, B.; Wen, Z.; Luo, X.; Xue, L.; Li, L. Label-Free Blood Serum Detection by Using Surface-Enhanced Raman Spectroscopy and Support Vector Machine for the Preoperative Diagnosis of Parotid Gland Tumors. *BMC Cancer* 2015, *15*, 1–9. doi:10.1186/s12885-015-1653-7
78. Tan, Y.; Yan, B.; Xue, L.; Li, Y.; Luo, X.; Ji, P. Surface-Enhanced Raman Spectroscopy of Blood Serum Based on Gold Nanoparticles for the Diagnosis of the Oral Squamous Cell Carcinoma. *Lipids Health Dis.* 2017, *16*, 1–9. doi:10.1186/s12944-017-0465-y
79. Xue, L.; Yan, B.; Li, Y.; Tan, Y.; Luo, X.; Wang, M. Surface-Enhanced Raman Spectroscopy of Blood Serum Based on Gold Nanoparticles for Tumor Stages Detection

- and Histologic Grades Classification of Oral Squamous Cell Carcinoma. *Int. J. Nanomedicine*. 2018, 13, 4977–4986. doi:10.2147/IJN.S167996
80. Lin, H.; Zhou, J.; Wu, Q.; Hung, T.-M.; Chen, W.; Yu, Y.; Chang, J. T.-C.; Pan, J.; Qiu, S.; Chen, R. Human Blood Test Based on Surface-Enhanced Raman Spectroscopy Technology Using Different Excitation Light for Nasopharyngeal Cancer Detection. *IET Nanobiotechnol.* 2019, 13, 942–945. doi:10.1049/iet-nbt.2019.0221
81. Liang, X.; Miao, X.; Xiao, W.; Ye, Q.; Wang, S.; Lin, J.; Li, C.; Huang, Z. Filter-Membrane-Based Ultrafiltration Coupled with Surface-Enhanced Raman Spectroscopy for Potential Differentiation of Benign and Malignant Thyroid Tumors from Blood Plasma. *Int. J. Nanomedicine*. 2020, 15, 2303–2314. doi:10.2147/IJN.S233663
82. Adeebea; Siddiqui, A. J.; Sherazi, S. T.; Ahmed, S.; Choudhary, M. I.; Rahman, A.; Musharraf, S. G. A Comparative Profiling of Oral Cancer Patients and High Risk Niswar Users Using FT-IR and Chemometric Analysis. *Spectrochim. Acta. Part A: Mol. Biomol. Spectrosc.* 2018, 203, 177–184. doi:10.1016/j.saa.2018.05.107
83. Brindha, E.; Rajasekaran, R.; Aruna, P.; Koteeswaran, D.; Ganesan, S. High Wavenumber Raman Spectroscopy in the Characterization of Urinary Metabolites of Normal Subjects, Oral Premalignant and Malignant Patients. *Spectrochim. Acta A. Mol. Biomol. Spectrosc.* 2017, 171, 52–59. doi:10.1016/j.saa.2016.06.048
84. Sahu, A.; Gera, P.; Pai, V.; Dubey, A.; Tyagi, G.; Waghmare, M.; Pagare, S.; Mahimkar, M.; Murali Krishna, C. Raman Exfoliative Cytology for Oral Precancer Diagnosis. *J. Biomed. Opt.* 2017, 22, 1–12. doi:10.1117/1.JBO.22.11.115003
85. Sarkar, R.; Chatterjee, K.; Ojha, D.; Chakraborty, B.; Sengupta, S.; Chattopadhyay, D.; RoyChaudhuri, C.; Barui, A. Liaison between Heme Metabolism and Bioenergetics Pathways—a Multimodal Elucidation for Early Diagnosis of Oral Cancer. *Photodiagn. Photodyn. Ther.* 2018, 21, 263–274. doi:10.1016/j.pdpdt.2018.01.002
86. Sun, L.; Xu, Z.; Huang, W.; Wu, S.; Lin, X.; Zhu, F.; Liu, N.; Huang, M.; Chen, R.; Zeng, H. Preliminary Study of Differentiating Smears from Cancerous and Non-Cancerous Nasopharyngeal Tissue Using Confocal Raman Spectroscopy. *J. Cancer Res. Clin. Oncol.* 2016, 142, 823–831. doi:10.1007/s00432-015-2082-3
87. Jeng, M.-J.; Sharma, M.; Sharma, L.; Huang, S.-F.; Chang, L.-B.; Wu, S.-L.; Chow, L. Novel Quantitative Analysis Using Optical Imaging (VELscope) and Spectroscopy (Raman) Techniques for Oral Cancer Detection. *Cancers* 2020, 12, 3364. doi:10.3390/cancers12113364
88. Vohra, P.; Strobbia, P.; Ngo, H.; Lee, W.; Vo-Dinh, T. Rapid Nanophotonics Assay for Head and Neck Cancer Diagnosis. *Sci. Rep.* 2018, 8, 1–7. doi:10.1038/s41598-018-29428-0
89. Chundayil Madathil, G.; Iyer, S.; Thankappan, K.; Gowd, G. S.; Nair, S.; Koyakutty, M. A Novel Surface Enhanced Raman Catheter for Rapid Detection, Classification, and Grading of Oral Cancer. *Adv. Healthcare Mater.* 2019, 8, 1801557. doi:10.1002/adhm.201801557
90. Hoesli, R. C.; Orringer, D. A.; McHugh, J. B.; Spector, M. E. Coherent Raman Scattering Microscopy for Evaluation of Head and Neck Carcinoma. *Otolaryngol. Head Neck Surg.* 2017, 157, 448–453. doi:10.1177/0194599817700388
91. Malik, A.; Sahu, A.; Singh, S. P.; Deshmukh, A.; Chaturvedi, P.; Nair, D.; Nair, S.; Murali Krishna, C. In Vivo Raman Spectroscopy-Assisted Early Identification of Potential Second Primary/Recurrences in Oral Cancers: An Exploratory Study. *Head Neck*. 2017, 39, 2216–2223. doi:10.1002/hed.24884
92. Bhattacharjee, A.; Hole, A.; Malik, A.; Sahu, A.; Singh, S. P.; Deshmukh, A.; Nair, S.; Chaturvedi, P.; Krishna, C. M. Risk Prediction by Raman Spectroscopy for Disease-Free Survival in Oral Cancers. *Lasers Med. Sci.* 2021, 1–10.
93. He, C.; Wu, X.; Zhou, J.; Chen, Y.; Ye, J. Raman Optical Identification of Renal Cell Carcinoma via Machine Learning. *Spectrochim. Acta A. Mol. Biomol. Spectrosc.* 2021, 252, 119520. doi:10.1016/j.saa.2021.119520
94. Liu, Y.; Du, Z.; Zhang, J.; Jiang, H. Renal Mass Biopsy Using Raman Spectroscopy Identifies Malignant and Benign Renal Tumors: potential for Pre-Operative Diagnosis. *Oncotarget* 2017, 8, 36012–36019. doi:10.18632/oncotarget.16419

95. Mert, S.; Özbek, E.; Ötünçtemur, A.; Çulha, M. Kidney Tumor Staging Using Surface-Enhanced Raman Scattering. *J. Biomed. Opt.* 2015, 20, 047002. doi:10.1117/1.JBO.20.4.047002
96. Sablinskas, V.; Bandzeviciute, R.; Velicka, M.; Ceponkus, J.; Urboniene, V.; Jankevicius, F.; Laurinavičius, A.; Dasevičius, D.; Steiner, G. Fiber Attenuated Total Reflection Infrared Spectroscopy of Kidney Tissue during Live Surgery. *J. Biophotonics*. 2020, 13, e202000018. doi:10.1002/jbio.202000018
97. Bai, Y.; Yu, Z.; Yi, S.; Yan, Y.; Huang, Z.; Qiu, L. Raman Spectroscopy-Based Biomarker Screening by Studying the Fingerprint Characteristics of Chronic Lymphocytic Leukemia and Diffuse Large B-Cell Lymphoma. *J. Pharm. Biomed. Anal.* 2020, 190, 113514. doi:10.1016/j.jpba.2020.113514
98. Féré, M.; Gobinet, C.; Liu, L. H.; Beljebbar, A.; Untereiner, V.; Gheldof, D.; Chollat, M.; Klossa, J.; Chatelain, B.; Piot, O. Implementation of a Classification Strategy of Raman Data Collected in Different Clinical Conditions: application to the Diagnosis of Chronic Lymphocytic Leukemia. *Anal. Bioanal. Chem.* 2020, 412, 949–962. doi:10.1007/s00216-019-02321-z
99. Li, X.; Yang, T.; Li, S.; Jin, L.; Wang, D.; Guan, D.; Ding, J. Noninvasive Liver Diseases Detection Based on Serum Surface Enhanced Raman Spectroscopy and Statistical Analysis. *Opt. Express*. 2015, 23, 18361–18372. doi:10.1364/OE.23.018361
100. Yu, Y.; Lin, Y.; Xu, C.; Lin, K.; Ye, Q.; Wang, X.; Xie, S.; Chen, R.; Lin, J. Label-Free Detection of Nasopharyngeal and Liver Cancer Using Surface-Enhanced Raman Spectroscopy and Partial Least Squares Combined with Support Vector Machine. *Biomed. Opt. Express*. 2018, 9, 6053–6066. doi:10.1364/BOE.9.006053
101. Zhang, K.; Hao, C.; Man, B.; Zhang, C.; Yang, C.; Liu, M.; Peng, Q.; Chen, C. Diagnosis of Liver Cancer Based on Tissue Slice Surface Enhanced Raman Spectroscopy and Multivariate Analysis. *Vib. Spectrosc.* 2018, 98, 82–87. doi:10.1016/j.vibspec.2018.07.010
102. Qian, K.; Wang, Y.; Hua, L.; Chen, A.; Zhang, Y. New Method of Lung Cancer Detection by Saliva Test Using Surface-Enhanced Raman Spectroscopy. *Thorac. Cancer*. 2018, 9, 1556–1561. doi:10.1111/1759-7714.12837
103. Xiao, R.; Zhang, X.; Rong, Z.; Xiu, B.; Yang, X.; Wang, C.; Hao, W.; Zhang, Q.; Liu, Z.; Duan, C.; et al. Non-Invasive Detection of Hepatocellular Carcinoma Serum Metabolic Profile through Surface-Enhanced Raman Spectroscopy. *Nanomed. Nanotechnol. Biol. Med.* 2016, 12, 2475–2484. doi:10.1016/j.nano.2016.07.014
104. Bangaol, R.; Santillan, A.; Angeles, L. M.; Abanilla, L.; Lim, A.; Ramos, M. C.; Fellizar, A.; Guevarra, L.; Albano, P. M. ATR-FTIR Spectroscopy as Adjunct Method to the Microscopic Examination of Hematoxylin and Eosin-Stained Tissues in Diagnosing Lung Cancer. *PloS One* 2020, 15, e0233626. doi:10.1371/journal.pone.0233626
105. Weng, S.; Xu, X.; Li, J.; Wong, S. T. Combining Deep Learning and Coherent anti-Stokes Raman Scattering Imaging for Automated Differential Diagnosis of Lung Cancer. *J. Biomed. Opt.* 2017, 22, 1–10. doi:10.1117/1.JBO.22.10.106017
106. McGregor, H. C.; Short, M. A.; McWilliams, A.; Shaipanich, T.; Ionescu, D. N.; Zhao, J.; Wang, W.; Chen, G.; Lam, S.; Zeng, H. Real-Time Endoscopic Raman Spectroscopy for in Vivo Early Lung Cancer Detection. *J. Biophotonics*. 2017, 10, 98–110. doi:10.1002/jbio.201500204
107. Akalin, A.; Mu, X.; Kon, M. A.; Ergin, A.; Remiszewski, S. H.; Thompson, C. M.; Raz, D. J.; Diem, M. Classification of Malignant and Benign Tumors of the Lung by Infrared Spectral Histopathology (SHP). *Lab. Invest.* 2015, 95, 406–421. doi:10.1038/labinvest.2015.1
108. Großerueschkamp, F.; Kallenbach-Thieltges, A.; Behrens, T.; Brüning, T.; Altmayer, M.; Stamatis, G.; Theegarten, D.; Gerwert, K. Marker-Free Automated Histopathological Annotation of Lung Tumour Subtypes by FTIR Imaging. *Analyst* 2015, 140, 2114–2120. doi:10.1039/C4AN01978D
109. Maitra, I.; Morais, C. L. M.; Lima, K. M. G.; Ashton, K. M.; Date, R. S.; Martin, F. L. Attenuated Total Reflection Fourier-Transform Infrared Spectral Discrimination in Human Bodily Fluids of Oesophageal Transformation to Adenocarcinoma. *Analyst* 2019, 144, 7447–7456. doi:10.1039/c9an01749f

110. Maitra, I.; Morais, C. L. M.; Lima, K. M. G.; Ashton, K. M.; Date, R. S.; Martin, F. L. Raman Spectral Discrimination in Human Liquid Biopsies of Oesophageal Transformation to Adenocarcinoma. *J. Biophotonics*. 2020, *13*, e201960132. doi:10.1002/jbio.201960132
111. Feng, S.; Zheng, Z.; Xu, Y.; Lin, J.; Chen, G.; Weng, C.; Lin, D.; Qiu, S.; Cheng, M.; Huang, Z.; et al. A Noninvasive Cancer Detection Strategy Based on Gold Nanoparticle Surface-Enhanced Raman Spectroscopy of Urinary Modified Nucleosides Isolated by Affinity Chromatography. *Biosens. Bioelectron* 2017, *91*, 616–622. doi:10.1016/j.bios.2017.01.006
112. Wu, Q.; Li, C.; Qi, Z.; Zong, L.; Hu, C.; Li, J.; Wang, X. Comparison of Hair Medulla from Esophageal Cancer Patients and Healthy Persons Using Synchrotron Radiation Infrared Microspectroscopy. *Infrared Phys. Technol.* 2020, *105*, 103201. doi:10.1016/j.infrared.2020.103201
113. Maitra, I.; Morais, C. L. M.; Lima, K. M. G.; Ashton, K. M.; Bury, D.; Date, R. S.; Martin, F. L. Discrimination of Oesophageal Transformation Stages to Adenocarcinoma in Human Tissue Samples Using Raman Microspectroscopy. *Vib. Spectrosc.* 2020, *111*, 103141. doi:10.1016/j.vibspec.2020.103141
114. Ishigaki, M.; Maeda, Y.; Taketani, A.; Andriana, B. B.; Ishihara, R.; Wongravee, K.; Ozaki, Y.; Sato, H. Diagnosis of Early-Stage Esophageal Cancer by Raman Spectroscopy and Chemometric Techniques. *Analyst* 2016, *141*, 1027–1033. doi:10.1039/c5an01323b
115. Wang, J.; Lin, K.; Zheng, W.; Yu Ho, K.; Teh, M.; Guan Yeoh, K.; Huang, Z. Simultaneous Fingerprint and High-Wavenumber Fiber-Optic Raman Spectroscopy Improves in Vivo Diagnosis of Esophageal Squamous Cell Carcinoma at Endoscopy. *Sci. Rep.* 2015, *5*, 1–10. doi:10.1038/srep12957
116. Wald, N.; Goormaghtigh, E. Infrared Imaging of Primary Melanomas Reveals Hints of Regional and Distant Metastases. *Analyst* 2015, *140*, 2144–2155. doi:10.1039/c4an01831a
117. Schleusener, J.; Gluszczynska, P.; Reble, C.; Gersonde, I.; Helfmann, J.; Fluhr, J. W.; Lademann, J.; Röwert-Huber, J.; Patzelt, A.; Meinke, M. C. In Vivo Study for the Discrimination of Cancerous and Normal Skin Using Fibre Probe-Based Raman Spectroscopy. *Exp. Dermatol.* 2015, *24*, 767–772. doi:10.1111/exd.12768
118. Zhao, J.; Lui, H.; Kalia, S.; Zeng, H. Real-Time Raman Spectroscopy for Automatic in Vivo Skin Cancer Detection: An Independent Validation. *Anal. Bioanal. Chem.* 2015, *407*, 8373–8379. doi:10.1007/s00216-015-8914-9
119. Zhao, J.; Zeng, H.; Kalia, S.; Lui, H. Wavenumber Selection Based Analysis in Raman Spectroscopy Improves Skin Cancer Diagnostic Specificity. *Analyst* 2016, *141*, 1034–1043. doi:10.1039/c5an02073e
120. Santos, I. P.; van Doorn, R.; Caspers, P. J.; Schut, T. C.; Barroso, E. M.; Nijsten, T. E.; Hegt, V. N.; Koljenović, S.; Puppels, G. J. Improving Clinical Diagnosis of Early-Stage Cutaneous Melanoma Based on Raman Spectroscopy. *Br. J. Cancer* 2018, *119*, 1339–1346.
121. Feng, X.; Moy, A. J.; Nguyen, H. T. M.; Zhang, Y.; Zhang, J.; Fox, M. C.; Sebastian, K. R.; Reichenberg, J. S.; Markey, M. K.; Tunnell, J. W. Raman Biophysical Markers in Skin Cancer Diagnosis. *J. Biomed. Opt.* 2018, *23*, 1–10. doi:10.1117/1.JBO.23.5.057002
122. Medipally, D. K. R.; Cullen, D.; Untereiner, V.; Sockalingum, G. D.; Maguire, A.; Nguyen, T. N. Q.; Bryant, J.; Noone, E.; Bradshaw, S.; Finn, M.; et al. Vibrational Spectroscopy of Liquid Biopsies for Prostate Cancer Diagnosis. *Ther. Adv. Med. Oncol.* 2020, *12*, 1758835920918499. doi:10.1177/1758835920918499
123. Medipally, D. K. R.; Nguyen, T. N. Q.; Bryant, J.; Untereiner, V.; Sockalingum, G. D.; Cullen, D.; Noone, E.; Bradshaw, S.; Finn, M.; Dunne, M.; et al. Monitoring Radiotherapeutic Response in Prostate Cancer Patients Using High Throughput FTIR Spectroscopy of Liquid Biopsies. *Cancers* 2019, *11*, 925. doi:10.3390/cancers11070925
124. Naseer, K.; Saleem, M.; Qazi, J. Optical Diagnosis of Typhoid Infection in Human Blood Sera Using Raman Spectroscopy. *Spectrosc. Lett.* 2020, *53*, 249–255. doi:10.1080/00387010.2020.1734841
125. Yunanto, A.; Utama, A. A.; Muthmainnah, N.; Suhartono, E. Early detection of neonatal sepsis using fourier transformation infrared spectroscopy (FTIR). in AIP Conference Proceedings. Jun 4, 2019 Jun 4; (Vol. 2108, No. 1, p. 020026) (AIP Publishing LLC). <https://>

- aip.scitation.org/doi/abs/10.1063/1.5110001?casa_token=moYWR97_78wAAAAA:OSGoEyVY C1Kqx7X3f3hsU6ezCsNS5NffeOnMwnvLEGZbb1q1t4iGVohuo7SymnMFIRmgT7m
126. Tien, N.; Lin, T.-H.; Hung, Z.-C.; Lin, H.-S.; Wang, I.-K.; Chen, H.-C.; Chang, C.-T. Diagnosis of Bacterial Pathogens in the Urine of Urinary-Tract-Infection Patients Using Surface-Enhanced Raman Spectroscopy. *Molecules* 2018, 23, 3374. doi:10.3390/molecules23123374
 127. Agbaria, A. H.; Beck, G.; Lapidot, I.; Rich, D. H.; Kapelushnik, J.; Mordechai, S.; Salman, A.; Huleihel, M. Diagnosis of Inaccessible Infections Using Infrared Microscopy of White Blood Cells and Machine Learning Algorithms. *Analyst* 2020, 145, 6955–6967. doi:10.1039/D0AN00752H
 128. Dinkelacker, A. G.; Vogt, S.; Oberhettinger, P.; Mauder, N.; Rau, J.; Kostrzewa, M.; Rossen, J. W. A.; Autenrieth, I. B.; Peter, S.; Liese, J.; et al. Typing and Species Identification of Clinical Klebsiella Isolates by Fourier Transform Infrared Spectroscopy and Matrix-Assisted Laser Desorption Ionization–Time of Flight Mass Spectrometry. *J. Clin. Microbiol.* 2018, 56, e00843-18. doi:10.1128/JCM.00843-18
 129. Wohlmeister, D.; Vianna, D. R. B.; Helfer, V. E.; Calil, L. N.; Buffon, A.; Fuentesfria, A. M.; Corbellini, V. A.; Pilger, D. A. Differentiation of *Candida albicans*, *Candida glabrata*, and *Candida krusei* by FT-IR and Chemometrics by CHROMagar™ *Candida*. *J. Microbiol. Methods.* 2017, 141, 121–125. doi:10.1016/j.mimet.2017.08.013
 130. Silva, S.; Tobaldini-Valerio, F.; Costa-de-Oliveira, S.; Henriques, M.; Azeredo, J.; Ferreira, E. C.; Lopes, J. A.; Sousa, C. Discrimination of Clinically Relevant *Candida* Species by Fourier-Transform Infrared Spectroscopy with Attenuated Total Reflectance (FTIR-ATR). *RSC Adv.* 2016, 6, 92065–92072. doi:10.1039/C6RA16769A
 131. Kourkoumelis, N.; Gaitanis, G.; Velegraki, A.; Bassukas, I. D. Nail Raman Spectroscopy: A Promising Method for the Diagnosis of Onychomycosis. An Ex Vivo Pilot Study. *Med. Mycol.* 2018, 56, 551–558. doi:10.1093/mmy/myx078
 132. Heraud, P.; Chatchawal, P.; Wongwattanakul, M.; Tippayawat, P.; Doerig, C.; Jearanaikoon, P.; Perez-Guaita, D.; Wood, B. R. Infrared Spectroscopy Coupled to Cloud-Based Data Management as a Tool to Diagnose Malaria: A Pilot Study in a Malaria-Endemic Country. *Malar. J.* 2019, 18, 348. doi:10.1186/s12936-019-2945-1
 133. Mwanga, E. P.; Minja, E. G.; Mrimi, E.; Jiménez, M. G.; Swai, J. K.; Abbasi, S.; Ngowo, H. S.; Siria, D. J.; Mapua, S.; Stica, C.; et al. Detection of Malaria Parasites in Dried Human Blood Spots Using Mid-Infrared Spectroscopy and Logistic Regression Analysis. *Malar. J.* 2019, 18, 341. doi:10.1186/s12936-019-2982-9
 134. Khan, S.; Ullah, R.; Saleem, M.; Bilal, M.; Rashid, R.; Khan, I.; Mahmood, A.; Nawaz, M. Raman Spectroscopic Analysis of Dengue Virus Infection in Human Blood Sera. *Optik* 2016, 127, 2086–2088. doi:10.1016/j.ijleo.2015.11.060
 135. Khan, S.; Ullah, R.; Khan, A.; Wahab, N.; Bilal, M.; Ahmed, M. Analysis of Dengue Infection Based on Raman Spectroscopy and Support Vector Machine (SVM). *Biomed. Opt. Express.* 2016, 7, 2249–2256. doi:10.1364/BOE.7.002249
 136. Khurram, M.; Khan, S.; Ali, H.; Ullah, R.; Khan, A.; Mahmood, A.; Ahmed, M. Evaluation of Raman Spectroscopy in Comparison to Commonly Performed Dengue Diagnostic Tests. *J. Biomed. Opt.* 2016, 21, 95005. doi:10.1117/1.JBO.21.9.095005
 137. Amin, A.; Ghouri, N.; Ali, S.; Ahmed, M.; Saleem, M.; Qazi, J. Identification of New Spectral Signatures Associated with Dengue Virus Infected Sera. *J. Raman Spectrosc.* 2017, 48, 705–710. doi:10.1002/jrs.5110
 138. Khan, S.; Ullah, R.; Khan, A.; Sohail, A.; Wahab, N.; Bilal, M.; Ahmed, M. Random Forest-Based Evaluation of Raman Spectroscopy for Dengue Fever Analysis. *Appl. Spectrosc.* 2017, 71, 2111–2117. doi:10.1177/0003702817695571
 139. Santos, M. C. D.; Nascimento, Y. M.; Monteiro, J. D.; Alves, B. E. B.; Melo, M. F.; Paiva, A. A. P.; Pereira, H. W. B.; Medeiros, L. G.; Morais, I. C.; Fagundes Neto, J. C.; et al. ATR-FTIR Spectroscopy with Chemometric Algorithms of Multivariate Classification in the Discrimination between Healthy vs. dengue vs. chikungunya vs. zika Clinical Samples. *Anal. Methods* 2018, 10, 1280–1285. doi:10.1039/C8AY90116C

140. Patel, S. K.; Rajora, N.; Kumar, S.; Sahu, A.; Kochar, S. K.; Krishna, C. M.; Srivastava, S. Rapid Discrimination of Malaria- and Dengue-Infected Patients Sera Using Raman Spectroscopy. *Anal. Chem.* 2019, *91*, 7054–7062. doi:10.1021/acs.analchem.8b05907
141. Sohail, A.; Khan, S.; Ullah, R.; Qureshi, S. A.; Bilal, M.; Khan, A. Analysis of Hepatitis C Infection Using Raman Spectroscopy and Proximity Based Classification in the Transformed Domain. *Biomed. Opt. Express.* 2018, *9*, 2041–2055. doi:10.1364/BOE.9.002041
142. Khan, S.; Ullah, R.; Khan, A.; Ashraf, R.; Ali, H.; Bilal, M.; Saleem, M. Analysis of Hepatitis B Virus Infection in Blood Sera Using Raman Spectroscopy and Machine Learning. *Photodiagnosis Photodyn. Ther.* 2018, *23*, 89–93. doi:10.1016/j.pdpdt.2018.05.010
143. Roy, S.; Perez-Guaita, D.; Bowden, S.; Heraud, P.; Wood, B. R. Spectroscopy Goes Viral: Diagnosis of Hepatitis B and C Virus Infection from Human Sera Using ATR-FTIR Spectroscopy. *Clin. Spectrosc.* 2019, *1*, 100001. doi:10.1016/j.clispe.2020.100001
144. Tong, D.; Chen, C.; Zhang, J.; Lv, G.; Zheng, X.; Zhang, Z.; Lv, X. Application of Raman Spectroscopy in the Detection of Hepatitis B Virus Infection. *Photodiagnosis Photodyn. Ther.* 2019, *28*, 248–252. doi:10.1016/j.pdpdt.2019.08.006
145. Lu, H.; Tian, S.; Yu, L.; Lv, X.; Chen, S. Diagnosis of Hepatitis B Based on Raman Spectroscopy Combined with a Multiscale Convolutional Neural Network. *Vib. Spectrosc.* 2020, *107*, 103038. doi:10.1016/j.vibspec.2020.103038
146. Sebba, D.; Lastovich, A. G.; Kuroda, M.; Fallows, E.; Johnson, J.; Ahoudi, A.; Honko, A. N.; Fu, H.; Nielson, R.; Carruthers, E.; et al. A Point-of-Care Diagnostic for Differentiating Ebola from Endemic Febrile Diseases. *Sci. Transl. Med.* 2018, *10*, eaat0944. doi:10.1126/scitranslmed.aat0944
147. Silva, L. G.; Péres, A. F. S.; Freitas, D. L. D.; Morais, C. L. M.; Martin, F. L.; Crispim, J. C. O.; Lima, K. M. G. ATR-FTIR Spectroscopy in Blood Plasma Combined with Multivariate Analysis to Detect HIV Infection in Pregnant Women. *Sci. Rep.* 2020, *10*, 1–7. doi:10.1038/s41598-020-77378-3
148. Chen, C.; Wang, J.; Chen, C.; Tang, J.; Lv, X.; Ma, C. Rapid and Efficient Screening of Human Papillomavirus by Raman Spectroscopy Based on GA-SVM. *Optik* 2020, *210*, 164514. doi:10.1016/j.ijleo.2020.164514
149. Zheng, X.; Wang, J.; Yin, L.; Luo, B.; Lv, X.; Wu, G. Label-Free Detection of High-Risk Human Papillomaviruses Infection Using Raman Spectroscopy and Multivariate Analysis. *Laser Phys. Lett.* 2020, *17*, 115601. doi:10.1088/1612-202X/abafbf
150. Mo, H.; Yang, L.; Wu, G.; Zheng, X.; Wang, J.; Yin, L.; Lv, X. Rapid and Non-Invasive Screening of High-Risk Human Papillomavirus Using Fourier Transform Infrared Spectroscopy and Multivariate Analysis. *Optik* 2020, *206*, 164292. doi:10.1016/j.ijleo.2020.164292
151. Barauna, V. G.; Singh, M. N.; Barbosa, L. L.; Marcarini, W. D.; Vassallo, P. F.; Mill, J. G.; Ribeiro-Rodrigues, R.; Campos, L. C. G.; Warnke, P. H.; Martin, F. L. Ultrarapid on-Site Detection of SARS-CoV-2 Infection Using Simple ATR-FTIR Spectroscopy and an Analysis Algorithm: High Sensitivity and Specificity. *Anal. Chem.* 2021, *93*, 2950–2958. doi:10.1021/acs.analchem.0c04608
152. Carlomagno, C.; Bertazioli, D.; Gualerzi, A.; Picciolini, S.; Banfi, P. I.; Lax, A.; Messina, E.; Navarro, J.; Bianchi, L.; Caronni, A.; et al. COVID-19 Salivary Raman Fingerprint: innovative Approach for the Detection of Current and past SARS-CoV-2 Infections. *Sci. Rep.* 2021, *11*, 1–13. doi:10.1038/s41598-021-84565-3
153. Wood, B. R.; Kochan, K.; Bedolla, D. E.; Salazar-Quiroz, N.; Grimley, S.; Perez-Guaita, D.; Baker, M. J.; Vongsvivut, J.; Tobin, M.; Bambery, K.; Christensen, D.; et al. Infrared Based Saliva Screening Test for COVID-19. *Angewandte Chemie* 2021, *133*, 2–8.
154. Simoens, S. Health Economic Assessment: A Methodological Primer. *IJERPH.* 2009, *6*, 2950–2966. doi:10.3390/ijerph6122950
155. Cui, L.; Butler, H. J.; Martin-Hirsch, P. L.; Martin, F. L. Aluminium Foil as a Potential Substrate for ATR-FTIR, Transfection FTIR or Raman Spectrochemical Analysis of Biological Specimens. *Anal. Methods* 2016, *8*, 481–487. doi:10.1039/C5AY02638E

156. Finlayson, D.; Rinaldi, C.; Baker, M. J. Is Infrared Spectroscopy Ready for the Clinic? *Anal. Chem.* 2019, *91*, 12117–12128. doi:10.1021/acs.analchem.9b02280
157. Wilson, B. C.; Jermyn, M.; Leblond, F. Challenges and Opportunities in Clinical Translation of Biomedical Optical Spectroscopy and Imaging. *J. Biomed. Opt.* 2018, *23*, 1–13. doi:10.1117/1.JBO.23.3.030901
158. Jamieson, L. E.; Byrne, H. J. Vibrational Spectroscopy as a Tool for Studying Drug-Cell Interaction: Could High Throughput Vibrational Spectroscopic Screening Improve Drug Development? *Vib. Spectrosc.* 2017, *91*, 16–30. doi:10.1016/j.vibspec.2016.09.003
159. Gray, E.; Butler, H. J.; Board, R.; Brennan, P. M.; Chalmers, A. J.; Dawson, T.; Goodden, J.; Hamilton, W.; Hegarty, M. G.; James, A.; et al. Health Economic Evaluation of a Serum-Based Blood Test for Brain Tumour Diagnosis: exploration of Two Clinical Scenarios. *BMJ Open.* 2018, *8*, e017593. doi:10.1136/bmjopen-2017-017593
160. Gray, E.; Cameron, J. M.; Butler, H. J.; Jenkinson, M. D.; Hegarty, M. G.; Palmer, D. S.; Brennan, P. M.; Baker, M. J. Early Economic Evaluation to Guide the Development of a Spectroscopic Liquid Biopsy for the Detection of Brain cancer. *Int. J. Technol. Assess. Health Care.* 2021, *37*, e41. doi:10.1017/s0266462321000143
161. Baker, M. J.; Trevisan, J.; Bassan, P.; Bhargava, R.; Butler, H. J.; Dorling, K. M.; Fielden, P. R.; Fogarty, S. W.; Fullwood, N. J.; Heys, K. A.; et al. Using Fourier Transform IR Spectroscopy to Analyze Biological Materials. *Nat. Protoc.* 2014, *9*, 1771–1791. <http://www.nature.com/nprot/journal/v9/n8/abs/nprot.2014.110.html>. #supplementary-information (2014). doi:10.1038/nprot110
162. Morais, C. L. M.; Paraskevaidi, M.; Cui, L.; Fullwood, N. J.; Isabelle, M.; Lima, K. M. G.; Martin-Hirsch, P. L.; Sreedhar, H.; Trevisan, J.; Walsh, M. J.; et al. Standardization of Complex Biologically Derived Spectrochemical Datasets. *Nat. Protoc.* 2019, *14*, 1546–1577. doi:10.1038/s41596-019-0150-x
163. Yang, H.; Yang, S.; Kong, J.; Dong, A.; Yu, S. Obtaining Information about Protein Secondary Structures in Aqueous Solution Using Fourier Transform IR Spectroscopy. *Nat. Protoc.* 2015, *10*, 382–396. doi:10.1038/nprot.2015.024
164. Afara, I. O.; Shaikh, R.; Nippolainen, E.; Querido, W.; Torniaainen, J.; Sarin, J. K.; Kandel, S.; Pleshko, N.; Töyräs, J. Characterization of Connective Tissues Using near-Infrared Spectroscopy and Imaging. *Nat. Protoc.* 2021, *16*, 1297–1329. doi:10.1038/s41596-020-00468-z
165. Kuepper, C.; Kallenbach-Thieltges, A.; Juette, H.; Tannapfel, A.; Großerueschkamp, F.; Gerwert, K. Quantum Cascade Laser-Based Infrared Microscopy for Label-Free and Automated Cancer Classification in Tissue Sections. *Sci. Rep.* 2018, *8*, 1–10. doi:10.1038/s41598-018-26098-w
166. Bassan, P.; Weida, M. J.; Rowlette, J.; Gardner, P. Large Scale Infrared Imaging of Tissue Micro Arrays (TMAs) Using a Tunable Quantum Cascade Laser (QCL) Based Microscope. *Analyst* 2014, *139*, 3856–3859. doi:10.1039/c4an00638k
167. Pilling, M. J.; Henderson, A.; Gardner, P. Quantum Cascade Laser Spectral Histopathology: Breast Cancer Diagnostics Using High Throughput Chemical Imaging. *Anal. Chem.* 2017, *89*, 7348–7355. doi:10.1021/acs.analchem.7b00426
168. Pilling, M. J.; Henderson, A.; Bird, B.; Brown, M. D.; Clarke, N. W.; Gardner, P. High-Throughput Quantum Cascade Laser (QCL) Spectral Histopathology: A Practical Approach towards Clinical Translation. *Faraday Discuss.* 2016, *187*, 135–154. doi:10.1039/c5fd00176e
169. Stevens, O.; Petterson, I. E. I.; Day, J. C.; Stone, N. Developing Fibre Optic Raman Probes for Applications in Clinical Spectroscopy. *Chem. Soc. Rev.* 2016, *45*, 1919–1934. doi:10.1039/c5cs00850f
170. Ramos, I. R. M.; Malkin, A.; Lyng, F. M. Current Advances in the Application of Raman Spectroscopy for Molecular Diagnosis of Cervical Cancer. *BioMed. Res. Int.* 2015, *2015*, 1–9. doi:10.1155/2015/561242
171. Pilling, M. J.; Henderson, A.; Shanks, J. H.; Brown, M. D.; Clarke, N. W.; Gardner, P. Infrared Spectral Histopathology Using Haematoxylin and Eosin (H&E) Stained Glass Slides: A Major Step Forward towards Clinical Translation. *Analyst* 2017, *142*, 1258–1268. doi:10.1039/c6an02224c